RELIABILITY TESTING AND HEAT TRANSFER ENHANCEMENT OF ORGANIC PHASE CHANGE MATERIALS

RAVI KUMAR SHARMA

A THESIS SUBMITTED IN FULFILLMENT OF THE REQUIREMENTS FOR THE AWARD OF THE DEGREE OF DOCTOR OF PHILOSOPHY

FACULTY OF ENGINEERING
UNIVERSITY OF MALAYA
KUALA LUMPUR

2016

UNIVERSITI MALAYA

ORIGINAL LITERARY WORK DECLARATION

Name of Candidate: Ravi Kumar Sharma

Registration/Matric No: KHA110122

Name of Degree: Doctor of Philosophy (PhD)

Title of Project Paper/Research Report/ Dissertation/Thesis ("this work"):

Reliability Testing and Heat Transfer Enhancement of Organic Phase Change Materials

Field of study: Mechanical Engineering

I do solemnly and sincerely declare that:

(1) I am the sole author/writer of this work;
(2) This work is original;
(3) Any use of any work in which copyright exists was done by way of fair dealing and for permitted purposes and any excerpt and extract from, or reference to or reproduction of any copyright work has been disclosed expressly and sufficiently and the title of the work and its authorship have been acknowledged in this work;
(4) I do not have any actual knowledge nor do I ought reasonably to know that making of this work constitutes an infringement of any copyright work;
(5) I hereby assign all and every right in the copyright to this work to the University of Malaya ("UM"), who henceforth shall be the owner of the copyright in this work and that any reproduction or use in any form or by any means whatsoever is prohibited without the consent of UM having been first had and obtained;
(6) I am fully aware that if in course of making this work I have infringed any copyright whether intentionally or otherwise, I may be subject to legal action or any other action as may be determined by UM.

Candidate's Signature Date

Subscribed and solemnly declares before,

Witness's Signature Date

Name:

Designation:

ABSTRACT

The design and development of a thermal energy storage device require discrete selection of the appropriate phase change material (PCM) and a suitable container to contain them. This study focuses on the selection of PCMs for solar thermal energy storage devices and the improvement in their thermophysical properties. In addition, a new shape of the PCM container is also investigated using computational fluid dynamics.

The accelerated thermal cycle test is an essential requirement to ensure the thermal and chemical stability of selected PCMs to be used in practical applications. Solar energy being an unlimited natural energy source is used in a large number of applications such as solar water/air heating, cooking, drying and other domestic and commercial applications. On the other hand, this energy also has limitations as this is available only in the daytime. Storage of this abundantly available solar energy can be effectively used in the night hours or when there are no sunny days. Four organic PCMs-paraffin wax, palmitic acid, myristic acid, and polyethylene glycol (PEG) 6000, all in the melting temperature range of 50-70 ˚C, have been considered in this study and the changes in their thermal and chemical properties have been measured using the differential scanning calorimetry and the Fourier transform infrared techniques. The results of this research work revealed that the changes in the melting temperature of paraffin wax, palmitic acid, myristic acid, and PEG 6000 were in the range of +0.72 ˚C to +3.27 ˚C, -0.29 ˚C to +1.76 ˚C, -2 ˚C to +1.2 ˚C, and 3.77 to 3.94 ˚C respectively. The variation in the latent heat of fusion was found in the range of -9.8 to 14%, 3.28 to 18%, 0.9 to 10%, and 13 to 25 % for paraffin wax, palmitic acid, myristic acid, and PEG 6000 respectively.

The low thermal conductivity of organic PCMs is a well-known drawback which limits their use in many domestic and industrial applications. A composite of palmitic acid and nano titanium dioxide (TiO_2) was prepared and its phase change behavior was investigated. TiO_2 nanoparticles of 0.5%, 1.0%, 3.0%, and 5.0% were dispersed into palmitic acid and the thermophysical properties of these nano composites were measured. The composite PCMs were characterized by FESEM, XRD, and FT-IR. The thermal properties, thermal stability and thermal reliability were ensured by DSC, TGA, and thermal cycle testing. FESEM images show the uniform dispersion of nanoparticles in the palmitic acid and FT-IR spectrum indicate that the composite PCM possesses good chemical stability and interaction between PCM and nanoparticles. The results of a thermal conductivity test show that the dispersion of the 5% nanoparticles enhances the thermal conductivity of palmitic acid by 80%.

Finally, a novel trapezoidal cavity is proposed for containing the PCM and a detailed parametric study was carried out using two nano enhanced PCMs, paraffin-Cu and water-Cu based on the computational study. The effect of side wall inclination angle, cold wall temperature, nanofluid's initial temperature, cavity inclination, Grashof number on the total solidification time of nanofluid was simulated. The total solidification time for different wt% of Cu nanoparticles was also investigated in the trapezoidal cavity. The enthalpy–porosity technique is used to trace the solid–liquid interface. The inclination angle can be used efficiently to control the solidification time. In addition, the average Nusselt number along the hot wall for different angles, nanoparticles volume fractions, and Grashof number are presented graphically. The proposed predictions are very helpful in developing an improved latent heat thermal energy storage for the solar heat collector and for casting and mold design.

ABSTRAK

Reka bentuk dan pembangunan peranti penyimpanan tenaga haba memerlukan pemilihan diskret bahan perubahan fasa yang sesuai (PCM), dan bekas yang sesuai untuk membendungnya. Kajian ini memberi tumpuan kepada pemilihan PCMS untuk peranti penyimpanan tenaga haba solar, peningkatan dalam hartanah termofizikal mereka dan reka bentuk bekas PCM novel.

Ujian kitaran haba adalah satu keperluan yang penting untuk memastikan kestabilan haba dan kimia bagi PCMS yang dipilih untuk digunakan dalam aplikasi praktikal. Tenaga solar sebagai sumber tenaga semula jadi boleh digunakan dalam sebilangan besar aplikasi seperti solar air / pemanasan udara, memasak, pengeringan dan aplikasi domestik dan komersial lain. Tetapi, tenaga ini juga mempunyai had kerana janya hanya boleh diterima pada siang hari. Penstoran tenaga solar ini boleh digunakan dengan berkesan pada waktu malam atau pada hari hujan. Empat organik PCMS iaitu lilin parafin, asid palmitik, asid Myritic, dan polietilena glikol (PEG) 6000, dalam lingkungan suhu lebur 50-70 C, telah dipertimbangkan dalam kajian ini dan perubahan dalam sifat haba dan kimia mereka telah diukur menggunakan kalorimeter dan jelmaan Fourier teknik inframerah. Hasil kajian menunjukkan bahawa perubahan dalam suhu lebur lilin parafin, asid palmitik, asid Myritic dan PEG 6000 adalah dalam lingkungan +0.72 ˚C hingga +3.27 ˚C, -0.29 ˚C kepada +1.76 ˚C, -2 ˚C kepada +1.2 ˚C, dan masing-masing 3.77-3.94 ˚C. Perubahan dalam haba pendam pelakuran ditemui dalam julat -9.8 kepada 14%, 3.28-18%, 0.9-10%, dan 13 hingga 25% untuk lilin parafin, asid palmitik, asid Myritic dan PEG 6000 masing-masing.

Kekonduksian haba yang rendah adalah kelemahan yang ketara untuk PCM organik yang menghadkan penggunaannya dalam aplikasi domestik dan industri.

Komposit palmitik asid dan nano titanium dioksida (TiO_2) serta perubahan fasa komposit tersebut akan dikaji. Nanopartikel TiO_2 sebanyak 0.5%, 1.0%, 3.0% dan 5.0% disertakan ke dalam asid palmitik dan termofizikal komposit tersebut juga diukur. PCM komposit akan dianalisis mengunakanFESEM dan FT-IR. Sifat haba, kestabilan terma dan kebolehpercayaan haba telah dikaji mengunakan DSC, TGA, dan ujian kitaran haba. Imej FESEM menunjukkan penyebaran seragam nanopartikel dalam asid Palmitic dan spektrum FT-IR menunjukkan bahawa PCM komposit mempunyai kestabilan kimia yang baik dan interaksi antara PCM dan nanopartikel. Keputusan ujian kekonduksian haba menunjukkan bahawa penyebaran 5% nanopartikel mempertingkatkan kekonduksian sebanyak 80%.

Akhir sekali, rongga trapezoid dicadangkan sebagai bekas PCMdan kajian parametrik terperinci telah dijalankan menggunakan dua nano-PCMS, iaitu parafin-Cu dan air-Cu. Kesan sudut dinding sebelah kecenderungan, suhu dinding sejuk, suhu awal NEPCM tersebut, kecondongan, nombor Grashof pada jumlah masa pemejalan daripada NEPCM telah disiasat mengunakan perisian komputer. Jumlah masa pemejalan untuk berat% yang berbeza daripada nanopartikel Cu turut disiasat dalam rongga trapezoid. Teknik entalpi-keliangan digunakan untuk mengesan antara muka pepejal-cecair. Sudut kecondongan boleh digunakan dengan cekap untuk mengawal masa pemejalan. Di samping itu, bilangan Nusselt purata di sepanjang dinding panas untuk sudut yang berbeza, nanopartikel pecahan isi padu, dan nombor Grashof di beri secara grafik. Ramalan yang dicadangkan adalah sangat berguna dalam aplikas haba pendam penyimpanan tenaga haba untuk pengumpul haba suria dan untuk tuangan dan reka bentuk acuan.

ACKNOWLEDGEMENTS

I would like to express my sincere thanks and deepest gratitude to my supervisor Dr. Poo Balan Ganesan for his constant encouragement, motivation, advice, support, and supervision throughout these few years of my study here in Malaysia. My special thanks goes to Dr. V.V. Tyagi, of Shri Mata Vaishno Devi University, Katra, India for his guidance in the area of phase change materials.

I would like to sincerely put on record the research assistantship I had received from Dr. Henk Metselaar, Department of Mechanical Engineering for completing this project, without this help I could not have sustained for the period I had spent in carrying out this research. This study would not have been possible without the funding from University of Malaya Research Grant and High Impact Research Grant. I am thankful to the directors of UMRG and HIR for the financial and moral support. I would also like to thank all of the faculty members, especially in the Department of Mechanical Engineering, University of Malaya for their support and advice during the various stages of this study.

A special thanks to my wife Babita and daughter Avani. I hope I can repay them the time they have lost not being together all these years. Words cannot express how grateful I am to my mother-in law, father-in-law, my mother, and father for all of the sacrifices that they have made on my behalf. I am also indebted to my fellow research friends, Sujit Singh, Amin Kazemzadeh, Mohammad Pourtousi, Manoj Tripathi, and Adarsh Pandey for their direct and indirect help during my study. I had truly enjoyed and benefited from all the discussions and time we have had.

TABLE OF CONTENTS

LIST OF FIGURES

LIST OF TABLES

CHAPTER 1: INTRODUCTION

This chapter presents the background and problem statement that are pertinent to the topic of this research study. This study is based on the development of a thermal energy storage using phase change materials, both experimentally and numerically. The first chapter of this thesis presents the background of the study, gives an overview of the research aim and objectives and describes the scope of study. This chapter also presents a summary of the thesis structure.

1.1 Research background

A continuous increase in the gap between the energy demand and supply and the depletion of fossil fuels has received the significant attention of researchers in the last few decades. This increasing demand forces researchers to develop renewable energy sources. But the storage of energy in a suitable form is as important as developing the new sources. The demand and supply gap can be efficiently bridged by employing an energy storage system. The capacity of energy storage in various forms and their depth of discharge are given in Figure 1.1. Among all of the different kinds of available energy, thermal energy is the only one which is available in abundance in the nature in the form of solar radiation, geothermal energy and thermally stratified layers in the ocean. This available energy, if stored in suitable storage units, can be used when solar energy is not available. As an example, the solar energy is not available in the night hours and cloudy days, so the heat stored in the day time can be utilized in the night hours. The thermal energy storage system can store the energy in the form of sensible heat in which the amount of energy stored changes with the temperature e.g. rock or water (Farid et al., 2004). Alternatively, they can store the energy in the form of latent heat which is absorbed or released when a substance changes its phase upon melting or

freezing. The temperature remains constant during this phase change process. Latent heat thermal energy storage (LHTES) are the devices which use phase change materials (PCMs) for energy storage and are more attractive due to their high energy storage density and constant charge and discharge temperature. Excess energy available in the lean hours can be used at the peak time, if it is stored properly. Every latent heat thermal energy storage device requires an appropriate type of PCM for a particular application. Solid-liquid phase change problems, sometime also known as moving boundary or Stefan problems are encountered in many industrial applications such as casting and laser drilling, latent heat thermal energy storage, food and pharmaceutical processing, microelectronics, and protective clothing. Depending upon the initial temperature of the material, they are categorized as one-region, two-region or multiple region problems (Faghri & Zhang, 2006). This phase change conversion (solid - liquid) absorbs latent heat during charging (melting) and release it during solidification (discharging).

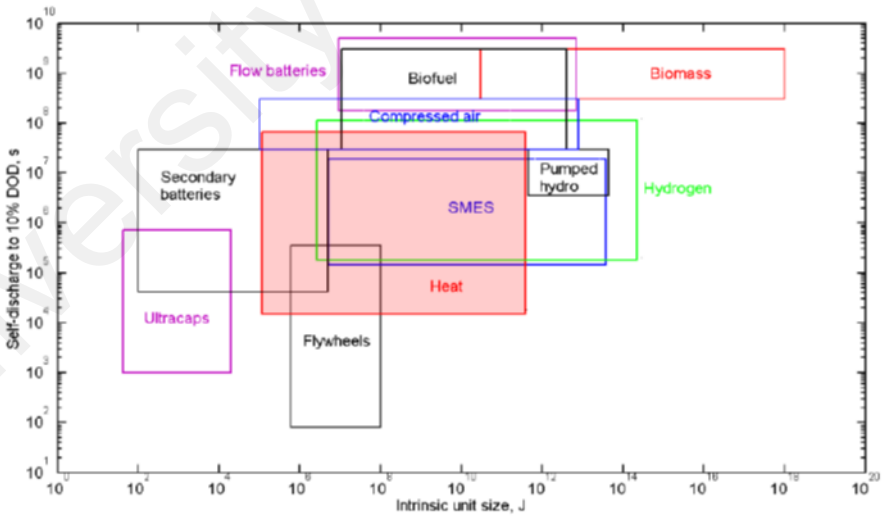

Figure 1.1 Storage capacity and discharge feature of various forms of energy storage units (Hammerschlag and Schaber, 2008)

LHTES have found their application in many industrial sectors such as, cooling of electronic devices, domestic refrigerators, building passive cooling, solar energy storage, food processing and transportation, medical, and textiles. Early work on the LHTES was mainly concerned with the thermal control in aeronautics and electronic devices in the middle of the twentieth century. A PCM for a specific application is selected on the basis of their melting/freezing temperature, chemical/thermal stability, latent heat of fusion, and cost, etc. A large number of review articles (Abhat, 1983; Hasnain, 1998; Zalba et al., 2003; Farid et al., 2004; Demirbas, 2006; Kenisarin & Mahkamov, 2007; Regin et al., 2008; Verma et al., 2008; Sharma et al., 2009; Agyenim et al., 2010; Cabeza et al., 2011; Dutil et al., 2011; Delgado et al., 2012; Tatsidjodoung et al., 2013; Nkwetta & Haghighat, 2014; Sharma et al., 2015) have been published in the past where thermophysical properties of PCMs, their encapsulation methods, applications, heat transfer enhancement and other related issues have been discussed in detail.

Low thermal conductivity of PCMs is the primary limitation in many engineering devices because it strongly suppresses the charging (melting) and discharging (freezing) rate of materials, however dispersion of solid metal particles enhances this property of the liquid substantially. The dispersion of solid particles can be done at micro or nano level. Dispersion of micrometer or millimeter sized particles may cause the clogging in the fluid flow and increase the pressure drop because of the rapid settling characteristics. Nano sized particles up to a 100 nm size behave like liquid particles, show little or no pressure drop and flow with or without little chance of clogging in the pipes. The mixture of these nanoparticles and fluid is termed as nanofluid (Choi & Eastman, 1995) and show considerably high thermal conductivity compared to the base fluids (Yu et al., 2008). Thermal conductivity of PCMs is also enhanced using various

fixed structures such as metallic fins and foams and carbon/graphite fibers (Fan & Khodadadi, 2011). However the proper configuration of these structures and their interaction with heat conduction and convection and the phase change process has always been a challenging issue. This study is concerned with the thermal conductivity enhancement only by the dispersion of solid nanoparticles. This study identifies a novel organic phase change material and proposes a novel composite material of organic PCM and metal oxide of nano size for efficient storage of thermal energy for applications such as water/air heating and drying. This study also introduces a new geometry for thermal energy storage devices.

1.2 Problem statement

The phase change materials used for the storing of the solar thermal energy undergo a large number of repetitive melting and freezing processes, which leads to the deterioration of their thermal and chemical properties. The sustainability of PCMs after a large number of melt/freeze cycles is a major concern for researchers and industries adopting them as energy storage materials. So, to be economically feasible the usage of thermal energy storage materials, they must be able to sustain their thermal properties after large numbers of thermal cycles. To date, several organic and inorganic phase change materials have been investigated for thermal energy storage, however, the variations in their chemical properties due to thermal cycle test is less explored. Another major concern of organic phase change materials is their low thermal conductivity which limits their use in many industrial and domestic applications. Insertion of metal matrix, fins, and metal particles of nano size has been found to be the proven way for enhancing the thermal conductivity of organic PCMs. In addition, the containment of PCMs for energy storage is also an area of great interest due to the fact that the shape of

the container affects the heat transfer process within the PCMs. Although many attempts have been made to overcome these issues globally, a more focused study on these mentioned aspects is still needed to understand the subject matter deeply.

1.3 Research objectives

This study aims to demonstrate the potential of adopting the organic phase change materials (O-PCMs) in a working temperature range of 50 and 70 °C for applications related to solar thermal energy storage such as solar water/air heating, crop drying, and space heating/cooling etc. The specific objectives of this study are:

1. To evaluate thermal and chemical properties of four types of organic PCMs, i.e. Polyethylene glycol of molecular weight 6000, palmitic acid, myristic acid, and paraffin wax for thermal energy storage in a melting temperature range of 50 °C to 70 °C through thermal cycle test.
2. To prepare, to characterize, and to investigate the thermal energy storage capacity of composite organic phase change material of palmitic acid and TiO_2 nanoparticles.
3. To investigate the details of the solidification phenomenon of organic and inorganic nano enhanced phase change materials filled in a trapezoidal cavity using computational fluid dynamics (CFD).

1.3.1 Scope

The scope of this study is on investigating the sustainability of organic PCMs when they undergo a large number of melt/freeze cycles and the suitability for domestic and commercial solar energy storage applications. This research also focuses on the thermal

properties enhancement of the organic PCM by dispersing the solid nano particles in various concentrations and to investigate the effect on the thermal and chemical properties of the base PCM. This will show the degree of thermal properties enhancement of the bas PCM. All of these experiments are to be performed in the University of Malaya premises and the facilities laid out by the university are to be used for all measurements and testing purposes. The shape of the PCM container plays an essential role in the thermal performance of the PCMs. In this regard, a novel trapezoidal geometry is proposed in this study that can be very useful for latent heat thermal energy storage for solar heat collector and for casting and mold design. A parametric investigation using CFD technique is carried out to see the effect of various pertinent parameters, such that geometry aspect ratio, hot and cold side temperature, Grashof, and Prandtl number. This numerical investigation will help the researchers in the design of a more effective thermal energy storage device.

The experimental part of this study is limited to the organic PCMs only due to their larger energy density. The thermal conductivity of organic PCM is low which is to be improved by the dispersion of metal oxide. In this study, it is limited to titanium dioxide (TiO_2) of a specific size and shape. The numerical study is limited to the investigation of solidification phenomenon of inorganic PCMs and Cu solid nanoparticles due to the availability of data in the literature.

1.4 Thesis structure

The structure of the thesis is based on the article style format. This thesis presents five articles which address various objectives of this research study in Chapter 2, Chapter 3, Chapter 4, and Chapter 5. This thesis is presented in total six chapters. The summary of each chapter is provided as follows.

Chapter 1: Introduction

This chapter presents an overview of the background to this research, research aim, research objectives and the scope of research study.

Chapter 2: Literature review

This chapter reviews the experimental and numerical approaches to investigate the suitability of various phase change materials (PCMs), in particular, organic PCMs (O-PCMs) for thermal energy storage. This review focuses on three aspects: the materials, encapsulation and applications of organic PCMs, and provides an insight on the recent developments in applications of these materials. The final section of this chapter presents the research gaps.

Chapter 3: Thermal cycle test of organic PCMs

This chapter presents the findings of the thermal cycle test of four PCMs from different subcategories of organic PCMs, for example, paraffin wax from paraffin family, palmitic acid and myristic acid from fatty acids, and polyethylene glycol of molecular weight 6000 from alcohol family. This study shows the variation in the thermal and chemical properties during the cycle tests of all mentioned PCMs.

Chapter 4: Enhancement in heat transfer of organic PCMs

This chapter reports the effects of titania nanoparticles on the thermal and chemical properties of the palmitic acid. A composite PCM of various nanoparticle wt% reveals the increasing thermal conductivity and improvement in other thermal properties with weight fraction which enhances the heat transfer rate.

Chapter 5: Mathematical modeling for enhanced solidification in an enclosure

This chapter reports on the findings of a parametric study carried out for organic and inorganic PCMs filled in a trapezoidal cavity. The effect of the nanoparticle concentration and cavity geometrical parameter on the total solidification time is measured and reported. The effect of various other pertinent parameters such as cold wall temperature, initial fluid temperature, and Grashof number is also discussed.

Chapter 6: Conclusions and future works

This chapter revisits the aims and objectives, provide a summary of the research process and research findings. This chapter also presents the contribution to theoretical knowledge, research limitations and research opportunities for future research and implications for practitioners.

CHAPTER 2: LITERATURE REVIEW

This chapter aims to review the experimental and numerical approaches to investigate the suitability of various phase change materials (PCMs), in particular, organic PCMs (O-PCMs) for thermal energy storage. This review focuses on three aspects: the materials, encapsulation and applications of organic PCMs, and provides an insight on the recent developments in applications of these materials. Organic PCMs have inherent characteristics of low thermal conductivity (0.15-0.35 W/mK), hence, a larger surface area is required to enhance the heat transfer rate. Therefore, attention is also given to the investigations related to the thermal conductivity enhancement of the materials, which helps to keep the area of the system to a minimum and helps to increase the heat transfer rate. Besides, various available techniques for material characterization adopted by researchers have also been discussed. This chapter also discusses the various shapes of the container adopted by the researchers for the holding of the PCMs for thermal energy storage.

2.1 Thermal energy storage

Thermal energy storage (TES) using phase change material (PCM) has been a key area of research in the last three decades and more, and has since been recognized as an important aspect after the 1973-74 energy crisis. Depletion of the fossil fuels and increase in the energy demand has increased the gap between energy demand and its supply. Excess energy stored in a suitable form has been able to bridge this energy demand/supply gap significantly. TES can be used for either short term or long-term storage. If the energy is stored for a few hours, it is termed as short term storage and is essential in many industrial and domestic applications; while if energy is stored for a month or more, it is generally considered as a long term storage device which may also

be required in some applications. Thermal energy storage plays a very important role when energy demand and supply are not equal. Excess energy available in the off peak time can be stored in TES devices for later use e.g. solar energy is available only in sunshine hours, thus, the excess heat may be stored in the day time and used later in the night hours. Energy storage helps in the saving of expensive fuels and reduces the wastage of energy and capital cost which leads to a cost effective system (Sharma et al., 2009). TES devices are majorly categorized as sensible heat storage and latent heat storage (LHS) devices. Although the most commonly used devices in industrial applications for thermal energy storage, is the sensible heat storage, but the latent heat thermal energy storage (LHTES) devices have attracted a wide range of industrial and domestic applications and will be discussed in the later sections of this chapter. LHTES provides large energy storage density with a smaller temperature change when compared to sensible heat storage devices (Paris et al., 1993; Ip & Gates, 2000). Previous studies have shown that PCMs have the capability to store about 3-4 times more heat per volume than what is stored as sensible heat in the temperature increment of 20 °C (Mehling & Cabeza, 2008). However, LHTES devices confront the difficulties that arise when the latent heat method is applied. This is due to the low thermal conductivity, changes in density, stability of thermal properties and subcooling of PCMs. Organic PCMs are a very important class of materials because of their unique thermal properties such as congruent melting and narrow melting/freezing temperature range. These properties make them suitable for many applications in solar energy storage, textiles, and cooling of electronic devices. Organic PCMs are the most suitable materials for cooling/heating of building.

2.1.1 Phase change materials

PCMs are latent heat storage materials that have high heat of fusion, high thermal energy storage densities when compared to sensible heat storage materials. They absorb and release heat at a constant temperature when undergoing a phase change process (e.g. solid -liquid). The storage capacity of LHTES devices is given by (Lane, 1983):

$$Q = \int_{T_i}^{T_m} mC_p dT + ma_m \Delta h_m + \int_{T_m}^{T_f} mC_p dT \tag{2.1}$$

$$Q = m\left[C_{sp}\left(T_m - T_i\right) + a_m \Delta h_m + C_{lp}\left(T_f - T_m\right)\right] \tag{2.2}$$

where Q is the storage capacity, C_p specific heat, T_i, T_m, and T_f are initial, melting and freezing temperature, and h is the enthalpy.

2.1.2 Classification of PCMs

Phase change materials are majorly classified as organic, inorganic, and eutectic and a comprehensive classification was given by Abhat (Abhat, 1983) and shown in Figure 2.1. Based on the melting/freezing temperature and latent heat of fusion, a large number of organic and inorganic materials can be treated as PCM. Even though, their melting/freezing temperature is within the operating range, many of the PCMs do not satisfy the criteria required for an adequate thermal energy storage device because no single material can have all of the properties required for the TES. Therefore, the available materials are to be used and their thermo physical properties are to be improvised by making suitable changes in systems design or by using external agents. For example, the thermal conductivity of PCMs can be increased by the dispersion of

metallic nanoparticle in the PCM or by inserting metallic fins in the systems design and supercooling can be suppressed by using a nucleating agent in the PCM.

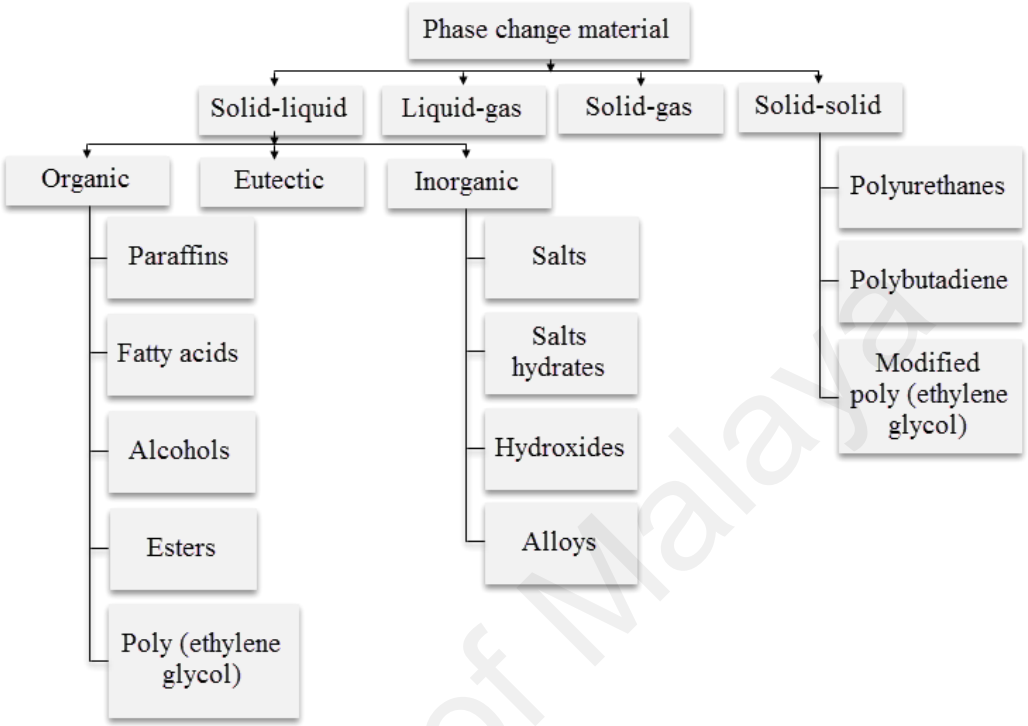

Figure 2.1: Classifications of phase change materials (Abhat, 1983; Zalba et al., 2003; Sharma et al., 2009; Kuznik, David, et al., 2011)

Organic PCMs such as paraffin wax consist of straight n-alkanes chain (CH_3-(CH_2)-CH_3) and fatty acids that are made up of straight chain hydrocarbons and are relatively expensive and possess combustible nature. Organic materials possess the capability of congruent melting without phase separation. These compounds are available in a wide range of melting points (Khudhair & Farid, 2004). Paraffin is safe, reliable, predictable, inexpensive, non-corrosive and chemically inert and stable below 500 °C but possesses extremely low thermal conductivity (0.1-0.3 W/mK) and is not suitable for encapsulation in plastic containers. Organic PCMs will be discussed in detail in the later sections of this chapter.

Inorganic materials are generally hydrated salts and metals and have a large number of applications in solar energy (Lane, 1986; Dincer & Rosen, 2002). As PCM, these materials are capable of maintaining the high heat of fusion (~ 350 MJ/m^3) even after a large number of cycles and relatively higher thermal conductivity (~ 0.5 W/m °C), but they melt incongruently. One of the cheapest inorganic materials which was studied by Telkas (1952) is Glauber salt ($Na_2SO_4.H_2O$), which contains 44% Na_2SO_4 and 56% H_2O in weight and is suitable to be used as thermal energy storage material. This salt has high latent heat (254 kJ/kg) and melting point of about 32.4 °C but it is highly prone to phase segregation and subcooling. The corrosion of the salt on metal container is also a concern (Farrell et al., 2006). The use of thickening agents e.g. Bentonite clay and nucleating agent e.g. Borax help to overcome the subcooling but they reduce the heat transfer rate by lowering the thermal conductivity. Generally, most of the salt hydrates encounter the same problem. An extensive review of hydrated salts was presented in the Chapter 1 of Lane (1983), Sharma et al. (2004), and Kenisarin and Mahkamov (2016).

The eutectic is a composition of two or more components such as organic-organic, organic-inorganic, inorganic-inorganic and each of them change their phase congruently and form a mixture of component crystal during crystallization (George, 1989). Eutectics generally melt and freeze congruently and leave no chances of separation of components (Sharma et al., 2009; Sharma et al., 2015).

2.1.3 Thermo-physical properties

Since thermo-physical properties of PCMs vary from one manufacturer to another, any of the available PCM cannot be simply used for designing an effective thermal energy storage device (Hasnain, 1998). The PCM to be used as thermal storage system should

possess the following thermal, physical, chemical, and economic properties (Abhat, 1983; Regin et al., 2008; Sharma et al., 2009; Soares et al., 2013; Waqas & Ud Din, 2013):

Thermal properties such as suitable phase change temperature, high specific heat, high latent heat, and high thermal conductivity in both, liquid and solid phases are expected from a suitable PCM. The operating temperature of heating or cooling should be matched with the phase change temperature of the PCM, which is to be selected for energy storage. High specific heat provides the additional sensible heat storage. High latent heat is desirable to store the large amount of energy in a small volume of PCM i.e. to minimize the physical size of thermal energy storage. Thermal conductivity should be high in order to minimize the temperature gradient required for the melting and freezing of the PCM.

High density materials require relatively small storage containers and little subcooling avoid the temperature range required for freezing or melting of the PCM and give a single value of phase change temperature i.e. high nucleation rate. Low vapor pressure and small volume change in the PCM help to reduce the complexity of the geometry of the container. Chemical properties such as prolonged chemical stability, compatible with capsule material, and nontoxic, nonflammable, and nonexplosive are advisable for a PCM. Continuous freezing and melting cycles may hamper the chemical composition of the PCM so it is highly desirable that the material maintains its chemical stability over a long period of time. The PCM is to be encapsulated in order to avoid the undesirable reaction with container materials.

2.1.4 Geometry of PCM container

The effects of capsule geometry have also been reported in the previous studies and found that the geometry can be a significant parameter to improve the thermal performance of PCMs. Regular geometries such as square (Khodadadi & Hosseinizadeh, 2007; Arasu & Mujumdar, 2012; Abdollahzadeh & Park, 2014), cylindrical (Ismail et al., 2001; Kim et al., 2011; Solomon & Velraj, 2013; Mahdaoui et al., 2014), and spherical (Assis et al., 2007; Tan, 2008; Hosseinizadeh et al., 2012; Amin et al., 2014; Chandrasekaran et al., 2014) have been extensively tested but the studies using irregular geometries such as triangular and trapezoidal are in scarce. Duggirala et al. (2006) investigated the solidification of binary mixture of ammonia and water in various concentrations filled in trapezoidal cavity. However, this study does not explicitly investigate the effect of the trapezoidal cavity on the solidification rate and is not based on solidification/melting of NEPCM. Recently, Sharma et al. (2014) numerically investigated the effect of trapezoidal cavity on the solidification of copper-water nanofluid. They performed the CFD simulation for various aspect ratios and calculated the solidification time for various initial fluid temperatures, cold wall temperatures, and Grashof number. This shape of the cavity was found to be a controlling parameter for the total solidification time of NEPCM.

2.2 Organic PCMs

Organic PCMs provide congruent melting and are further classified as paraffins and non-paraffins. These materials provide the congruent melting without phase segregation over the large number of melting/freezing cycles at the cost of degrading latent heat of fusion and do not suffer from supercooling. Hale (1971) provided the data related to the material properties of more than 500 PCMs required by thermal design engineers to

build efficient thermal energy storage devices. This was followed by numerous studies that focused on organic PCMs. Paraffin waxes, poly(ethylene glycol)s, fatty acids and their derivatives are the major classification of organic PCMs, which undergo a solid-liquid phase transition during heating and subsequent cooling. Polyalcohols and polyethylene are the other groups of organic PCMs, which undergo a solid-solid phase transition. Such a kind of phase transition occurs at a fixed temperature by absorbing / releasing large amounts of the latent heat. A detailed list of organic PCM candidates can be found in the literature (Lorsch et al., 1976; Abhat, 1983; Zalba et al., 2003; Farid et al., 2004; Demirbas, 2006; Cabeza et al., 2011; Sharma et al., 2015). Apart from the many listed advantages of organic PCMS, their major drawbacks are low thermal conductivity which curb the charging/discharging rate, super cooling effect in cooling cycles, and leakage of PCMs in the containers (Choi et al., 2001; Alkan, 2006; Agyenim et al., 2010).

2.2.1 Paraffins

Paraffin or paraffin wax is a mixture of straight chain *n*-alkanes which is represented by the chemical formula C_nH_{2n+2}, where $20 \leq n \leq 40$. Depending on the chain length of the alkane, paraffins may be even-chained (n-paraffin) or odd-chained (iso-paraffin) (Abhat, 1983). Studies conducted in the recent years on paraffins are summarized in Table 2.1. The molecular chain of paraffin wax involves large amount of latent heat during the crystallization/fusion. The melting temperature of these compounds increases with increase in the number of alkane chains in the molecules (Himran et al., 1994) as seen in Table 2.1. This increment in the melting temperature is because of the elevated induced dipole attraction between n-alkane chains (Sarier & Onder, 2012) e.g. the melting point of C14 is 4.5 °C and that of C18 is 28 °C. Many previous studies (Parks et

al., 1946; Parks et al., 1949; Finke et al., 1954; Messerly et al., 1967; Atkinson et al., 1969; M. Zábranský et al., 1996; van Miltenburg, 2000; Zábranský et al., 2001) have shown that paraffin waxes are capable of absorbing, storing, and releasing a great amount of heat over a large number of phase change cycles. They are excellent materials for energy storage, particularly in the buildings with a heat capacity of 2.14-2.4 kJ/kg K, and latent heat of 200-220 kJ/kg. Paraffins show no phase segregation even after many phase transition cycles and exhibit many favorable characteristics as PCMs such as they are chemically inert, non-corrosive, colorless, durable, inexpensive, available abundantly, ecologically harmless and nontoxic (Abhat, 1983; Lane, 1983; Hasnain, 1990; Hasnain, 1998). On the contrary, Lane (1983) reported that paraffin shows slow oxidation when exposed to oxygen, therefore, it requires leak-proof containers. They are generally compatible with all metallic containers but on the other hand they make some plastic containers soften (Lane, 1983).

Table 2.1 Thermo-physical properties of some paraffins, paraffin waxes, and its blends used as latent heat storage

Compound	**T_m (°C)**	**H_f (kJ/kg)**	**C_p (kJ/ kg K)**	***k*** **(W/ m K)**	**ρ (kg/m^3)**	**Ref.**
Decane	-29.65	202	-	-	726 (l)	(Himran et al., 1994)
Undecane	-25.6	177	-	-	737 (l)	(Himran et al., 1994)
Dodecane	-9.6	216	-	-	745 (l)	(Himran et al., 1994)
Tridecane	-5.4	196	2.21 (l)	-	753 (l)	(Himran et al., 1994)
Paraffin C14	4.5	165	-	-	-	(Abhat, 1983)
Tetradecane.	5.5	227	2.07 (s)	0.15	825 (s)	(Himran et al., 1994)

Table 2.1 continued…

Compound	T_m (°C)	H_f (kJ/kg)	C_p (kJ/ kg K)	k (W/ m K)	ρ (kg/m^3)	Ref.
Paraffin C15-C16	8	153	2.2 (s)	-	-	(Abhat, 1983)
Paraffin C16-C18	20-22	152	-	-	-	(Tyagi & Buddhi, 2007)
Paraffin C13-C14	22-24	189	2.1	0.21	790 (l) 900 (s)	(Tyagi & Buddhi, 2007) (Mehling & Cabeza, 2008)
Paraffin C18	28	244	2.16	0.15	814	(Abhat, 1983)
Nonadecane	32	222	-	-	785	(Paris et al., 1993)
Eicosane	36.6	247			788	(Paris et al., 1993)
Heneicozane	40.2	213	-	-	791	(Paris et al., 1993)
Paraffin C20-C33	48-50	189	2.1	0.21	769 (l) 912 (s)	(Abhat, 1983)
Paraffin C22-45	58-60	189	2.1	0.21	795 (lC) 920 (s)	(Abhat, 1983)
1-Tetradecanol	38	205	-	-	825	(Hawes et al., 1993)
Paraffin C23-C45	62-64	189	2.1	0.21	0.915	(Abhat, 1983)
Paraffin wax	64	173.6 266.0	-	0.167 (l) 0.346 (s)	790 (l) 916 (s)	(Lane, 1980) (Dincer & Rosen, 2002)

Table 2.1 continued…

Compound	**T_m (°C)**	**H_f (kJ/kg)**	**C_p (kJ/ kg K)**	***k*** **(W/ m K)**	**ρ (kg/m^3)**	**Ref.**
Paraffin C21-C50	66-68	189	-	0.21	830 (l) 930 (s)	(Abhat, 1983)
Biphenyl	71	119.2	-	-	994 (l) 1166 (s)	(Lane, 1980) (Dincer & Rosen, 2002)
Propionamide	79	168.2	-	-	-	(Lane, 1980)
Napthelene	80	147.7	2.8	0.132 (l) 0.341 (s)	976 (l) 1145 (s)	(Lane, 1980) (Durupt et al., 1995)
Tetradecane + octadecane	-4.02 - 2.1	227.52	-	-	-	(Kenisarin & Mahkamov, 2007)
91.67% Tetradecane + 8.33% hexadecane	1.70	156.20	-	-	-	(Cabeza et al., 2011)
Tetradecane + docosane	1.5-5.6	234.33	-	-	-	(Cabeza et al., 2011)
Paraffin blend (n = 14–16)	5-6	152	-	-	783 (s)	(Lorsch et al., 1975)
Paraffin blend (n = 15–16)	8	147-153	-	-	751.6	(Lorsch et al., 1975)
Paraffin blend (n = 16–18)	20-22	152	-	-	-	(Lorsch et al., 1975)
Octadecane + heneicosane	25.8-26	193.93	-	-	-	(Cabeza et al., 2011)
Octadecane + docosane	25.5-27	203.80	-	-	-	(Cabeza et al., 2011)

2.2.2 Fatty acids

Non-paraffins are generally found in the form of acid and represented by the formula $CH_3(CH_2)_{2n}COOH$ (Demirbas, 2006). The fatty acids are basically derived from vegetable and animal sources which ensure nonpolluting source of supply (Feldman et al., 1995a) and are divided into six groups: caprilic, capric, lauric, myristic, palmitic and stearic (Abhat, 1983). Unlike paraffins, the individual material in this category has its own properties (Sharma et al., 2009). When compared with paraffins, these materials show excellent phase change (solid - liquid) properties but are about three times more expensive than paraffins (Hasnain, 1998). An extensive survey of organic materials was done by Abhat et al. (1981) and Buddhi and Sawhney (1994) and the number of esters, fatty acids, alcohol's and glycol's were identified to be suitable as latent heat storage. These materials are highly flammable and should avoid exposure to high temperature, flames and oxidizing agents. Fatty acids and palmitoleic acids, which have a low melting point, are the most common among others in the category. The melting temperatures of fatty acids vary between -5 and 70 °C and the latent heat between 45 and 210 kJ/kg (Kenisarin & Mahkamov, 2007). These materials have the capability to be retained in the shape of host material due to their high surface tension of 2.3×10^{-4} N/cm. A great insight of fatty acids was recently presented by Yuan et al. (2014). Some of the fatty acids investigated in the past are presented in Table 2.2. PCMs based on fatty acids can be categorized as follows (Rozanna et al., 2005):

1. Hydrates of acids of triglycerides and their mixtures.
2. Esters of fatty acids of naturally occurring triglycerides.
3. Refined/synthesized triglyceride products produced by a combination of fractionation and transesterification processes.

4. Synthesized fatty acid derivatives that have the desired freezing point temperatures.
5. Refined fatty acid hydrates that have the desired freezing point temperatures.
6. Prepared mixtures produced by essentially any of the previous processing approaches with other chemicals (preferable cheap and nontoxic) to produce eutectic compositions with the desired freezing point temperature range.

Fatty acids possess superior properties such as congruent melting, good chemical and thermal stabilities, nontoxicity, biodegradability, and melting temperature range suitable for many latent heat storage applications. They are also capable of thousands of thermal (melting/freezing) cycles without any notable degradation in thermal properties (Feldman et al., 1989; Feldman et al., 1991; Feldman et al., 1995a). The fatty acids and their eutectic mixtures have been recently investigated extensively as possible phase change materials for low/medium energy storage applications such as solar energy storage and residential applications. Thermal properties of fatty acids such as capric, lauric, palmitic and stearic acids were evaluated by Feldman et al. (1989) and they found that these materials are very promising to be used as PCMs in space heating applications. The melting point of these acids was measured between 30 °C and 65 °C and latent heat between 153 kJ/kg and 182 kJ/kg. Feldman et al. (1995b) further investigated the behavior of fatty acids and their thermal stability as PCMs. The thermal performance of myristic acid was investigated by Sari and Kaygusuz (2001) and they found that this acid shows better stability at low temperature. They also observed that this PCM is more effective when the heat exchanger is in horizontal position. Sari and Kaygusuz (2002a) studied the thermal performance of palmitic, stearic and oleic acids as well as their binary and ternary mixtures and they found that the presence of oleic acid in binary and ternary mixtures produce melting points at different levels of

temperatures. Subsequently Sari et al. studied the thermal performance of stearic acid (Sari Ahmet & Kaygusuz Kamİl, 2001) and palmitic acid (Sari & Kaygusuz, 2002b) as thermal energy storage. The thermal properties and the crystal structure of odd numbered fatty acids ($C_nH_{2n+1}COOH$) from tridecanoic acid ($C_{12}H_{25}COOH$) to tricosanoic acid ($C_{22}H_{45}COOH$) have been studied by Karaipekli et al. (2009). A detailed review of organic PCMs can be found in Rozanna et al. (2005), and Sarier and Onder (2012).

Table 2.2: Thermo-physical properties of some fatty acids used as latent heat storage

Compound (wt. %)	**T_m (°C)**	**H_f (kJ/kg)**	**Ref.**
CA-LA (90-10)	13.3	142.2	Regin et al. (2008)
CA-LA (64-36)	19.62	149.95	Karaipekli and Sarı (2010)
CA-LA (65.1-34.9)	19.67	126.56	Shilei et al. (2006)
CA-LA (45-55)	17-21	143	Kenisarin (2010)
CA-LA (70-30)	21.09	123.98	Sharma et al. (2013)
CA-MA (70-30)	21.79	123.62	Sharma et al. (2013)
CA-LA (66.75-33.25)	22.76	127.2	Ke et al. (2013)
CA-PA (76.5-23.5)	23.12	156.44	Karaipekli and Sarı (2010)
CA-SA (70-30)	23.40	104.90	Sharma et al. (2013)
$C_{14}H_{28}O_2$-$C_{10}H_{20}O_2$ (34-66)	24	147.7	Sharma et al. (2009)
CA-SA (83-17)	24.68	178.69	Karaipekli and Sarı (2010)
CA-SA (83-17)	25.39	188.15	Karaipekli and Sarı (2010)
CA-MA (78.39-21.61)	26.02	155.2	Ke et al. (2013)
CA-PA (70-30)	27.07	142.61	Sharma et al. (2013)
CA-PA (89-11)	28.71	141.4	Ke et al. (2013)
LA-MA (60-40)	28.8-40.8	172	Kenisarin (2010)

Table 2.2 continued…

LA-MA-SA (55.8-32.8-11.4)	29.29	140.9	Liu et al. (2014)
LA-MA-PA (55.24-29.75-15.02)	31.14	142.6	Zhang N. et al. (2013)
CA-SA (94.47-5.53)	31.17	156.8	Ke et al. (2013)
LA-PA (65-35)	32.8-37.1	170.2	Kenisarin (2010)
LA-SA (60.3-39.7)	33.8-47.6	189.8	Sari and Kaygusuz (2002a)
MA-SA (50-50)	35.2-51.8	189.2	Kenisarin (2010)
LA-SA (75.1-24.9)	36.9-37.6	183.4	Kenisarin and Mahkamov (2007)
MA-PA (50-50)	39.1-45.4	173.7	Kenisarin and Mahkamov (2007)
MA-PA (50-50)	47.91	153.12	Fauzi et al. (2013)
PA-SA (60-40)	51.2-54.2	183.7	Kenisarin and Mahkamov (2007)
CA-LA (65-35)	18	148	(Dimaano & Watanabe, 2002)
CA-LA (45–55)	21	143	(Hawes et al., 1993)

In order to improve the thermal performance and widen the application scope of organic PCMs, many researches have been preparing the eutectics of fatty acids and other PCMs. For a low temperature thermal energy storage, a mixture of capric and lauric acids was evaluated as possible phase change material by Shilei et al. (2006). Later Dimaano and Watanabe (2002) in their research, mixed pentadecane in the capric-lauric mixture and found that 50% of pentadecane in the mixture provides the highest heat charged. The solid-liquid phase transition in lauric, palmitic, stearic acid and their binary systems was investigated by Fauzi et al. (2013), whereby they found that

thermal properties of 23% lauric-palmitic acid eutectic system remained stable after 100 heating-cooling cycles at 32.8 °C. Sari et al. (2004) evaluated the thermal properties of lauric-stearic, myristic-palmitic, and palmitic-stearic acid and tested the thermal stability for 360 melting-freezing cycle and concluded that these materials can be effectively used for a one year period. Later, Sari (2005) studied the thermal performance of eutectic mixtures of lauric-myristic acid, lauric-palmitic acid, and myristic-stearic acid as PCM and found that these PCMs have a good thermal stability at least for four years. Subsequently, Sari and Kaygusuz (2006) investigated the thermal behavior of the eutectic mixture of myristic acid and stearic acid that can be effectively used as PCMs in low temperature thermal energy storages. Some of the studies carried out on eutectic mixtures are shown in Table 2.3.

Table 2.3: Thermo-physical properties of compound of fatty acids used as latent heat storage.

Compound (wt. %)	**T_m (°C)**	**H_f (kJ/kg)**	**Ref.**
CA-LA (90-10)	13.3	142.2	Regin et al. (2008)
CA-LA (64-36)	19.62	149.95	Karaipekli and Sarı (2010)
CA-LA (65.1-34.9)	19.67	126.56	Shilei et al. (2006)
CA-LA (45-55)	17-21	143	Kenisarin (2010)
CA-LA (70-30)	21.09	123.98	Sharma et al. (2013)
CA-MA (70-30)	21.79	123.62	Sharma et al. (2013)
CA-LA (66.75-33.25)	22.76	127.2	Ke et al. (2013)
CA-PA (76.5-23.5)	23.12	156.44	Karaipekli and Sarı (2010)
CA-SA (70-30)	23.40	104.90	Sharma et al. (2013)
$C_{14}H_{28}O_2$-$C_{10}H_{20}O_2$ (34-66)	24	147.7	Sharma et al. (2009)

Table 2.3 continued…

CA-SA (83-17)	24.68	178.69	Karaipekli and Sarı (2010)
CA-SA (83-17)	25.39	188.15	Karaipekli and Sarı (2010)
CA-MA (78.39-21.61)	26.02	155.2	Ke et al. (2013)
CA-PA (70-30)	27.07	142.61	Sharma et al. (2013)
CA-PA (89-11)	28.71	141.4	Ke et al. (2013)
LA-MA (60-40)	28.8-40.8	172	Kenisarin (2010)
LA-MA-SA (55.8-32.8-11.4)	29.29	140.9	Liu et al. (2014)
LA-MA-PA (55.24-29.75-15.02)	31.14	142.6	Zhang N. et al. (2013)
CA-SA (94.47-5.53)	31.17	156.8	Ke et al. (2013)
LA-PA (65-35)	32.8-37.1	170.2	Kenisarin (2010)
LA-SA (60.3-39.7)	33.8-47.6	189.8	Sari and Kaygusuz (2002a)
MA-SA (50-50)	35.2-51.8	189.2	Kenisarin (2010)
LA-SA (75.1-24.9)	36.9-37.6	183.4	Kenisarin and Mahkamov (2007)
MA-PA (50-50)	39.1-45.4	173.7	Kenisarin and Mahkamov (2007)
MA-PA (50-50)	47.91	153.12	Fauzi et al. (2013)
PA-SA (60-40)	51.2-54.2	183.7	(Kenisarin & Mahkamov, 2007)
CA-LA (65-35)	18	148	(Dimaano & Watanabe, 2002)
CA-LA (45–55)	21	143	(Hawes et al., 1993)

2.2.3 Sugar alcohol

Sugar alcohol, also known as polyalcohols are considered as medium temperature (90-200 ° C) PCMs and have received less attention by researchers. Previous studies revealed that alcohols such as xylitol, erythritol, and mannitol possess a much higher value of latent heat than other materials in this family. Alcohols have been tested as potential phase change materials in the last four decades. Hormansdorfer (1989) first proposed the use of polyalcohols as a PCM and their phase change behavior was discussed by Talja and Roos (2001) and Kaizawa et al. (Kaizawa et al., 2008). They observed that some polyalcohols possess latent heat of almost double than that of the other organic PCMs. Among sugar alcohols, erythritol has shown excellent suitability as a thermal energy storage material (Kakiuchi et al., 1998). Its melting point is 20 °C and latent heat of fusion is 339.8 kJ/kg. Shukla et al. (2003) performed a thermal cycling test of erythritol and observed no degradation for the 75 thermal cycles and experienced a supercooling of 15 °C. At a certain temperature, they observed the phase separation in the liquid state. When compared to lower temperature organic PCMs, sugar alcohol exhibited a much larger degree of super cooling which can hamper the efficiency of the thermal energy storage. This has been addressed in a number of research articles (Chihara et al., 1998; Ona et al., 2001; Elefsiniotis et al., 2014; Jiang et al., 2014). These materials also undergo a 10-15% volume expansion when melting (Kaizawa et al., 2008).

Sole et al. (2014) tested sugar alcohols D-mannitol, myo-inositol, and glactitol as potential PCMs by thermal cycle test. It was found that for the chosen set of parameters, myo-inositol sustained well during the cycling test, however, FT-IR images show changes in chemical structure, which does not affect the thermal properties. Some

polymorphic changes were noticed when myo-inositol was analyzed between 50 and 260 °C but these almost disappeared in the temperature range of 150 to 260 °C. Glactitol showed poor cycling stability and at the 18th cycle, its freezing temperature was measured as 60°C, which was 102 °C before starting the cycle test. D-mannitol showed the reaction with oxygen in the atmosphere which leads to non-stable materials with a lower thermal energy storage capacity.

Memon et al. (2013) developed a novel form stable alcohol based PCM by preparing a composite of lauryl alcohol and kaolin using the vacuum impregnation method, shown in Figure 2.2 (a). Simultaneous heating checked the exudation of this composite during impregnation process. A leakage testing was performed to check the maximum absorption ratio. The composite was placed in the oven for 30 min at a certain temperature above the melting point. This composite was checked for thermal reliability by performing cycling test. An experimental set up, Figure 2.2(b), which consists of a test room, a 150 W infrared lamp (as heating source), a hollow PVC envelope, and the thermocouple, was designed and developed. The leakage test showed that the maximum 24% lauryl acid can be retained by this composite. DSC measured the melting point of this composite as 19.14 °C, which is less than that of the pure lauryl acid and latent heat of fusion 48.08 kJ/kg, which is higher when compared to that of the lauryl acid 205.4 kJ/kg. The thermal cycling test revealed that after one month of complete cycling test, the melting point of the composite dropped by 0.39 °C and latent heat of fusion was dropped by 0.7 kJ/kg.

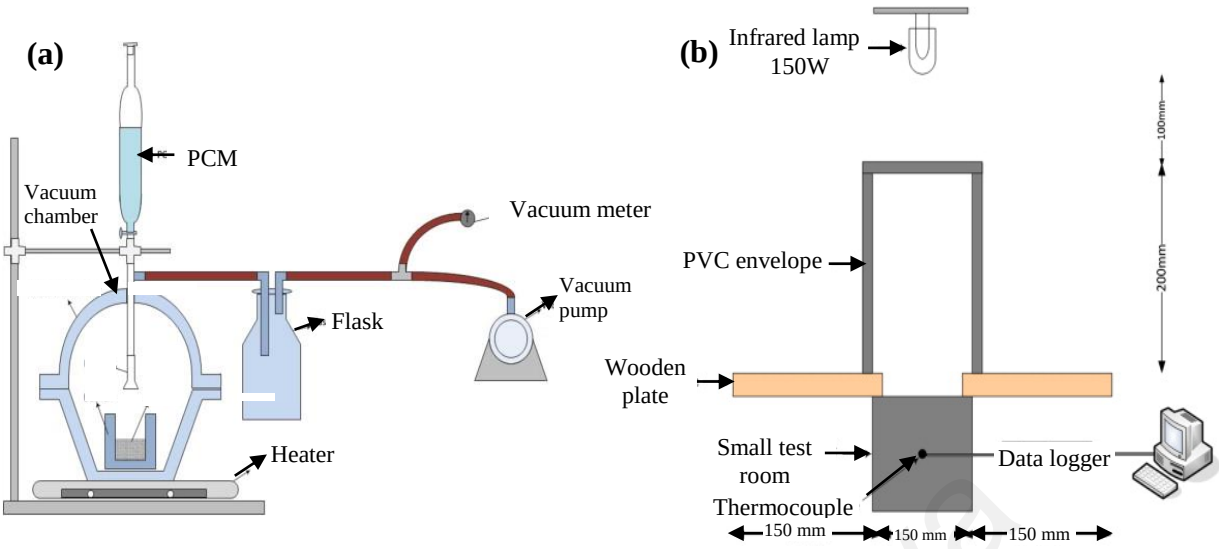

Figure 2.2 (a) Vacuum impregnation method, (b) schematic of thermal performance test (Ali Memon et al., 2013).

2.2.4 Poly(ethylene glycol)s

Polyethylene glycol (PEG) also known as polyoxyethylene (POE) or polyethylene oxide (PEO) is composed of dimethyl ether chains, $HO\text{-}CH_2\text{-}(CH_2\text{-}O\text{-}CH_2\text{-})_n\text{-}CH_2\text{-}OH$. Having the hydroxyl group at the end, makes them soluble in water as well as in organic compounds. PEGs in various grades (400, 600, 1000, 3400, 10000, 20000, 35000, 100000, and 1000000) (Pielichowska & Pielichowski, 2014) have been extensively investigated numerically and experimentally in the past and they are found to be chemically and thermally stable, nonflammable, non-toxic, non-corrosive and inexpensive (Burchill, 1983; Mathur & Moudgil, 1997; Meng & Hu, 2008; Constantinescu et al., 2010; Chen et al., 2011). As reported by Sarier and Onder (2012), the melting point and latent heat of fusion increase with an increase in molecular weight (MW), e.g. melting point of PEG (MW 400) is 3.2 °C and latent heat 91.4 kJ/kg, PEG (MW 2000) is 51 °C and latent heat 181.4 kJ/kg, and PEG (MW 20000) is 68.7 °C and

latent heat 187.8 kJ/kg. Ahmad et al. (2006) experimentally and numerically investigated the thermal performance of a wallboard filled with PEG 600. The apparent heat capacity method was adopted to numerically simulate the phase change process in a vertical panel. A sinusoidal variation of the outdoor temperature (Equation 2.3) was considered in the numerical simulation, which represents the daily variation in the outside temperature. Simulations started with the investigation of using paraffin in a gypsum wallboard, later in order to overcome the conductivity issue due to the presence of air, the polycarbonate and PVC panels were filled with PEG 600 and investigated experimentally. Results showed that the use of polycarbonate panel filled with PEG is not suitable for a light envelope for buildings but PVC panels filled with PEG 600 serves this purpose. During the thermal cycle test, no degradation in the thermal properties of the PVC panel with PEG 600 was noticed in the 400 cycles. A numerical simulation model also validated these experimental results.

$$T_e\ (°C) = 24 + 8 \sin(\omega t) \tag{2.3}$$

Like other organic PCMs, PEG is also subjected to low thermal conductivity and a large number of experimental and numerical studies have been carried out to enhance this property. Wang et al. (2009) prepared a form stable composite of SiO_2 and PEG and this composite was characterized by the SEM, FTIR and DSC. The PEG of molecular weight 10,000 and SiO_2 composite were prepared by dissolving the PEG and SiO_2 in water and stirring for 12 h. Then the mixture was heated in the oven at 100 °C for 24 h, followed by heating it under a reduced pressure of 70 °C for 24 h. SEM images showed that the PEG is dispersed into the network of solid SiO_2, which shows the mechanical strength of the composite. Polarizing optical microscope (POM) micrographs show that SiO_2 serves as a supporting material and help to prevent leakage of liquid PEG. DSC

graphs showed that the latent heat of PEG/SiO_2 composite is less and thermal conductivity is more than that of the plane PEG. The thermal conductivity of the solid PEG is 0.2985 W/m K, while it is 0.3615 W/m K for PEG/20% SiO_2 (w/w) which is 21% higher and 0.5124 for PEG/50% SiO_2, which is 71.7% higher than a normal PEG. More studies based on PEG/SiO_2 composite can be found in the references (Hawes et al., 1992; Hwang et al., 2006; Wang et al., 2007; Tang et al., 2012; Feng et al., 2013).

The blends of PEG and fatty acids have also been studied in the past to obtain the desired range of melting temperature and latent heat. It has been possible to obtain a homogeneous PEG/fatty acid blend by mixing both materials in a liquid state followed by subsequent freezing. An experimental study carried out by Pielichowski and Flejtuch (2003b) indicated that the melting range of such a blend lies between 30 and 72 °C. They investigated a series of blends of PEG with capric, lauric, myristic, palmitic, and stearic acid of different molecular weights as a thermal energy storage material. Their latent heat of fusion was observed between 168 and 208 kJ/kg, which is higher than that of the pure fatty acid, and PEG. In their further research Pielichowski et al. (2008) investigated the thermal properties of a blend of PEG 10000 with lauric acid and stearic acid. The results revealed that the crystallinity of PEG/lauric acid was 52% and PEG/stearic acid 43%. FT-IR images confirm the presence of hydrogen bonds in the blend, both in liquid and solid state that defines their synergies. During the phase change process, a synergistic effect was observed due to the formation and decay of hydrogen bonding. In similar studies by Pielichowski and Flejtuch (2003a), Flejtuch (2004), and Pielichowski (2005), the blend of PEG of different grades and fatty acids were prepared and tested for their thermal reliability as energy storage materials and was found that these materials are potential materials to be used as TES.

2.3 Enhancement of thermal conductivity of organic PCMs

An organic phase change materials has a well-known drawback of having low thermal conductivity, which substantially limits the heat transfer rate during the phase transition. A large number of research articles have been published in the last two decades, reporting the enhanced thermal conductivity of these materials by various means, such as, dispersion of high conductivity solid particles (micro/nano size) in the PCM (Zalba et al., 2003), insertion of metal matrices (Zalba et al., 2003; Khateeb et al., 2004), chunks of metal (stainless steel and copper) pieces (Cabeza et al., 2002), carbon fibers (Fukai et al., 2000; Fukai et al., 2002), and the impregnation of porous graphite matrix in the PCM (Py et al., 2001; Cabeza et al., 2002; Mills et al., 2006; Moeini Sedeh & Khodadadi, 2013). Jegadheeswaran and Pohekar (2009) presented a detailed review on the performance enhancement in latent heat thermal storage system. They discussed the various techniques such as impregnation of porous materials, dispersion of high conductivity particles, placement of metal structures, and use of high conductivity and low-density materials to enhance the thermal conductivity of PCMs. A nano composite of graphene and 1-octadecanol (stearyl alcohol) was prepared by Yavari et al. (2011) and thermal conductivity was investigated as a function of graphene content. They observed a 2.5 times higher thermal conductivity of the composite by the addition of 4% (by weight) graphene at a loss of 15.4% heat of fusion. Cui et al. (2011) added carbon nanofiber (CNF) and carbon nanotube (CNT) in the PCM (soya wax and paraffin wax) and observed that the addition of both CNF and CNT increases the thermal conductivity of the base PCM. A detailed review of studies regarding the thermal conductivity enhancement can be found in (Fan & Khodadadi, 2011; Liu et al., 2012). In the past, graphite has been extensively used as heat transfer enhancer due to its high thermal conductivity (Sarı & Karaipekli, 2007; Mehling & Cabeza, 2008; Lopez et al., 2010;

Zhang et al., 2010; Zhang et al., 2012; Zhang N. et al., 2013; Zhang Z. et al., 2013). Fan et al. (2013) investigated the effect of carbon nanofillers (CNT, CNF, and GNP) on the thermal conductivity of paraffin based PCM using hot wire method. The concentrations were varied from 1 to 5% at an increment of 1%. They found that the GNP enhanced the thermal conductivity most, at approx. 164% at the loading of 5% w/w. Li (2013) prepared a composite of paraffin and nano graphite (NG) and reported a high thermal conductivity of this composite. Nano graphite of particle diameter 35 nm was added to paraffin in 1%, 4%, 7%, and 10% w/w at 60 °C. The thermal conductivity of the paraffin was measured 0.1264 W/m K and the conductivity of the composite PCM were measured to be 2.89 times and 7.41 times higher for the 1% and 10% NG respectively. Nano graphite in different forms has been added to the numerous organic PCMs to enhance their thermal conductivity (Chen et al., 2013; Fang et al., 2013; Li H. et al., 2013; Choi et al., 2014; Goli et al., 2014; Li et al., 2014; Zeng et al., 2014).

2.4 Characterization techniques for organic PCMs

There are numerous techniques available to characterize the thermal and chemical properties of organic PCMs. The morphology of the reference material is investigated using a spectrum electron microscope (SEM) (Alkan et al., 2009; Li W. et al., 2013; Mehrali et al., 2013; Meng et al., 2013; Motahar et al., 2014b) and particle size distribution (PSD) (Alkan et al., 2009; Xu & Li, 2013; Song et al., 2014). The SEM produces images of a sample by focusing an electron beam on it and the PSD lists the values that define the relative amount of a substance into a mixture. The PSD sometimes is also known as grain size distribution. Chemical compatibility of the mixture is tested using the Fourier transform infrared spectroscopy (FT-IR) technique in which infrared (IR) radiation is passed through the sample. Some of the IR radiation is

transmitted through the sample and some absorbed into it. There have been numerous studies which have identified the properties of the materials using FT-IR technique (Feldman et al., 1989; Cho et al., 2002; Zhang et al., 2004; Sarı, Alkan, et al., 2009; Jiao et al., 2012; Pan et al., 2012; Memon et al., 2013; Konuklu et al., 2014). A Differential scanning calorimetry (DSC) (Sari & Kaygusuz, 2002b; Sarı & Karaipekli, 2007; Alkan et al., 2009; Ma et al., 2013; Mehrali et al., 2013; Konuklu et al., 2014; Sarı, 2014) and differential thermal analysis (DTA) (Buddhi et al., 1987) are the measurement techniques used to determine the latent heat of fusion, heat capacity and melting temperature of a material. In DSC, the sample and the reference material (with known thermal properties) are maintained at the same temperature and the thermal properties of the sample materials are calculated by measuring the difference of the heat absorbed between the sample and the reference. While in the DTA, the heat is applied to the sample only and the properties are evaluated by measuring the temperature difference between the sample and reference material. Yinping and Yi (1999) proposed a method, called the T-history method for the measurement of the melting temperature, degree of supercooling, thermal conductivity, specific heat, and heat of fusion of PCMs. Later, this method was modified by Hong et al (2004) and Peck et al. (2006) to make it more suitable for appropriate measurements.

The SEM, FT-IR, TEM, DSC, TGA and hot wire methods have been widely used to measure the thermal properties of pure and composite PCMs. Therefore, to ensure the accurate measurement and minimize the uncertainties in the measured values it is necessary that these equipment be calibrated before they are used. This will also help to avoid repetitive measurements, which are taken to ensure that the correct data is obtained. Most of the previous studies have concentrated on the measurement of the melting temperature and latent heat of prospective materials and very few studies have

considered the variations in the thermo-physical properties such as conductivity, density and viscosity with temperature. Almost all of the previous studies reported the use of DSC for thermal property evaluation. This technique uses a very small amount and requires almost uniform sample of PCM, which is unrealistic in the case of PCM based composite materials because they are not homogeneous.

2.5 Applications of organic PCMs

2.5.1 Cooling/heating of buildings

Consumption of electricity is significantly varied during the day and night, summer and winter seasons, depending upon the demand of industrial, commercial, and residential activities. Because of these variations, the pricing of energy use is also varied during peak and off peak season. A suitable thermal energy management system can help to keep the energy stored during off peak seasons, which can be used during peak seasons when the demand is more. For this purpose, the phase change materials can be used to enhance the thermal energy storage in building walls, floors and ceilings.

2.5.1.1 PCM walls and wallboard

Wallboards are easily available, effective and comparatively less expensive to use in the buildings and these characteristics make them highly suitable for PCM encapsulation. In wallboards, the PCM is imbedded into a gypsum board, plaster or other building structures. Stovall (1995) reported that a normal wallboard can contain up to 30% of PCMs. In their study, they found that it is a good energy saver for a passive solar system with a payback period of five years. In an early work (Athienitis et al., 1997), an experimental and numerical study was carried out over a gypsum board impregnated with a PCM (Butyl stearate) in a direct gain outdoor test room and it was observed that

the room temperature can be reduced by a maximum of 4 °C during the day time. Thermal dynamics of the PCM (fatty acid and paraffin wax) impregnated wallboards which is subjected to diurnal variation of room temperature was carried out by Neeper (2000). The results of this study showed that when the PCM melting temperature is close to the room temperature, the wallboard stores maximum diurnal energy and this energy decreases if the phase change occurs over a range of temperatures, Figure 2.3. Kuznik and Virgone (2009) experimentally investigated the thermal performance of PCM copolymer composite wallboard in a full scale test room for the summer, mid-season and winter and found that the PCM wallboards can reduce the overheating effect for all cases. Later Kuznik et al. (2011) monitored a building for almost a year for heat variation in two identical rooms. One room was equipped with the DuPont de Nemours® PCM wallboard and another was without any wallboard and found that the one with wallboard performed better.

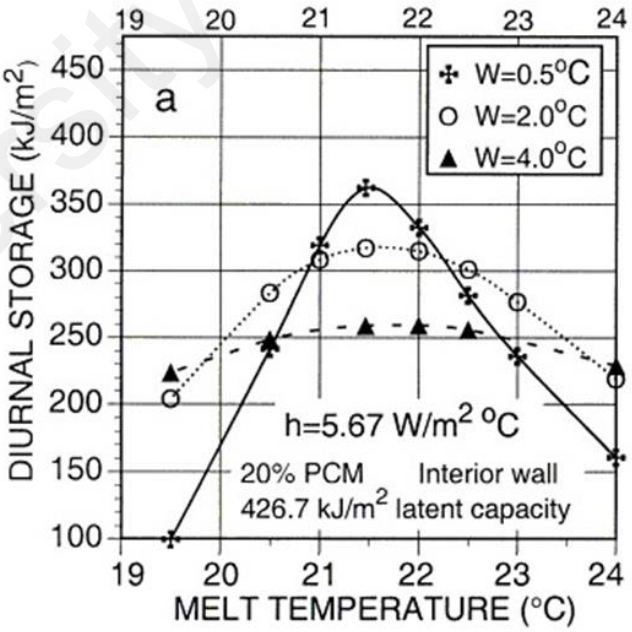

Figure 2.3 Diurnal energy storage versus melt temperature for an interior wall (Neeper, 2000).

Oliver (2012) prepared a new construction material: gypsum board containing of PCM 45 wt% and carried out its thermal characterization. They found that a 1.5 cm-thick board of gypsum with PCMs, stores 5 times more thermal energy than a laminated gypsum board, and the same energy as a 12 cm-thick brick wall within the comfort temperature range (20–30 °C). A nano-PCM (n-heptadecane+graphite nanosheets) enhanced wallboard was prepared by Biswas et al. (2014) and they simulated the thermal performance of this system, Figure 2.4, numerically and validated experimentally. Three temperature range were selected for this study: 23.3 °C that was well-above the phase change temperature range, 22 °C that was near the higher end of the melting temperature range and 21 °C that was at about the center of the melting range. No change in heat gain was observed at 22 and 23.3 °C but at 21 °C cooling set point, during peak summer, the nano-PCM wallboard reduced the peak heat gains and also delayed the heat flowing into the interior space. Recently, a new kind of composite PCM was developed by A. Sari (2014) which consists of polyethylene glycol (PEG 600) as the base PCM with gypsum and natural clay and a thermal analysis was carried out. The maximum absorption ratio of PEG 600 in gypsum-based and natural clay-based composites was found to be 18 weight% and 22 weight%, respectively. The thermal cycling test shows that this material has good thermal and chemical stability along with good thermal reliability. This material also showed an excellent cooling and heating performance.

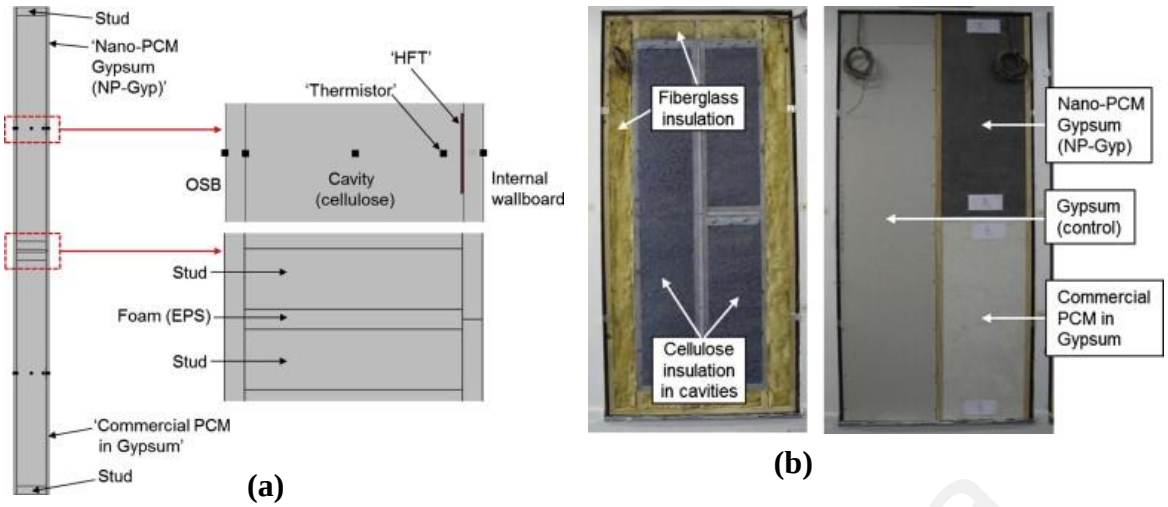

Figure 2.4 (a) Numerical model of nano-enhanced wallboard (b) Wallboard embedded with nanoPCM for experimental study (Biswas et al., 2014).

2.5.1.2 PCM Floors and ceilings for passive solar heating

The ceiling and floor are two important sides of a building block and can be effectively utilized for heating/cooling of a building space. Organic PCMs have been effectively incorporated either directly or in the encapsulated form in these parts in the past to store the solar radiation. Figure 2.5 shows an insulation system proposed by Turnpenny et al. (2000). They developed a latent heat storage unit by incorporating the embedded heat pipes in phase change material. This system stored coolness during the night and released it in the daytime. Stritih and Butala (2010) experimentally analyzed the cooling building using paraffin (melting point 22 °C) impregnated ceiling board as shown in Figure 2.6. They monitored the cooling of the PCM at night for seven consecutive days and it was observed that during this period the outside temperature remained stable. The amount of cold released from the PCM was calculated from zero to 300 min. They found that this system was very helpful for the cooling of buildings.

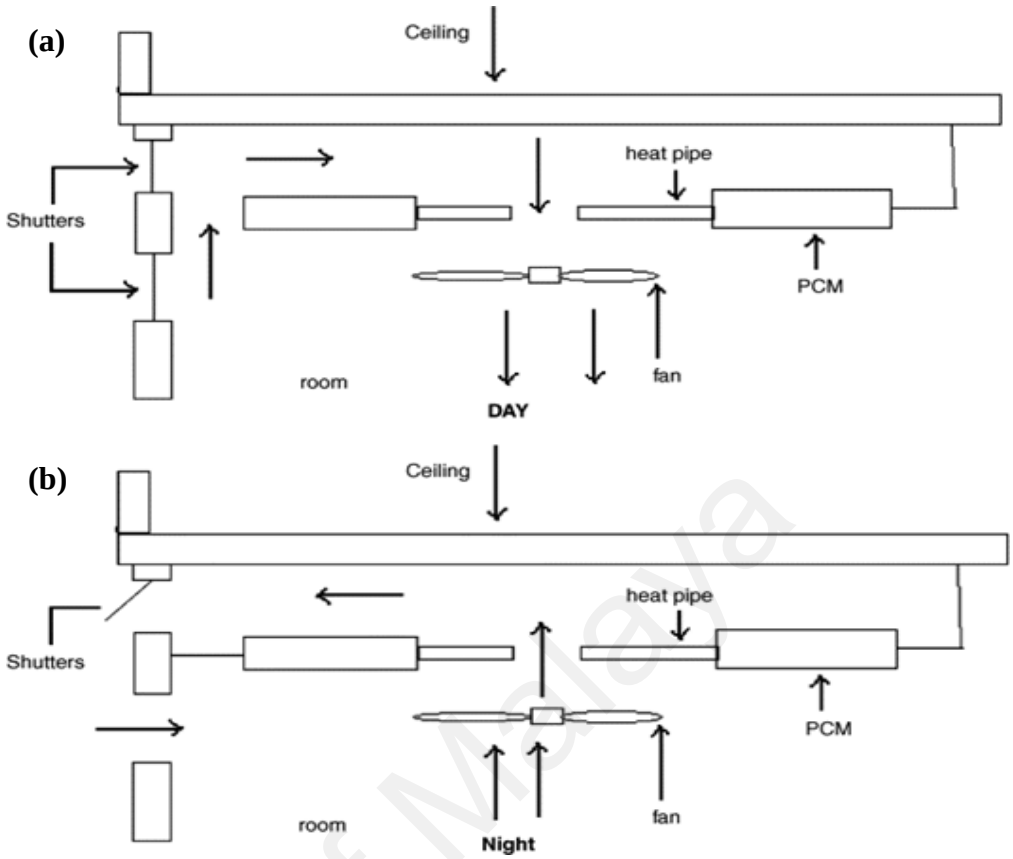

Figure 2.5 Outline of heat pipe/PCM insulation system (Turnpenny et al., 2000)

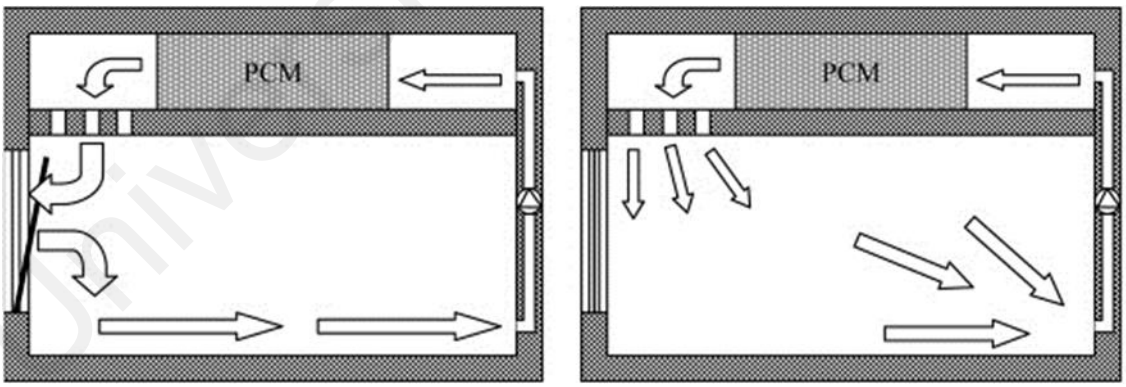

Figure 2.6 Principal function of PCM "free-cooling system": (left) cooling of PCM at night, (right) cooling of building during the day (Stritih & Butala, 2010).

Floor heating is also very important as they may provide a comfortable indoor environment than convective heating systems (Athienitis & Chen, 2000). Organic PCMs have a great potential to be used as thermal energy storage media in floors. Some of the organic PCMs used in floor heating are given in Table 2.5. Lin et al. (2005) experimentally investigated the thermal performance of under-floor electric heating systems (Figure 2.7) with a shape-stabilized phase change material (75% paraffin wax + 25% polyethylene). This system can charge heat by using cheap nighttime electricity and discharge the heat stored at daytime. During the duration of the experiment the average indoor temperature was 31 °C and the temperature difference between day and night was 12 °C. This resulted in a higher indoor temperature with no change in the temperature swing.

Table 2.5 Organic PCM used for floor heating (Jeon et al., 2013)

Compound	**Melting point (°C)**	**Heat of fusion (kJ/kg)**
Paraffin C_{16}-C_{18}	20-22	152
Polyglycol E600	22	127.2
Paraffin C_{13} – C_{24}	22-24	189
1-Dodecanol	26	200
Paraffin C_{18}	27.5	243.5
Vinyl Stearate	27-29	122
1-Tetradecanol	38	205
Paraffin C_{16} – C_{28}	42-44	189
Paraffin C_{20} – C_{33}	48-50	189
Paraffin wax	63	173.6

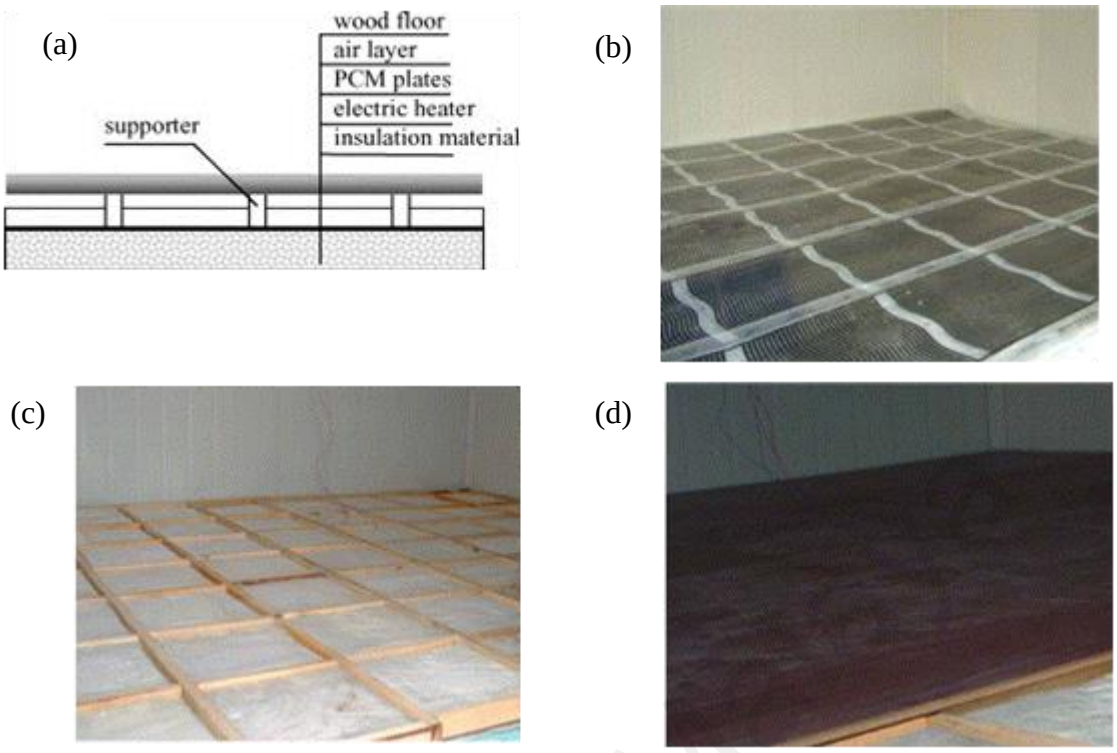

Figure 2.7 Under-floor electric heating system (a) Schematic of electric floor heating system with shape-stabilized PCM plates, (b) electric heaters, (c) shape-stabilized PCM plates, (d) wood floor (Lin et al., 2005).

2.5.2 Solar energy storage

Solar radiation is considered as one of the prospective sources of energy and this can be effectively utilized in large-scale by proper storage of it. PCMs are one of the most effective techniques to store the solar energy during daytime, which can be utilized at night or on cloudy days. The general principle of the solar energy storage and technologies to store it was summarized in ref. (HP Garg et al., 1985) and latent heat storage for solar energy was discussed in detail by Lane (1983, 1986) and Dincer and Rosen (2002). Organic PCMs are found in a large number of applications related to solar energy storage such as water and air heating, drying, solar cooking systems and solar thermal power plants which can be divided in two major groups, low temperature and high temperature solar energy storage. Kenisarin and Mahkamov (2007) and Sharma et al. (2009) presented a detailed review on tested PCMs for solar energy

storage to date. In this current review paper, we have divided this section into two major sub-sections, viz.: (i) low temperature energy storage, which includes water, air, and dryer heating using solar energy, and (ii) high temperature energy storage e.g. solar cooker.

2.5.2.1 Solar water/air heating

Solar water heating is relatively inexpensive and simple to fabricate and maintain. Barry (1940) designed one of the first kinds of solar water heating systems as shown in Figure 2.8. A copper made upwardly tapered coil is fitted inside the dome shaped shell. The lower end of this coil is connected to the inflow, which is connected to the bottom of the water container. The upper end of the coil is connected to the outlet of hot water, which is eventually connected to the top of the storage tank. The solar water heater integrated with the PCM is the upgraded version of the conventional solar water heaters which takes advantage of the ability of the PCM to store excess energy and which can be utilized in off-peak hours.

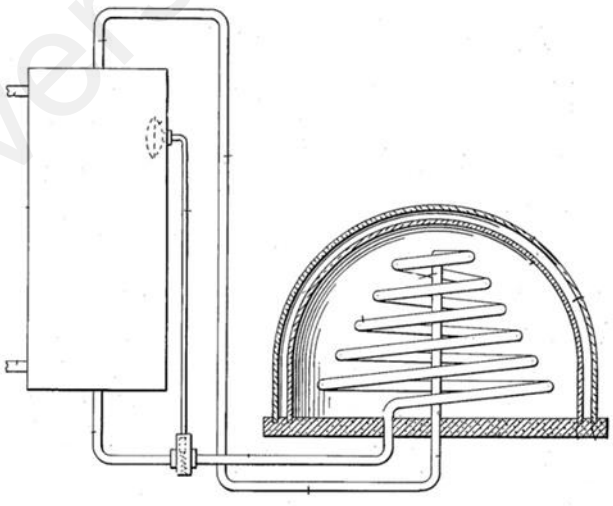

Figure 2.8 Design of solar water heater (Barry, 1940)**.**

Prakash et al (1985) developed a built-in thermal energy storage type water heater which contains a layer of PCM at the bottom which helped to provide hot water during off sunshine hours and substitute hot water by cold water. They analyzed the performance of such a system for two depths of PCMs and flow rates and found that this system is a potential solar water heater with improved heating characteristics. Organic PCMs as thermal energy storage media have been extensively used in the past and a detailed review was presented by Shukla et al. (2009). Bansal and Buddhi (1992) theoretically studied a cylindrical storage as a part of domestic hot water system with a flat plate collector for it charging and discharging. During the charging of the PCM (paraffin wax P-16 and stearic acid), the cylindrical capsule is in the close loop with a solar water heater, and while discharging, the liquid flowing in the storage unit absorbs the stored energy in the PCM. The performance of a PCM based solar water heating system with a heat pump was investigated by Kaygusuz (2000) for the data collected during November to April. The solar collector used in this system was constructed by modifying the flat-plate water-cooled collectors and the absorber unit consists of nine copper tubes of 1.8 m length and 0.022 m external diameter. Sheet iron was used to construct the storage tank with diameters of 1.30 m and 3.20 long, which contained the PCM, filled PVC containers. This design was helpful to save the energy substantially.

Hinti et al. (2010) experimentally investigated the effect of the paraffin filled capsules contained in a container used for water heating by solar radiation. This system consisted of four south facing flat plate of 1.94m × 0.76m × 0.15m collectors with a tilt angle 30°. This system works on the principle of open and closed loop system, which is enabled by the set of three valves, connected to the hot water storage tank. 1 kg of paraffin is filled in a thin walled cylindrical aluminum container of 1.3 l each. Thirty-eight such containers are fixed into a storage tank made up of steel having a length of

675 mm, inner diameter 450 mm and a volume of 107.4 l; see Figure 2.9 (a). The total volume of PCM containers are 49.4 l and remaining 58 l volume is occupied with water. Results revealed that over the test period of 24 hours, the water temperature was measured to be 30 °C higher than the ambient temperature as shown in Figure 2.9 (b).

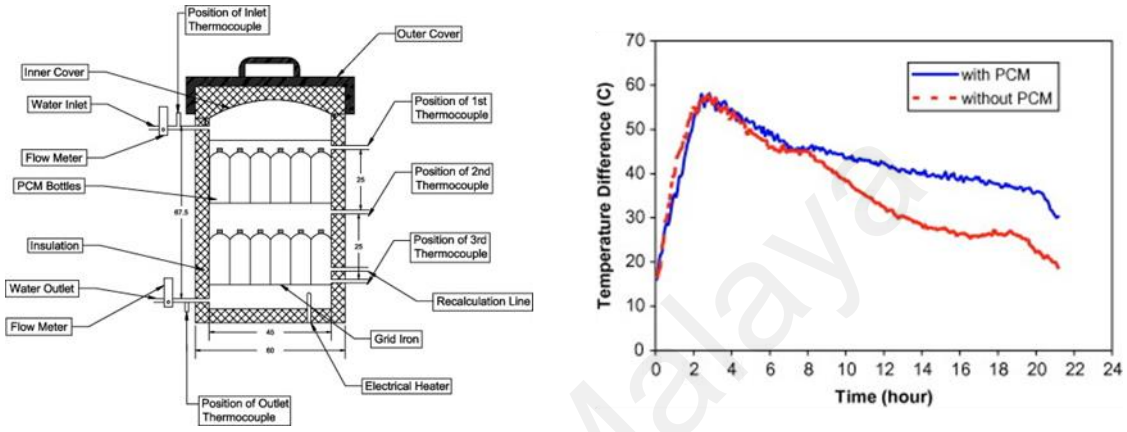

(a) **(b)**

Figure 2.9. (a) cross sectional view of the storage tank (b) Temperature variations with time (Al-Hinti et al., 2010).

Paraffin was encapsulated in spherical capsules as the PCM in a jacket shell type solar tank and the effect of the PCM encapsulation on water heater was investigated by Fazilati and Alemrajabi (2013). One hundred and eighty spherical capsules made up of HDPE having 38 mm diameter each, which occupy the 55% of the total volume of the tank was embedded inside the tank. Copper wire 380 mm long and 0.3 mm in diameter was inserted into the paraffin to enhance its thermal conductivity. It was observed that the use of the PCM in the tank increased the storage density by 39% and the exergy efficiency by 16%. It was also observed that such a PCM inbuilt solar water heater can supply hot water for up to 25% longer time. Khalifa et al. (2013) designed a storage tank consisting of six copper pipes of 80 mm diameter each, connected in series and paraffin wax filled in between the pipes as shown in Figure 2.10. Various performance factors such as top loss coefficient, water useful heat gain and heat transferred between

water and the PCM were considered to evaluate the thermal performance of such a system. Experiments were conducted on clear and semi-cloudy days of January, February and March. Results indicate that the plate temperature increases up to a distance of 2.5 m from entrance, after which a nearly steady temperature is noticed for the remaining 7.6 m of the total length (see Figure 2.10 b) which is in contrast to previously published results by many researchers.

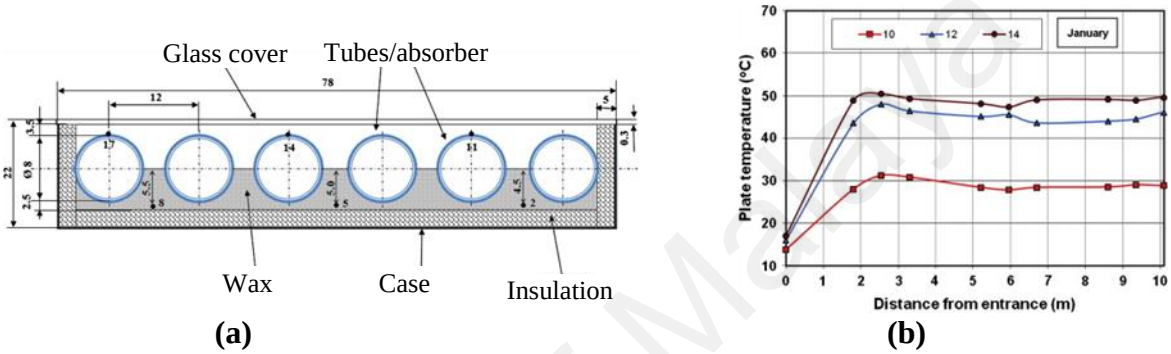

Figure 2.10 (a) Schematic diagram of storage tank, (b) variation of the pipe surface temperature with distance from entrance (Khalifa et al., 2013)

Recently, Mahfuz et al. (2014) experimentally investigated the thermal behavior of paraffin integrated solar water heating system. Their proposed system, shown in Figure 2.11 is made of three major components, a solar collector unit, a shell ad tube thermal energy storage, and an insulated water storage tank. During sunny hours, the valve 1 was open and valve 2 remained closed. The cold water from the water storage tanks passes through the solar collector and gains the heat and flows back to the storage tank. A part of this hot water goes through the thermal energy storage tank for the charging of the PCM. The excess water will automatically flow out of this tank and move towards the main water storage tank. In the night when there is no sun light, valve 2 is opened to allow the water to pass through the PCM tank so that it will extract the heat from the PCM, becomes heated up, and flow back to the main storage tank. The results show that when the water flow rate is 0.033 kg/min the energy efficiency of such

a system is 63.88% while it is 77.41% when the flow rate is 0.167 kg/min. For the first flow rate the total life cycle cost was calculated as $ 654.61 while for the later one, the total cost was predicted to be USD 609.22. This shows that when the flow rate increases, the life cycle cost decreases. Chaabane et al. (2014) carried out a numerical study on a PCM integrated solar water heater system. They used one organic PCM, myristic acid, and one organic-inorganic mixture of Rubitherm 42-graphite for this investigation. The results show that the myristic acid integrated water heating system performs better than other systems under the same environmental conditions.

Many previous research shows that organic PCMs are immensely used as thermal storage media in the solar water heating systems. The use of organic PCMs in solar water heating can also be found in the work of Elsyaed et al. (1994), Fath (1995), Salyer (2000), Ettouney et al. (2005), Sharma et al. (2009), Mazman et al. (2009), Talmatsky and Kribus (2008), Sadhishkumar and Balusamy (2014), Mettawee and Assassa (2006), Shabtay and Black (2014), Nkwetta et al. (2014), Bouadila et al. (2014).

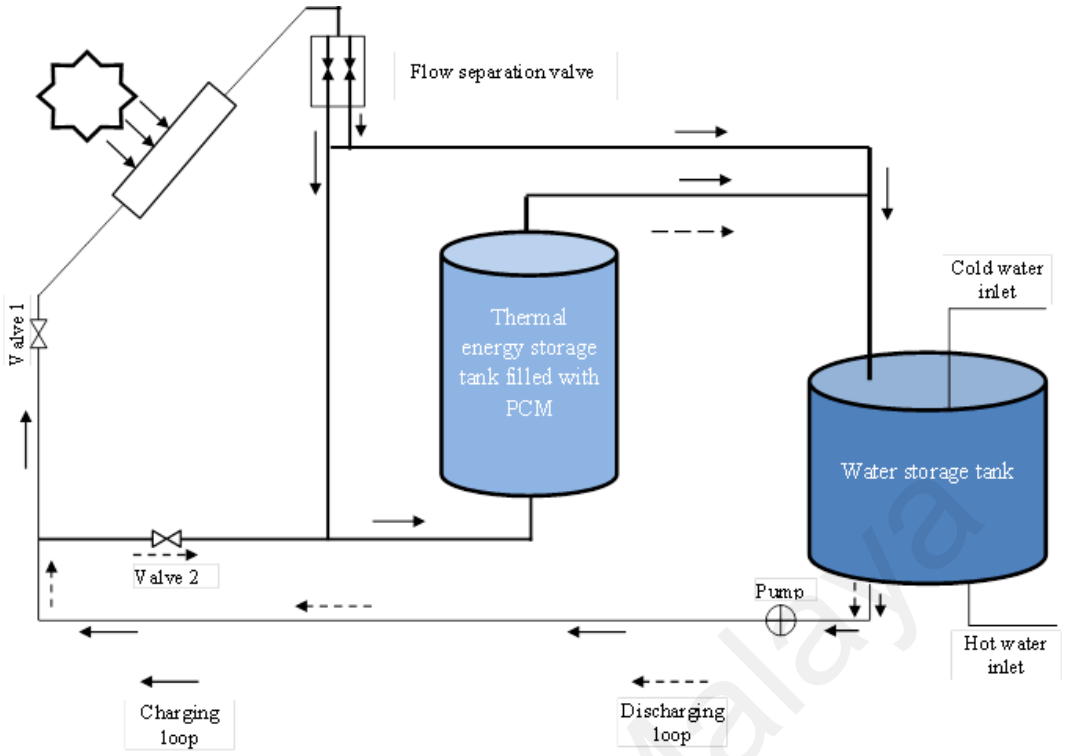

Figure 2.11 Solar water heating system with PCM (Mahfuz et al., 2014).

Solar air heating is the technique to heat or condition the air for use in building spaces or other applications. The use of PCMs is an effective way to make the sustainable solar air heating system (Lane, 1980). Morrison, Khalik and Jurinak in their different studies (Jurinak & Abdel-Khalik, 1978; Morrison & Abdel-Khalik, 1978; Jurinak & Abdel-Khalik, 1979a, 1979b) numerically investigated the performance of solar energy based air heating systems integrated with organic and inorganic phase change materials. They determined the effect of latent heat and melting temperature of PCM on the performance of an air heating system. The effect of semi-congruent melting of the phase-change material (PCM) on system performance was also examined. Results show that the PCM should be selected based on melting point rather than latent heat.

Enibe (2002) evaluated the performance of PCM based solar air heating system works on the principle of natural convection as shown in Figure 2.12. Paraffin as PCM is prepared in thin rectangular blocks, which is equispaced in the collector as shown in

Figure 2.12 (b) and behaves like thin fins. The space between two modules is utilized as air heater. The cold ambient air flows into the collector and passes through the spaces between PCM modules, which serve as air heater. Ambient air gets heat up and flows to the space chamber. Author suggested that such system is suitable for use as a solar cabinet crop dryer for aromatic herbs, medicinal plants and other crops, which do not require direct exposure to sunlight. Later in his work (Enibe, 2003), a transient numerical investigation was carried out for the same setup. Energy balance equations are developed for each major component of the heater and linked with heat and mass balance equations for the heated air flowing through the system. The numerically predicted results of the system were compared with previously published experimental data under daytime no-load conditions over the ambient temperature range of 19–41 °C and daily global irradiation of 4.9–19.9 MJ/m^2. Predicted temperatures at specific locations on the absorber plate, heat exchanger plate, glazing, and heated air were in good agreement with experimental data to within 10, 6, 8, and 10 °C, respectively. Maximum predicted cumulative useful and overall efficiencies of the system were within the ranges 2.5–13 % and 7.5–18%, respectively.

Alkilani et al. (2011) presented an up to date review on solar air collector based on thermal energy storage materials. They reviewed the published articles based on space heating, heat transfer in packed beds, green house systems and solar air heaters integrated with phase change materials. Entrop et al. (2011) experimentally evaluated the effect of microencapsulated paraffin of melting point 23 °C on the total heat load requirement for a building space when it is mixed with concrete. This experimental setup consists of four insulated boxes (1130 mm × 725 mm × 690 mm each) having window in south direction to allow the solar radiation to go inside the space, see Figure 2.13, and the data acquisition unit. The floor of two out of the four boxes contains micro

encapsulated PCM. Results of the data collected in 2010 revealed that the boxes having PCM floor are able to maintain their temperature well compared to the boxes without PCM as shown in Table 2.6.

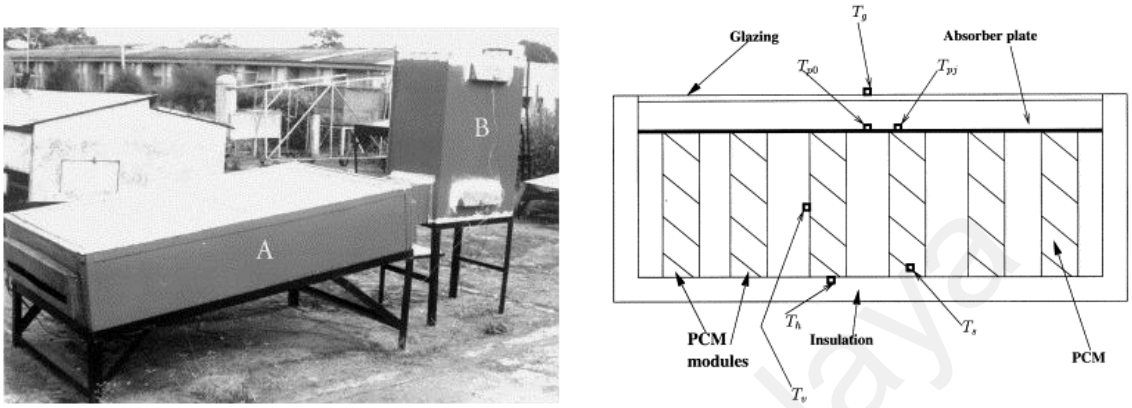

(a) **(b)**

Figure 2.12 (a) Air heating system, A, collector assembly with PCM and air-heating subsystem; B, heated space, (b) arrangement of PCM modules in the collector (Enibe, 2002).

Figure 2.13 Four test boxes at the site (Entrop et al., 2011).

Table 2.6 Minimum and maximum temperatures (±0.5 °C) in the boxes per day (Entrop et al., 2011).

Date	Test box 1	Test box 2	Test box 3	Test box 4
	Min–Max (°C)	Min–Max (°C)	Min–Max (°C)	Min–Max (°C)
24-6	20.9–24.4	23.0–29.2	19.9–25.2	20.2–28.9
25-6	23.2–25.2	25.1–29.8	22.4–25.7	22.1–28.8
26-6	23.1–25.6	23.8–30.3	21.1–26.2	20.1–29.4
27-6	23.7–27.7	24.8–32.2	22.1–28.6	21.3–31.7
28-6	24.7–30.0	27.0–33.9	23.9–31.0	23.7–33.5
29-6	26.3–30.3	28.3–33.9	24.4–30.6	24.4–32.5
30-6	25.7–30.2	27.3–33.4	24.0–29.2	23.1–30.7
1-7	24.4–28.5	25.4–31.4	23.2–28.5	22.0–30.7

Recently Karthikeyan et al. (2014) performed a numerical study on the performance of a packed bed storage unit as shown in Figure 2.14, integrated with encapsulated paraffin wax. The effect of parameters such as flow rate of heat transfer fluid (i.e. air), its temperature at inlet, ball size of the PCM capsule and effective thermal conductivity were investigated. Selected parameters for this study are given in Table 2.7. Results revealed that for a constant flow rate of air 0.035kg/s, inlet air temperature of 70 °C, and effective thermal conductivity of 0.7 W/m K, the charging/discharging time continuously increases with increasing ball diameter, increasing mass flow rate of air increases the charging time for all selected bed height. It was also observed that the effect of increasing thermal conductivity beyond 1 W/m K does not produce significant heat transfer enhancement.

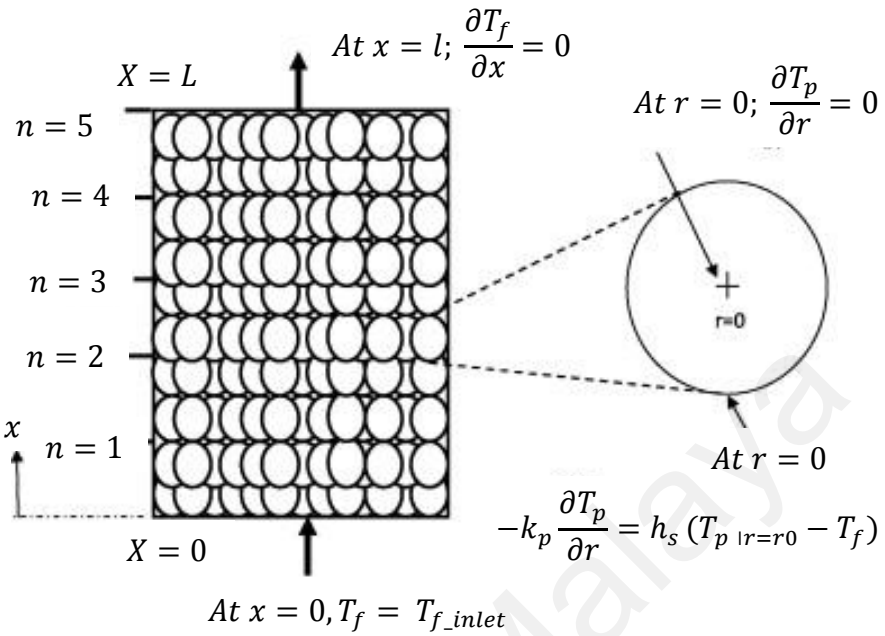

Figure 2.14 Arrangement of the packed bed model (Karthikeyan et al., 2014)

Table 2.7. Parameters considered and their range of values (Karthikeyan et al., 2014)

Parameters	**Values**
PCM ball size (mm)	60, 70, 80, 100
HTF inlet fluid temperature (°C)	67, 70, 75, 80
Mass flow rate of HTF (kg s^{-1})	0.05, 0.035, 0.015
Effective thermal conductivity of PCM (W m^{-1} K^{-1})	0.4, 1.0, 2.0

Charvat et al. (2014) numerically and experimentally analyzed a RT42 (Rubitherm®) based solar thermal system for air heating. They used 100 aluminum panels (450 mm × 300 mm × 10 mm each) filled with PCM and contained in heat storage unit as shown in Figure 2.15. Experiments were performed to validate the numerical model and then a parametric study was performed to assess the performance of such system. The TRNSYS simulation tool was used to simulate the transient one

dimensional heat transfer problem. The schematic of numerical model of heat storage unit is shown in Figure 2.15 (b). The effect of inlet air temperature and airflow rate in the performance of system was analyzed. The results revealed that this can be a potential system to be used as latent heat thermal storage system for air heating purpose.

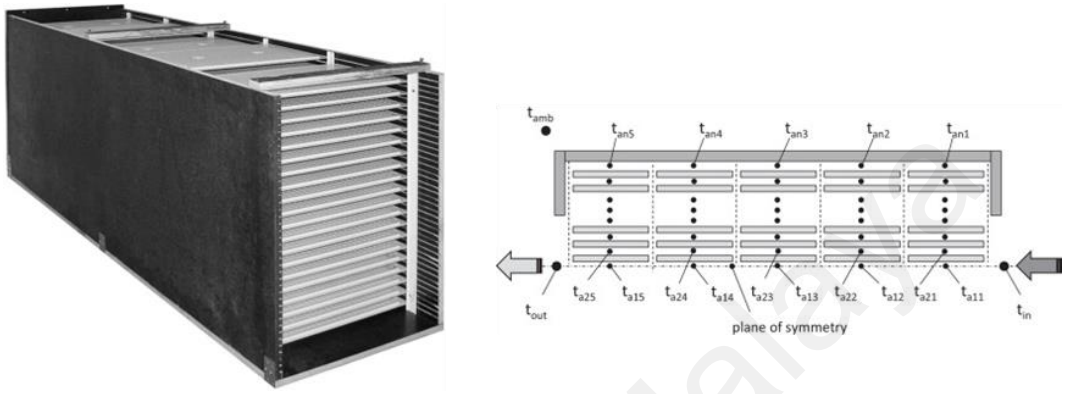

(a) **(b)**

Figure 2.15 (a) heat storage unit with front and top walls, (b) numerical model (Charvát et al., 2014)

Tyagi et al. (2012) performed the experimental investigation of a solar heater embedded with paraffin wax and hytherm oil. A total of 12 evacuated tube collector (ETC), four filled with paraffin, four filled with oil, and remaining 4 without any storage material were used in the solar heat collector as shown in Figure 2.16. The glass length exposed to sunlight is 172 cm and inclined at 45°. The results revealed that the outlet temperature of the heater with PCM was more than that of one without PCM. As the mass flow rate increases, the outlet temperature in all three considered cases increases. Later, Tyagi et al. (2012), presented a comparative energy and exergy analysis of a solar air heat collector integrated with paraffin wax and hytherm oil as PCMs. They observed that both energy and exergy efficiencies of the air heating system was higher with PCM based system than that of one without PCM.

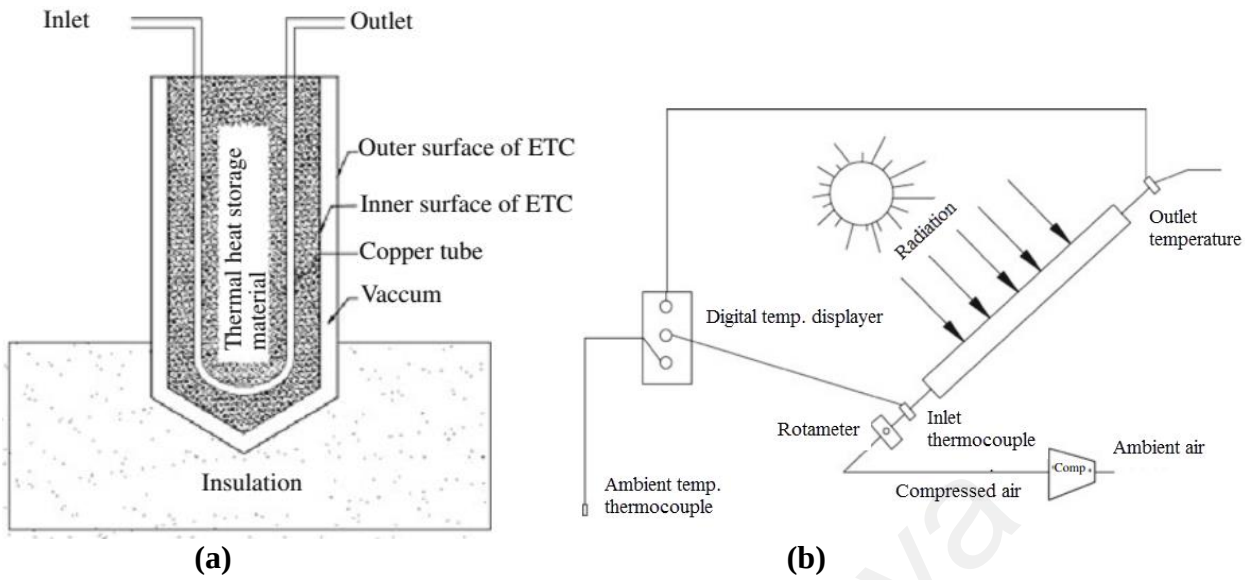

Figure 2.16 (a) Cross-sectional view of ETC tube with TES, (b) schematic of the experimental set-up (Tyagi, Pandey, Kaushik, et al., 2012)**.**

2.5.2.2 Solar dryer

Solar dryers are the devices used to dehydrate the substances using solar radiation. Depending upon the interaction of substances, they can be majorly divided into direct and indirect solar dryers. For preservation of agricultural products, especially, fruits and vegetables, the use of a moderate temperature range (40-75 °C) dryer is an essential device and the use of thermal energy storage in this temperature range has gained immense popularity in the last few decades due to their high energy storage capacity. Phase change materials, especially paraffin are one of the mostly used organic PCMs in solar dryers as energy storage media. Butler and Troeger (1981) constructed a solar collector-cum-rock bed storage for peanut drying and experimentally evaluated its performance. They found that in the drying time range of 22-24 hours, the moisture level was reduced from 20% to a safe storage moisture level.

Bal et al. (2010) presented a state of the art solar dryer with thermal energy storage for agricultural food products. They divided this review into five major sections viz. thermal energy storage, comparison of sensible and latent heat storage system, phase change materials, classification of PCMs, and solar dryer with thermal energy storage device. They emphasized on the advantage and drawbacks of various dryer designs using the thermal storage unit. The authors also mentioned that there is a need to focus on hybrid solar dryers and pointed out that heat loss is a major problem as a future research gap of the back panel of the solar dryer, which can be corrected by adding a coating of polyurethane. In their subsequent study (Bal et al., 2011), they presented an up to date review of solar dryer embedded with latent heat storage system. They mentioned that intermittent nature of the solar energy is the major drawback for solar dryer, which can be corrected if the dryer is embedded with phase change materials. Later, Vijaya Venkata Raman et al. (2012) presented a detailed review on solar drying technologies with and without PCMs. This review has listed the technological developments in the developing countries over a period of time and the various designs of solar dryers, classification and performance analysis are reviewed. Recently, Shalaby et al. (2014) presented a review on the solar dryer system integrated with phase change materials as thermal energy storage media. They also presented the various techniques used for thermal conductivity enhancement of PCMs such as, carbon fibers, expanded graphite, graphite foam etc.

In a recent investigation, Reyes et al. (2014) designed and developed a hybrid solar dryer for dehydration of mushrooms, cut in 8 mm and 12 mm slices, and consisting of an exposed surface of 10 m^2 and paraffin wax as energy storage media. The hybrid solar dryer, as shown in Figure 2.17, consists of a solar panel (3 m × 1 m) which contains a glass sheet of 5 mm thick and a black zinc plate. 14 kg of paraffin wax

are distributed in 100 copper pipes of 144 mm inner diameter and these pipes are placed in the solar energy accumulator. The mushrooms were soaked in a diluted 10% benzalkonium chloride solution for 5 min and then rinsed. The drying run started at 10:00 am and for the first 8 hours, no energy was taken from the accumulator. To maintain the temperature of the drying air at 60 °C, the energy was taken from the solar panel or the electrical resistances. After 6 pm, when the solar radiation started getting weak, the energy was taken from an energy storage device, i.e. paraffin. The authors recommended the use of low air recycle and level and thin slices of mushrooms in such a drying system. The results revealed that the color parameters significantly affected the drying process. The maximum moisture content after rehydration was 1.91 ± 0.24. The thermal efficiency of this system varied from 0.22 to 0.67 and the maximum energy fraction supplied by the accumulator was found to be 0.20.

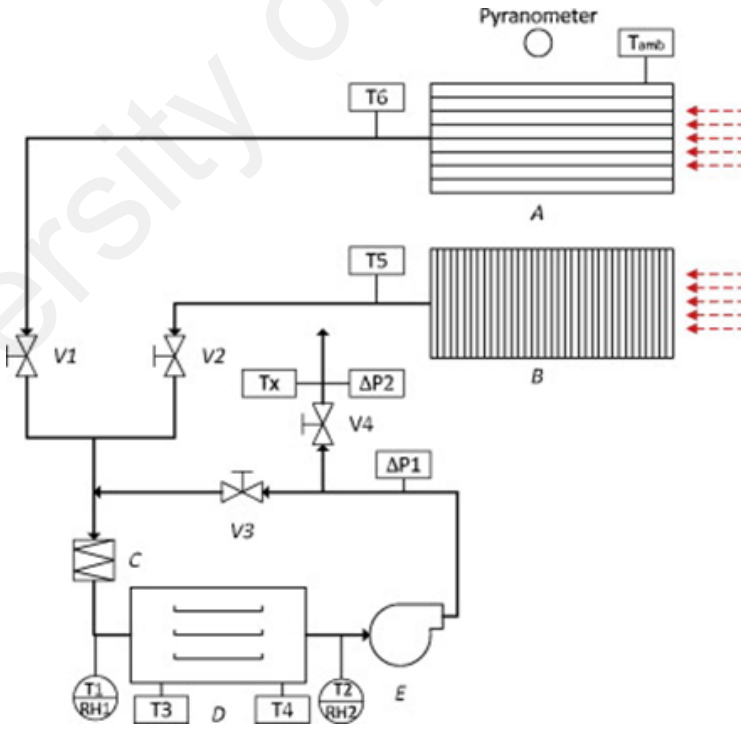

Figure 2.17 Hybrid-solar dryer for mushroom, A, Solar panel, B, Solar energy accumulator, C, Electrical heater, D, Chamber drying, E Centrifugal fan (Reyes et al., 2014).

Shalaby and Bek (2014) designed a novel indirect solar dryer (Figure 2.18) integrated with paraffin wax as a PCM with a melting temperature of 49 °C. This system consists of two identical solar heaters, one drying compartment, and a blower. The solar radiation on a tilted plate was measured in the month of September 2013 using Pyranometer and the temperature of drying air was monitored. A three-phase induction motor of 1.75 HP and 2610 rpm served the purpose of blower for dryer compartment. The experiments were conducted with and without paraffin and it was observed that after using the PCM, the temperature of the drying air was 2.5-7.5 °C higher than the ambient air for 5 hours minimum after sunset. Figure 2.18 (b) shows the hourly variation of the dry air temperature and it was observed that the average drying air temperature when using the PCM was less than that of the ones without the PCM between 8:00 am to 2:00 pm which indicates the large amount of energy storage in PCM. It was also observed that this design provides the dryer temperature with 3.5-6.5 °C higher when used with the PCM.

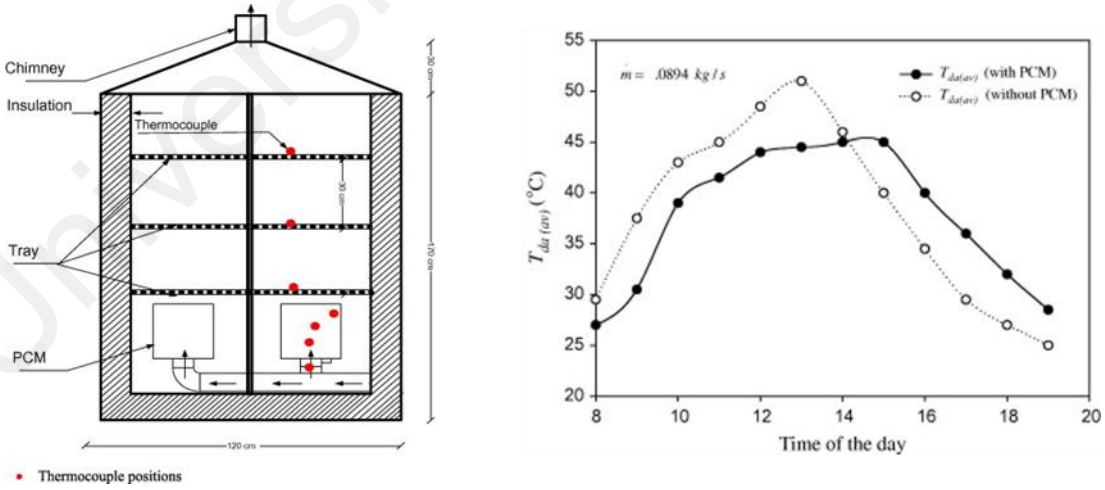

(a) (b)

Figure 2.18 (a) drying compartment, (b) variation in the temperature of the drying air (Shalaby & Bek, 2014).

2.6 Accelerated thermal cycle test

The latent heat storage materials undergo a large number of melt/freeze cycles during its entire period of application. Generally, a thermal energy storage material undergoes one melt/freeze cycle per day, however, when it undergoes a higher number of melt/freeze cycles in a laboratory under controlled conditions, it is termed as accelerated thermal cycle test (Sharma et al., 1999). An accelerated thermal cycle test of $Na_2SO_4.nH_2O$ for 1000 cycles was conducted by Ting et al. (1987), but, they did not report the variation in the thermal properties during the cycle test. a variation in the melting temperature and the latent heat of fusion was first measured by Porisini (1988) during a cycle testing of salt hydrates as the PCM. Hasan and Sayigh (1994) investigated the thermal energy storage characteristics in myristic acid, palmitic acid, and stearic acid for solar water heating system considering the moderate life of the 450 melt-freeze cycles. The results of this study revealed that the degradation of the thermophysical properties was negligible when the freezing and melting temperatures were kept between 20 and 80 ˚C. However, this reduction was up to one-third in the latent heat when the maximum temperature range was between 20 and 150 ˚C. (Shukla et al., 2008) performed an accelerated thermal cycle test for organic materials paraffin wax and erythritol, inorganic materials, sodium hydroxide, di-sodium borate, ferric nitrate, and barium hydroxide. They found that none of the inorganic material is suitable to use as thermal energy storage after a few number of cycles. However, paraffin wax and erythritol were found to be promising PCMs even after a large number of cycles. Rathod and Banerjee (2013) in their review discussed the thermal cycle test carried out for various low temperature melting points (30-60 °C) of organic and inorganic PCMs and concluded that organic PCMs exhibit better stability than inorganic materials during thermal cycle

testing. Recently, Desgrosseilliers et al. (2013) performed thermal cycle testing of lauric acid for 500 cycles.

2.7 Summary and research gap

This chapter has discussed the various commercial and lab grade organic PCMs investigated in the past studies for low and medium temperature solar energy storage applications such as building, solar water/air heater, and food industries. Numerous research work using organic PCMs and their eutectic mixture have been reported in the past in these domestic and commercial applications. Since the complete melting/solidification of the PCM in every cycle is difficult to achieve therefore, an appropriate design of a heat exchanger is essential to ensure the complete phase change process. It was also found that most of the studies have focused on the investigation of the melting/freezing phenomenon in regular geometry, however, irregular shapes have not been thoroughly studied.

On the basis of the literature reviewed, the following research gaps have been identified:

1. There is a lack of focus on studies relating to variations in the chemical structure and the compositional/functional group when PCMs undergo a large number of melt/freeze cycles.
2. The studies related to the accelerated thermal cycle testing of the polyethylene glycol based materials are lacking in the literature, thus a detailed investigation to use them as solar thermal energy storage materials is needed.
3. There is a lack of a thorough investigation of the chemical and thermophysical variation of a titania based nano enhanced phase change material when it undergoes a large number of melt/freeze cycles.

4. There is no solidification analysis of the NEPCM filled in a differentially heated trapezoidal cavity and a thorough parametric investigation is needed to ascertain the suitability of such shapes.

CHAPTER 3: THERMAL CYCLE TESTING OF ORGANIC PCMs

3.1 Introduction

As discussed in the literature review (Chapter 2), the organic phase change materials whose melting temperature are falling in the range of 50 and 70 °C are very much useful in many solar energy storage applications such as solar water/air heater and solar dryer etc. The literature review (Section 2.6) shows that there are a large number of investigations carried out on the accelerated thermal test but very few have considered a large 1500 thermal test cycles and more importantly there is extreme lack of findings on degradations of thermal properties due to changes in chemical structure during thermal cycle tests. Therefore, the present chapter investigates the thermal reliability and chemical stability of four selected commercial grade organic PCMs viz. palmitic acid, myristic acid, polyethylene glycol of molecular weight 6000, and paraffin wax. Except paraffin, all PCMs possess a purity of $\geq 98\%$. The variations in the melting temperature and latent heat of fusion during the cycle tests have been measured using differential scanning calorimeter (DSC) after every certain number of cycles and results are presented and discussed. Variations in the compositional/functional group during the cycle is also measured using the Fourier transformed infrared (FT-IR) spectroscopy and the effect of thermal cycle on chemical properties have been discussed. The selection of 1500 thermal cycles has been done on the basis of their use in the thermal energy storage for five years, considering that a latent heat storage material undergoes one melt-freeze cycle per day in a solar system and 300 in a year. Rest of the days may be considered as cloudy/rainy days.

3.2 Methodology

3.2.1 Materials

Commercial grade organic PCMs viz. palmitic acid (PA), myristic acid (MA), polyethylene glycol (PEG) of molecular weight 6000 with purity more than 98%, and paraffin wax were selected for thermal cycle testing in this study. The PA, MA, and paraffin were purchased from the R&M Chemicals, UK and PEG 6000 from Merck Company. The value of their melting temperature and the latent heat of fusion quoted by the company and obtained from the DSC are given in the Table 3.1. All of the materials were tested as they were received without any further purification.

3.2.2 Equipment

The melting temperature and the latent heat of fusion were obtained by a differential scanning calorimeter (Mettler Toledo-DSC 820-Error ± 0.25 °C) at a constant heating rate of 10 °C/min. The samples and the reference materials in the DSC tests were heated at a constant rate and the temperature difference between them was caused by the differences in the heat flow between both materials. The latent heat of fusion was obtained by calculating the area under the DSC curve and the melting temperature was approximated by drawing a tangent on the highest slope on the face portion of the peak. In order to determine the changes in the compositional/functional group during the cycle test, the Fourier Transform Infrared (FT-IR) spectroscope (Brand: Bruker, Model: IFS66v/S) was used between wavenumbers 400 to 4000 cm^{-1} with the spectral resolution of 2 cm^{-1}. The DSC facility was used at the Advanced Materials Research laboratory, Department of Mechanical Engineering and FT-IR was used at NANOCAT Laboratory of University of Malaya.

3.2.3 Experimental test rig for accelerated thermal cycle testing

The thermal stability of all selected PCMs was determined by using an in-house design (University of Malaya). The schematic of the thermal cycle tester is shown in Figure 3.1. A fan (12VDC) which is located in front of the PCM in the system was used as cooling medium and heater (24VDC) for heating purpose. A digital indicating controller (Shinko-ACS-13A) is attached to control the freezing and melting process and a communication converter (Shinko-IF-400) to transfer data to the PC and controller program. Relays (Idec-SM25) were used to monitor the power supplies to the heater and fans. A cartridge heater was glued outside to the PCM container and its heat flux was set at 80 W and 24 V respectively. A cooler type of heat sink was attached on the other side of the PCM container for the cooling of the materials. The material was heated up to 100 ˚C at heat rate of 10 ˚C/min and then naturally allowed to cool down to 30 ˚C using ethanol as the cold fluid. As soon as the heater goes up to a preset temperature of 100 °C, it gets turned off automatically due to the received signal from the feedback system. This is immediately followed by a freezing cycle of up to 30 °C by starting the fan. K-type thermocouples in the temperature range of 0-1260 °C with an error of ± 0.7% were used to sense the temperature of the PCMs. When the temperature sensor measures the set minimum temperature, the fan automatically turns off and turns on the heater for the heating of the next cycle. This accelerated thermal cycle test is a very well calibrated and established tester and has been installed at the Advanced Materials Research Laboratory of Department of Mechanical Engineering. The tester has been used in many previous work of the University (Mehrali et al., 2013; Tahan Latibari et al., 2013) and the work has already been published in the international journals of repute, thus confirming the reliability and accuracy of the tester.

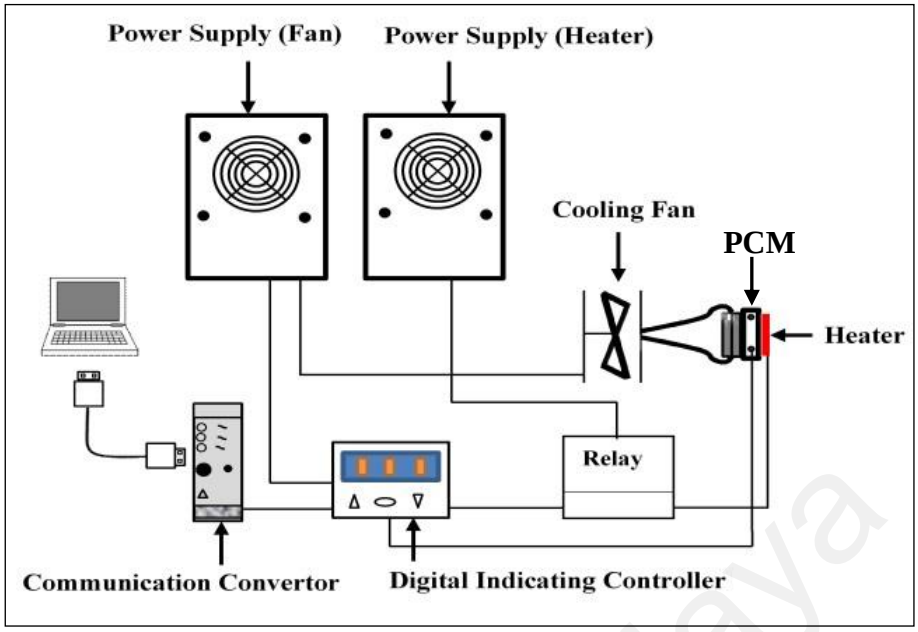

Figure 3.1 Schematic of thermal cycle tester

3.2.4 Experimental method

As mentioned in Section 3.2.1, the four organic PCMs with melting temperatures of between 50 and 70 °C were selected for the accelerated thermal cycle testing for 1500 melt/freeze cycles in this chapter. The minimum and maximum temperature of 30 °C and 100 °C were set in the thermal cycle tester. Since every selected PCM has a melting temperature somewhere between 50 and 70°C, this range of temperature is selected in order to ensure the complete melting and solidification of the PCMs. An amount of 6~9 mg of PCM is kept inside the DSC pan and it was hermetically sealed to avoid the contact of the PCM with the environment and to protect leakage. These DSC pans were placed in the tray of the DSC machine and it was run between the temperatures of 30 and 100 °C. At both extreme temperatures, the DSC was kept idle for 2 mins to remove the thermal history, if any. The thermophysical properties such as the melting

temperature and latent heat of fusion of paraffin, palmitic acid, myristic acid, and PEG 6000 were measured between the 0-1500 thermal test cycles (0^{th}, 100^{th}, 500^{th}, 1000^{th}, and 1500^{th}) and values of these thermophysical properties at zeroth cycle (fresh material) were considered as the reference values. The selection of the 1500 cycles have been made on the basis of their use as thermal energy storage materials for five consecutive years which is a significantly valid period for pay back.

3.3 Results and discussion

3.3.1 Thermophysical properties of O-PCMs before cycle test

The thermophysical properties such as melting temperature and the latent heat of fusion of fresh (uncycled) paraffin wax, palmitic acid, myristic acid, and PEG 6000 were measured using the DSC and obtained curves are shown in Figures 3.2 to Figure 3.5. As can be seen in the Figures, the paraffin wax possesses the minimum latent heat and that of palmitic acid is 59.7%, myristic acid is 66%, and PEG 6000 are 72.9% higher than that of paraffin wax.

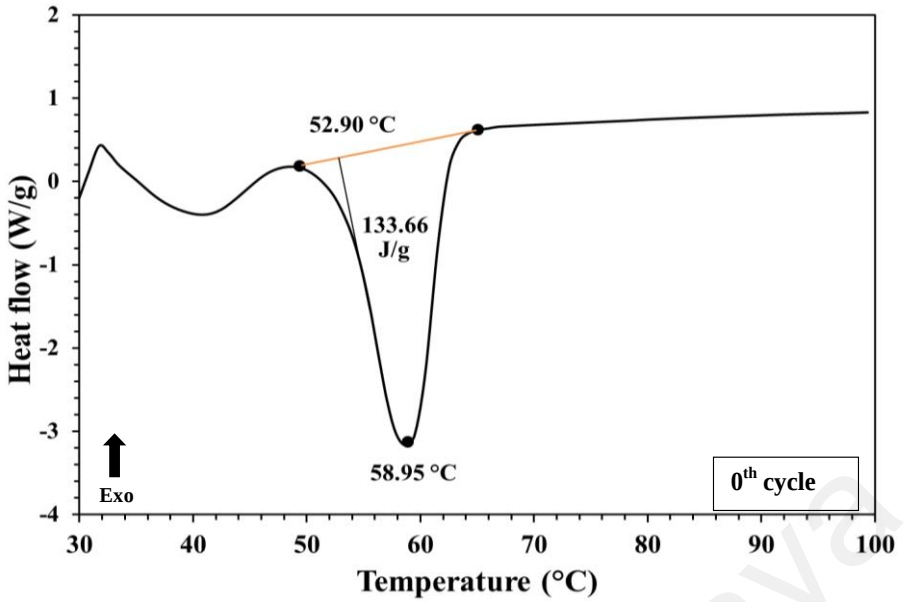

Figure 3.2 DSC curve of paraffin wax at 0th thermal cycle

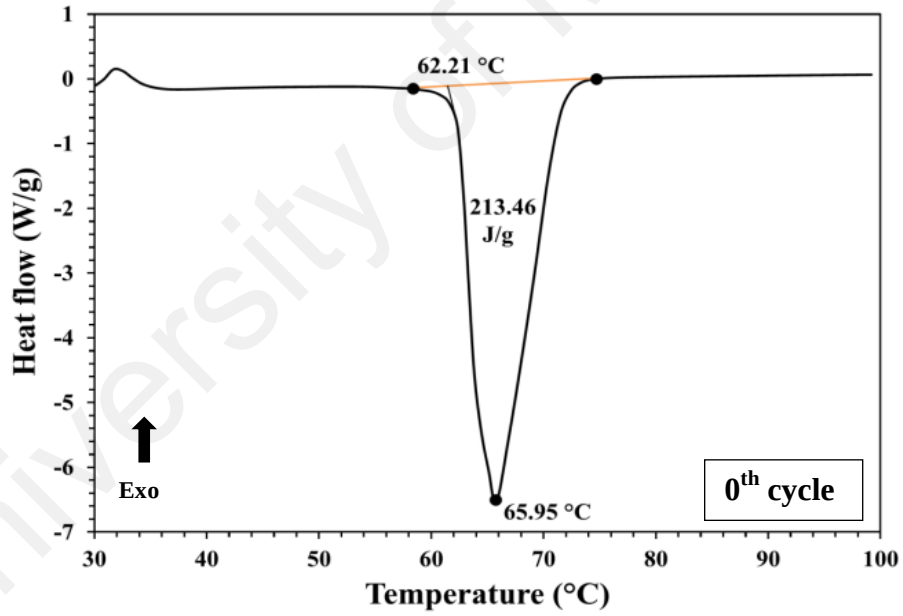

Figure 3.3 DSC curve of palmitic acid at 0th thermal cycle

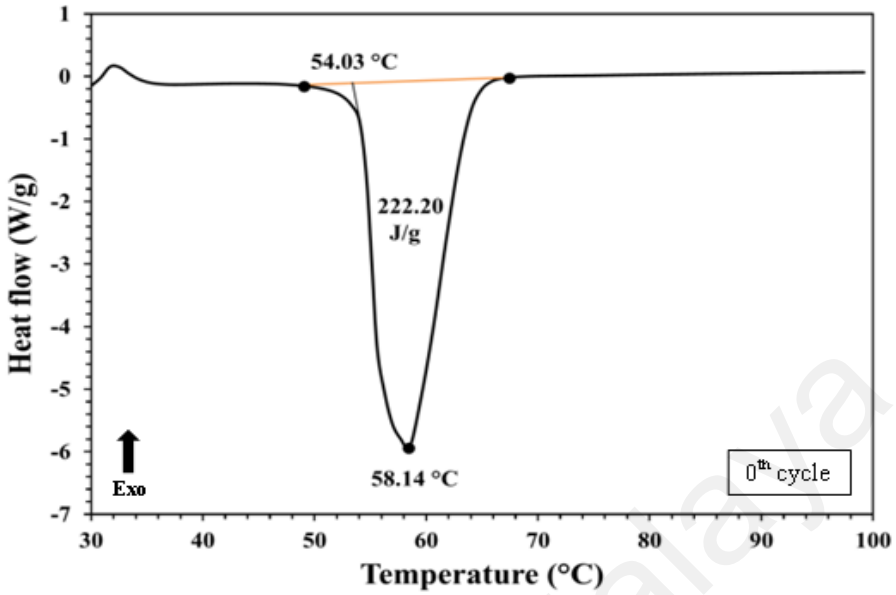

Figure 3.4 DSC curve of myristic acid at 0^{th} thermal cycle

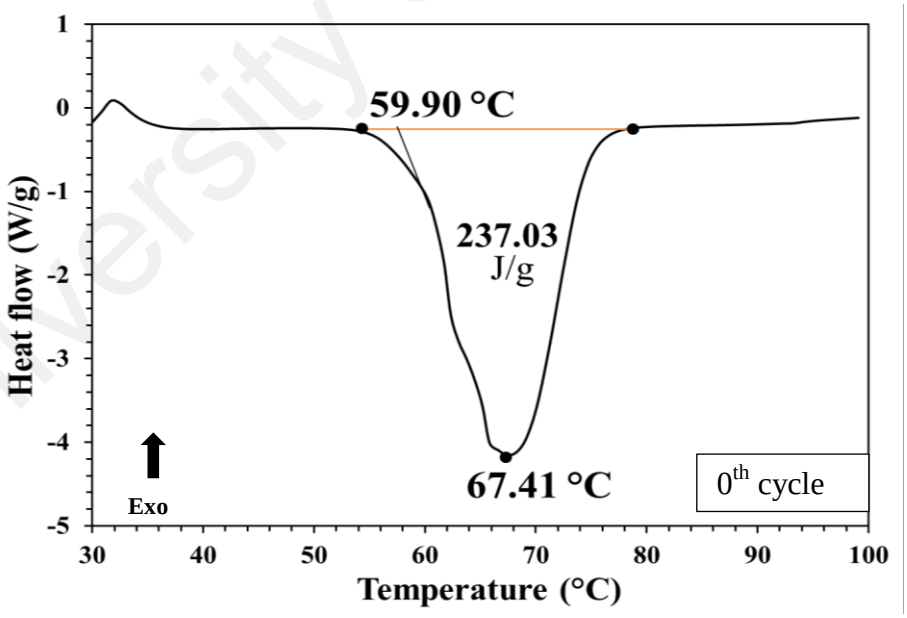

Figure 3.5 DSC curve of PEG 6000 at 0^{th} thermal cycle

The measured and obtained values of the melting temperatures of O-PCMs are compared and presented in Table 3.1. As seen in the Table the measured value of the melting temperature of paraffin wax, palmitic acid, and myristic acid do not fall in the range quoted by the companies, while, the melting temperature of the PEG 6000 falls within the quoted range. This Table signifies that the thermophysical properties of any PCM must be measured before implementing them into real usage due to the fact that their actual values may differ from the quoted ones. This measurement can provide a clear picture to practicing engineers for their usage in particular applications.

Table 3.1 Thermophysical properties of PCMs selected for accelerated thermal cycle test

PCM	**Chemical formula**	**Purity (%)**	**Melting temperature (°C)**		**Latent heat of fusion, ΔH(J/g)***
			Quoted	**Measured***	
Paraffin wax	-	-	56-58	52.90	133.66
Palmitic acid	$CH_3(CH_2)_{14}COOH$	≥ 98	60-62	62.21	213.46
Myristic acid	$CH_3(CH_2)_{12}COOH$	≥ 98	51-54	54.03	222.20
PEG 6000	$HO(C_2H_4O)_nH$	≥ 98	55-60	59.90	231.03

*Obtained from differential scanning calorimeter (DSC)

3.3.2 Thermophysical properties of O-PCMs after cycle test

The thermophysical properties (melting temperature and latent heat of fusion) of the O-PCMs were measured after the 100^{th}, 500^{th}, 1000^{th}, and 1500^{th} melt freeze cycles and the DSC curves were obtained. A detailed analysis of the individual PCMs are presented in the sections below.

3.3.2.1 Paraffin wax

A commercial grade paraffin wax of thermo physical properties as mentioned in Table 3.1 was selected for thermal cycle testing. A certain amount of paraffin was placed in a container and sealed with a lid to avoid leakage when the PCM is in a molten state. The experimental procedure is kept same as mentioned in Section 3.2.4. The DSC curves showing the heat flow variation with temperature are presented in Figures 3.6 to Figure 3.9 and the corresponding data are presented in Tables 3.2 and 3.3. As can be seen in these tables and Figures, no regular variations in the thermophysical properties of paraffin wax was observed during the accelerated thermal cycle test. From Figure 3.2 and 3.6-3.9, it can also be seen that the variations in the melting temperatures and latent heat of fusion with an increasing number of thermal cycles is notable.

The maximum observed variations in the melting temperature and the latent heat of fusion of paraffin wax were around 6% after 500 melt/freeze cycle and 14% after 1500 cycles respectively. Figure 3.10 shows the comparison of all the DSC curves taken after different tested thermal cycles by plotting all of them within the same graph. As can be seen, all of the curves show similar patterns during the melting process, but the onset and peak points can be clearly pointed. Also, it can be noted that after the 1500^{th} cycle, the melting temperature decreased by 2.57 °C and the latent heat of fusion decreased by 18.5 J/g. Also, it can be noted that if 300 melt/freeze cycles are considered in a year, then, this material can be used for 5 consecutive years which is a significant period for a PCM to be used as a latent heat thermal energy storage.

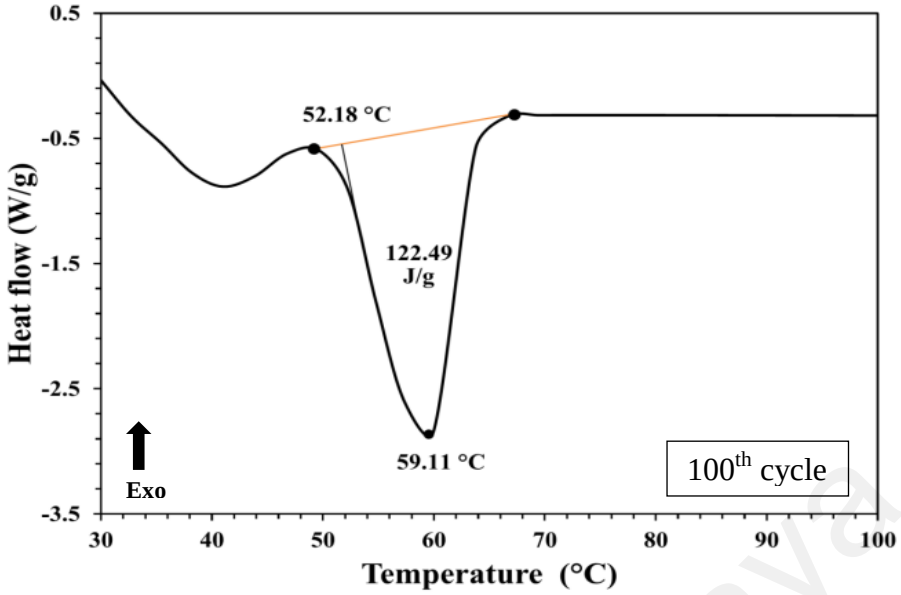

Figure 3.6 DSC curve of paraffin wax after 100th thermal cycle

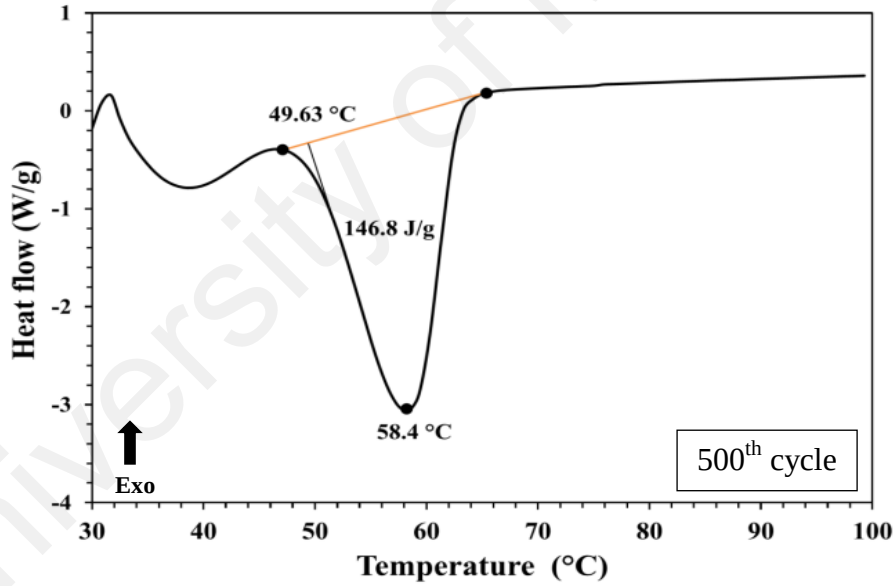

Figure 3.7 DSC curve of paraffin wax after 500th thermal cycle

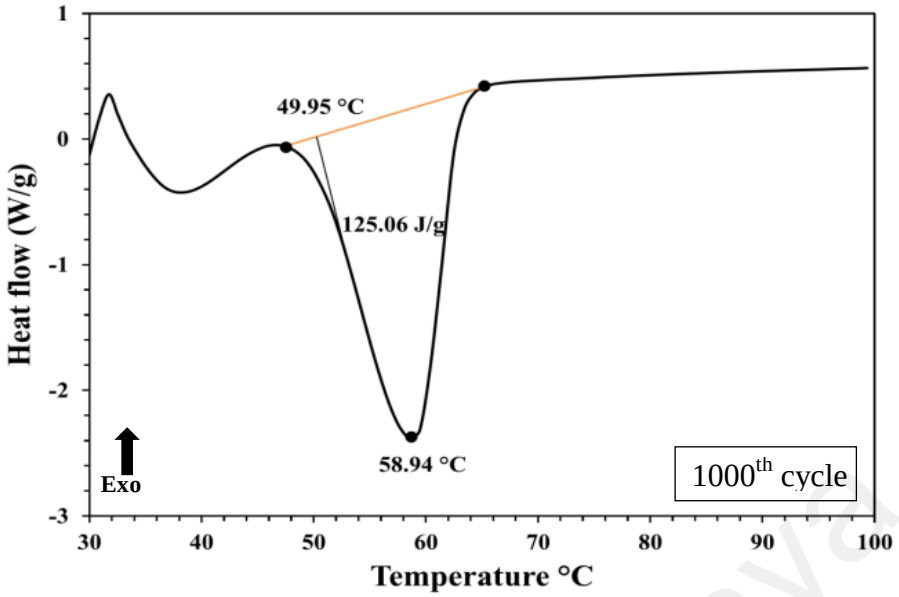

Figure 3.8 DSC curve of paraffin wax after 1000th thermal cycle

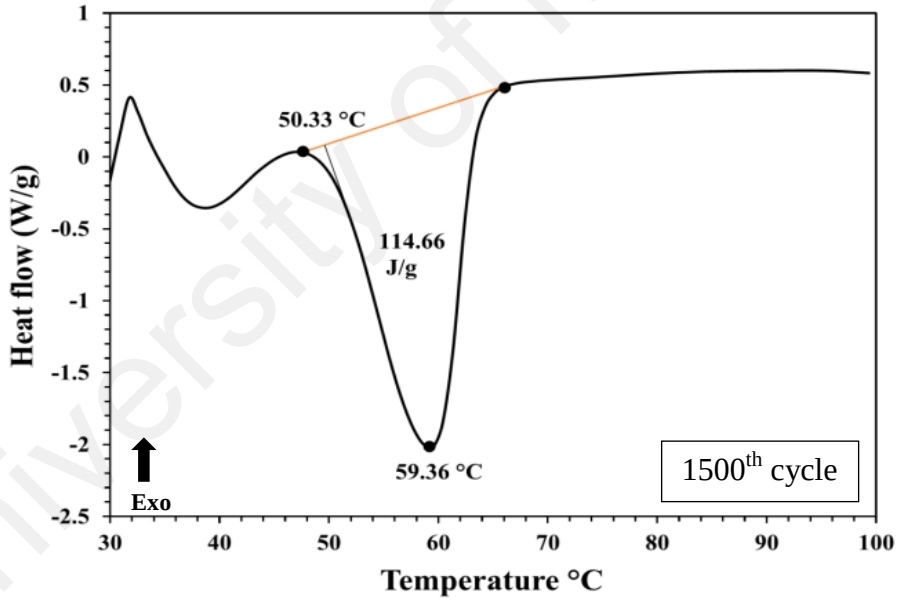

Figure 3.9 DSC curve of paraffin wax after 1500th thermal cycle

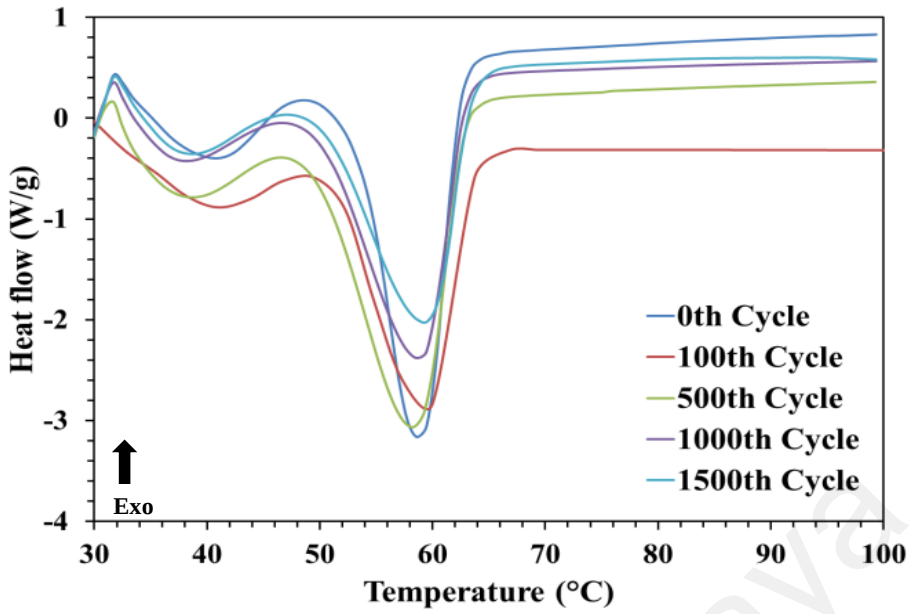

Figure 3.10 DSC curves of paraffin wax at different number of cycles during the thermal cycle test

3.3.2.2 Palmitic acid

For the cycle test of palmitic acid, a similar process as mentioned in Section 3.2.4 was followed. The thermal cycle test was conducted for 1500 thermal cycles and the DSC measurement was taken at the 0^{th} and after the 100^{th}, 500^{th}, 1000^{th}, and 1500^{th} cycles. The DSC curves obtained are shown in Figures 3.3 and 3.11-3.14 and their measured melting temperatures and latent heat of fusion are presented in Tables 3.2 and 3.3. As seen in the Figures and Tables, the melting temperatures of PA do not vary too much during the entire thermal cycle test. The onset value of the temperature shows a variation of between -0.29 °C (after 500^{th} cycles) to +1.76 °C (after 1500^{th} cycles). Similarly, the latent heat also shows an irregular variation with the increasing number of thermal cycles. This is noteworthy. The maximum variation of almost 18% has been observed after 1500 thermal cycles. Also, it can be inferred from the Figures and Tables that the PA is repeating its thermal properties after the 500^{th} thermal cycle by getting almost the same melting temperature and latent heat of fusion. Figure 3.15 shows all of

the DSC curves obtained in one graph and it can be seen that the DSC curves at the 0th cycle and after 500th cycles are almost similar, this signifies the thermal stability of the PCM.

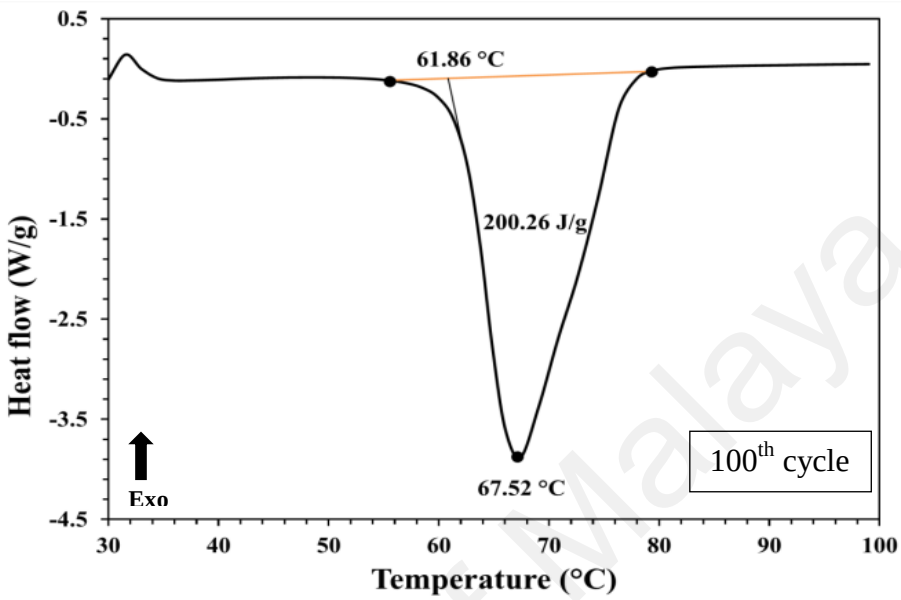

Figure 3.11 DSC curve of palmitic acid after 100th thermal cycle

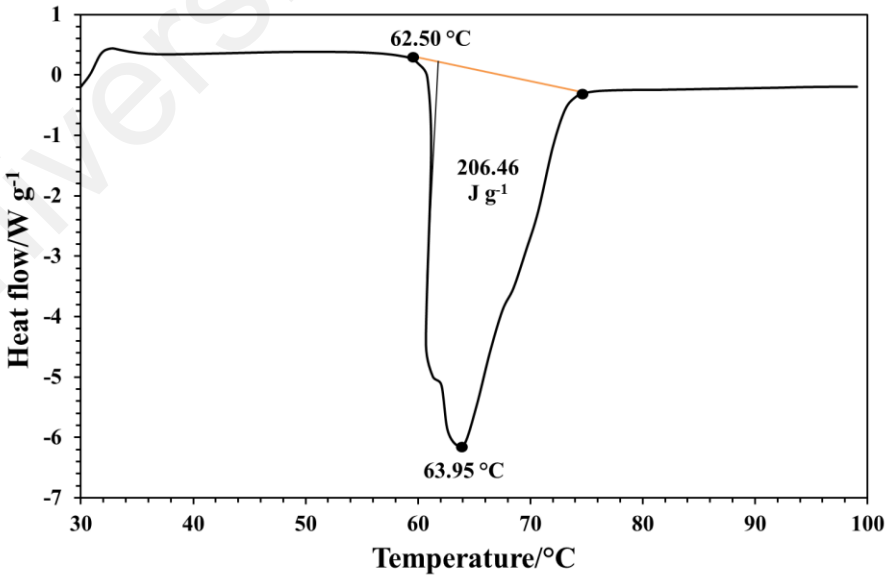

Figure 3.12 DSC curve of palmitic acid after 500th thermal cycle

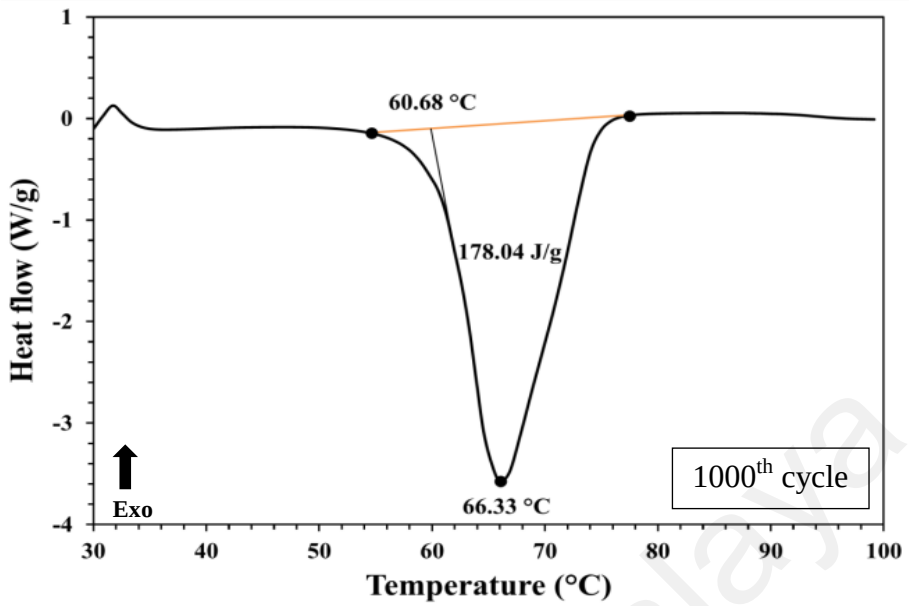

Figure 3.13 DSC curve of palmitic acid after 1000th thermal cycle

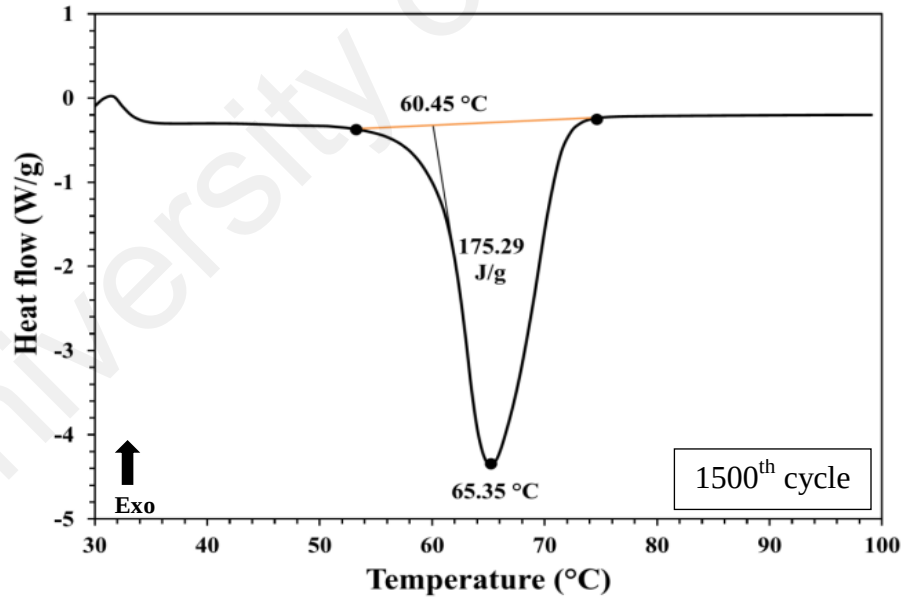

Figure 3.14 DSC curve of palmitic acid after 1500th thermal cycle

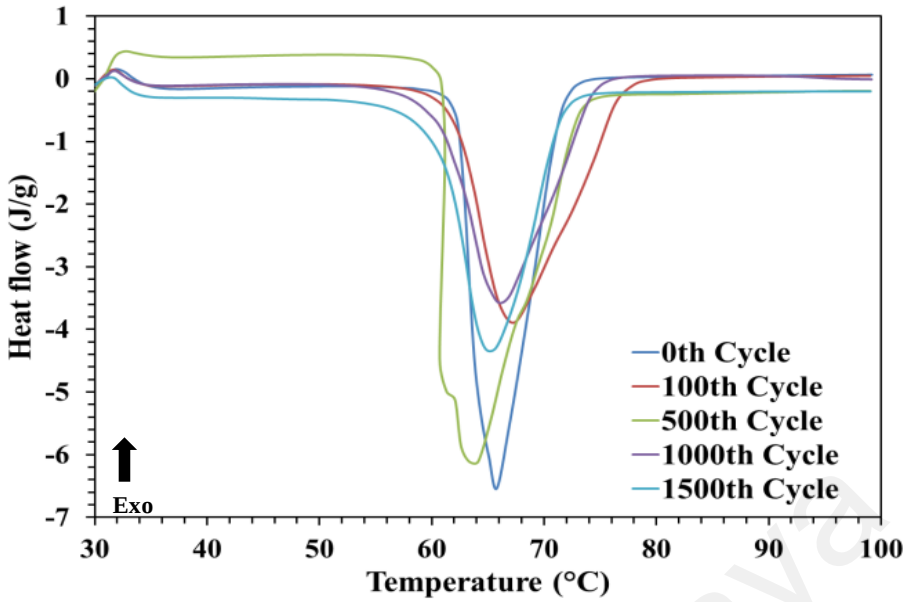

Figure 3.15 DSC curves of palmitic acid during thermal cycle test

3.3.2.3 Myristic acid

The thermal cycle test for myristic acid was also conducted in a fixed temperature range (30 to 100 °C) of the thermal tester as described in Section 3.2.4. The DSC measurements were taken at the 0^{th} cycle and after the 100^{th}, 500^{th}, 1000^{th}, and 1500^{th} thermal cycles and presented in Figure 3.4 and Figure 3.16-3.19 and presented in Table 3.2 and 3.3. After a short number of 100 thermal cycles, the change in the latent heat of fusion was decreased by 1.13 %, which became higher up to almost 10% after 500 thermal cycles. After 1000^{th} and 1500^{th} thermal cycle the changes in the latent heat of fusion were 0.9% and 0.6%, respectively. Similar irregular variations have been observed in the melting temperatures. A variation of -2.09 °C in the melting temperature was observed after 500 thermal cycles, while the variation of 1.25 °C and 1.07 °C was observed after 1000 and 1500 thermal cycles, respectively. A small peak at 62 °C also appears which can be attributes as the two phase transition. Based on the above

discussion, it can be stated that, overall not much variations have been noticed in the melting temperatures and latent heat of fusion of myristic acid for 1500 thermal cycles. A detailed comparison of all of the obtained DSC curves can be seen in Figure 3.20.

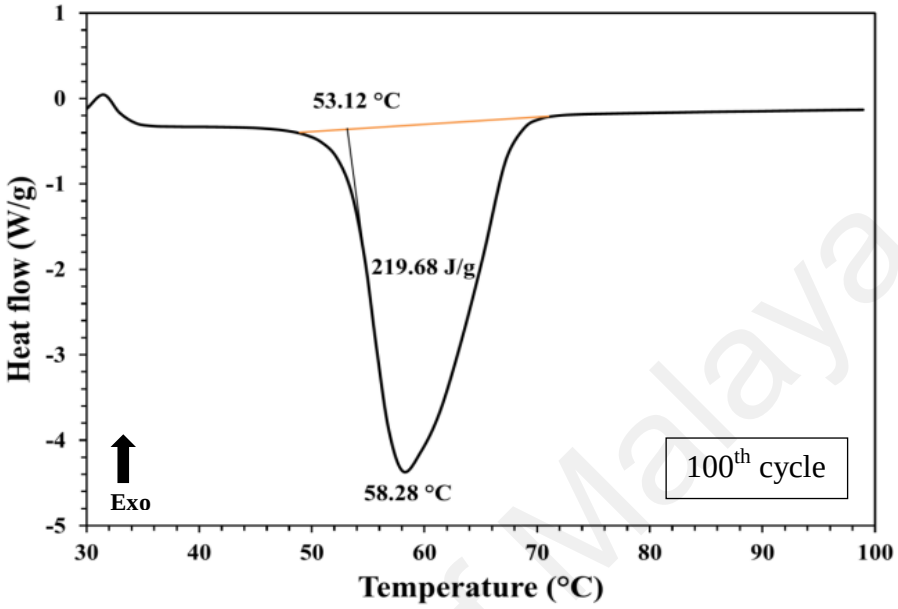

Figure 3.16 DSC curve of myristic acid after 100th thermal cycle

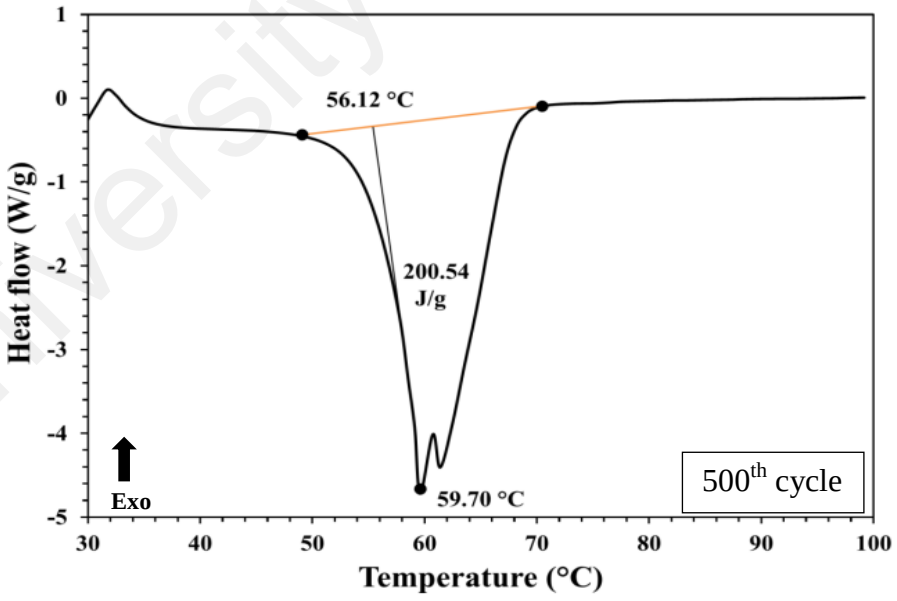

Figure 3.17 DSC curve of myristic acid after 500th thermal cycle

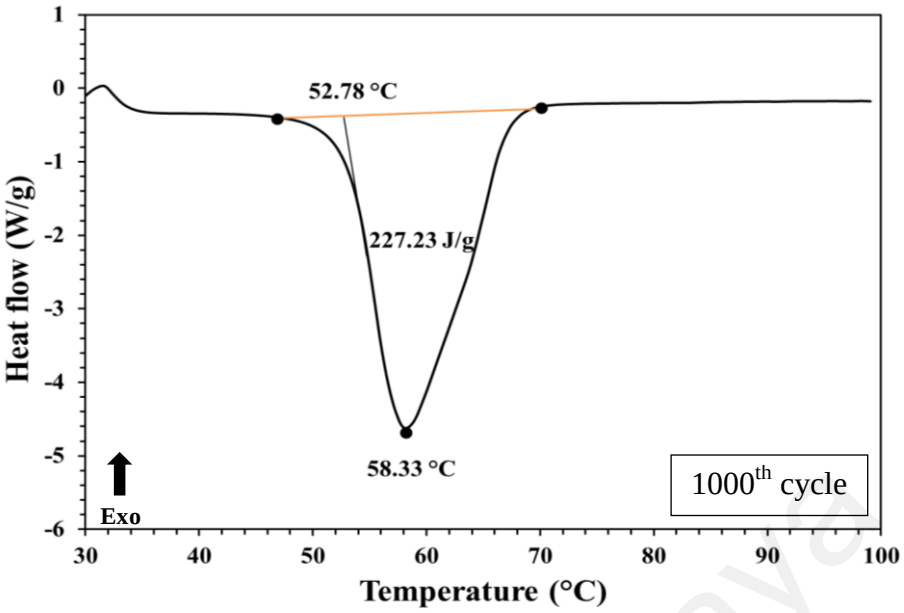

Figure 3.18 DSC curve of myristic acid after 1000th thermal cycle

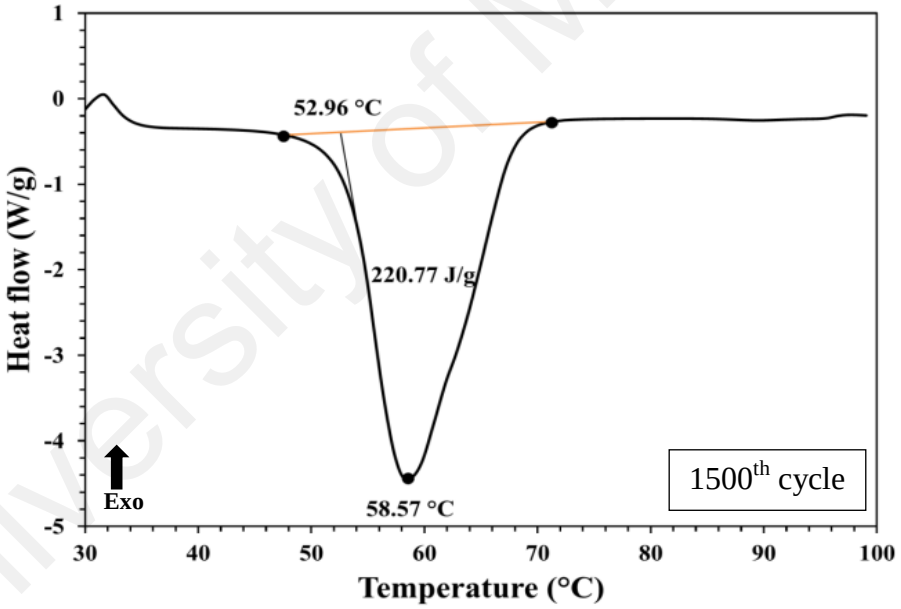

Figure 3.19 DSC curve of myristic acid after 1500th thermal cycle

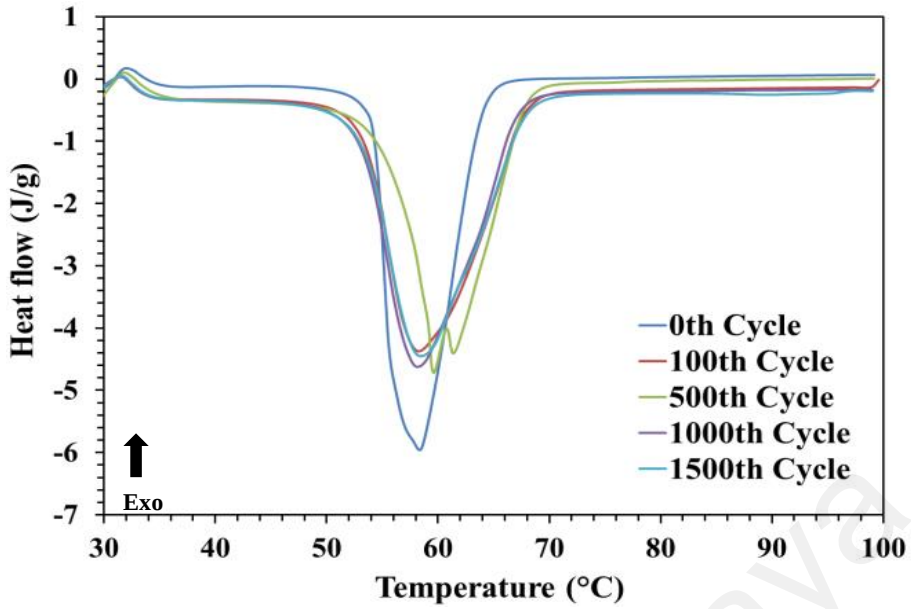

Figure 3.20 DSC curves of myristic acid during thermal cycle test

Paraffin and fatty acids, palmitic and myristic acids have shown reasonably good thermal stability. Some decrease in the melting temperatures and latent heat of fusion were observed after 500 thermal cycles but overall no major changes in these properties has been noticed. Similar irregular decrease in melting temperature and latent heat of fusion after 500 thermal cycles were observed for paraffin by Shukla et al. (2008) and for palmitic and myristic acid by Hasan and Sayigh (1994) and Sari (2003) with 95% purity. All of these three materials can be utilized as PCMs for latent heat thermal energy storage for approximately five years without experiencing much change in their thermophysical properties.

3.3.2.4 Polyethylene glycol 6000

For the accelerated thermal cycle tests, the lower and higher range of the temperatures in the thermal cycle tester of melting and freezing of the PEG 6000 was kept as 30 °C and 100 °C, respectively. The value of the latent heat of fusion and melting

temperatures of PEG were measured by the DSC at the heat flow rate of 10 °C/min at 0^{th}, and after the 100^{th}, 500^{th}, 1000^{th}, and 1500^{th} cycles. The values at the 0^{th} cycle were considered as reference values. The obtained value of the melting temperature of the fresh (uncycled) PEG 6000 from the DSC was 59.9 °C, which remained in the range of 55-60 °C, as quoted by Merck Company and the measured latent heat of fusion 231.03 J/g as shown in Figure 3.5. The variation in the heat flow against the temperatures as obtained from the DSC between the 0^{th} and 1500^{th} cycles and the curves are shown in Figure 3.21 to Figure 3.24.

A variation of +3.77 °C in the melting temperature of PEG 6000 was observed after the 100^{th} melt/freeze cycles, see Figure 3.21. Beyond the 100^{th} thermal cycles, not much variation in the melting temperature has been observed in the rest of the thermal cycle testing process. A maximum variation of +3.86 °C in the melting temperature after the 1000^{th} cycles (Figure 3.23) was observed when compared with that of the fresh material (zeroth cycle). It can be noted that for the first 500 melt-freeze cycles, the melting temperature decreases, but after 1000 cycles, an increase in this value was observed. A further enhancement in the value of the melting temperature was recorded after 1500 cycles, see Figure 3.24. This variation after the 100^{th}, 500^{th}, 1000^{th}, and 1500^{th} cycle is +3.77 °C, +3.94 °C, +3.86 °C, and +3.79 °C, respectively, compared with the 0^{th} cycle. Also, it can be noticed that all the variations in the melting temperature are within the standard temperature range quoted by Merck Company.

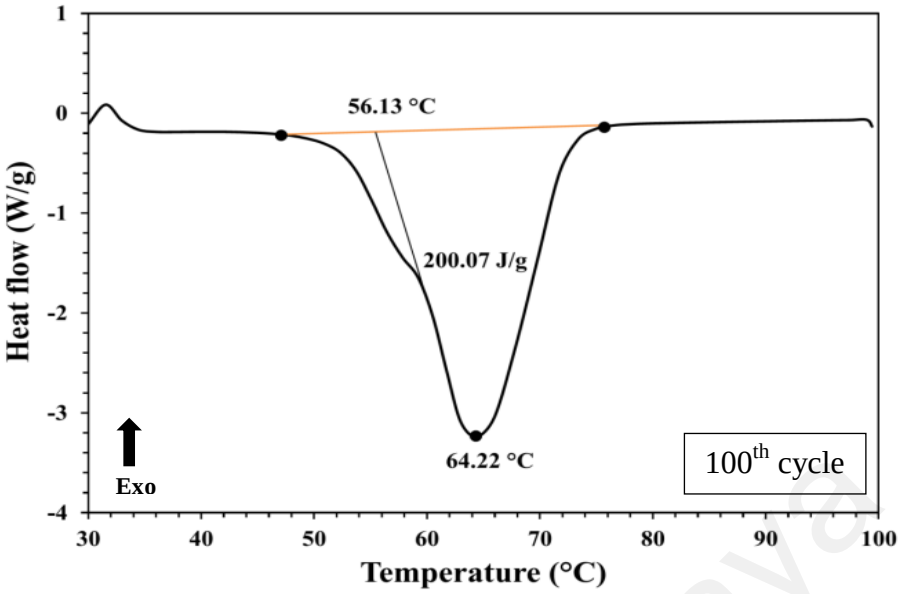

Figure 3.21 DSC curve of PEG 6000 after 100th thermal cycle

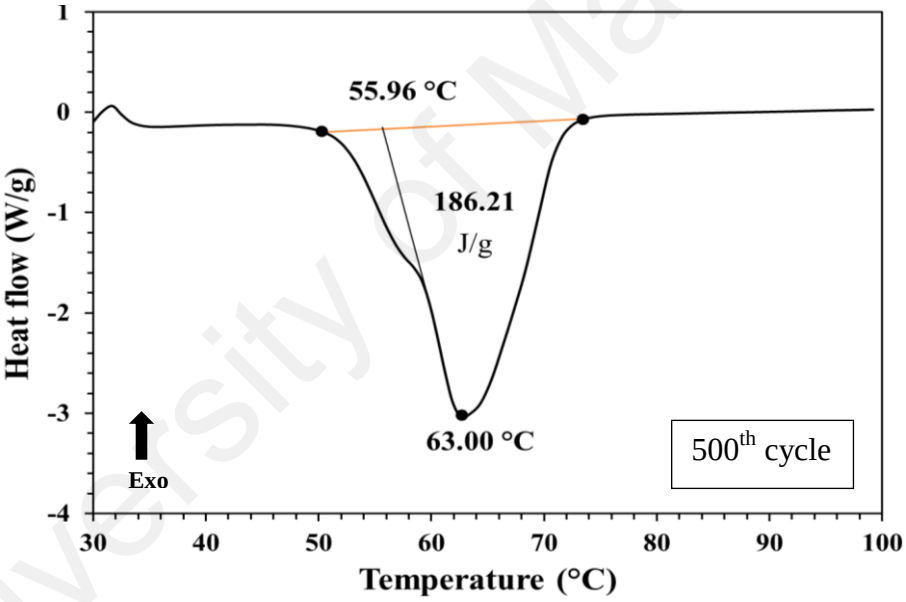

Figure 3.22 DSC curve of PEG 6000 after 500th thermal cycle

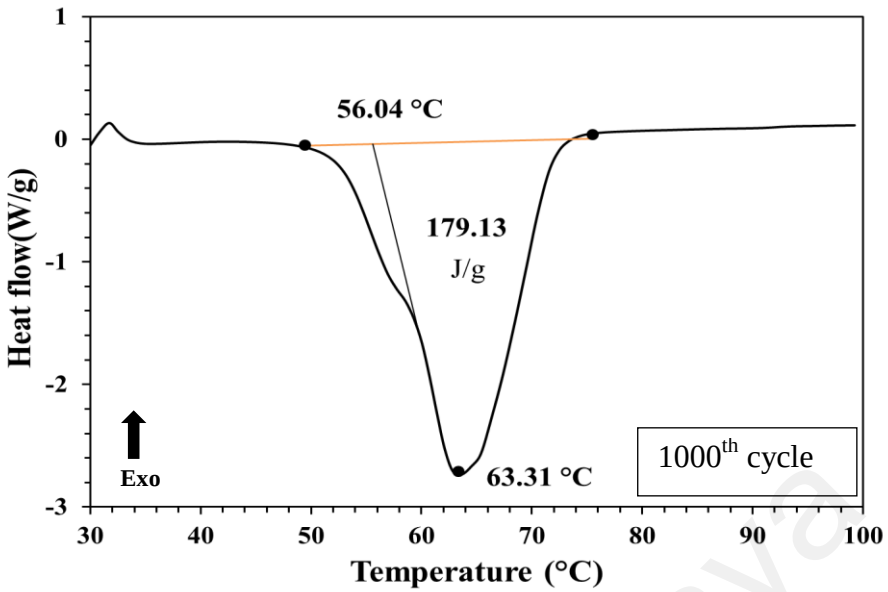

Figure 3.23 DSC curve of PEG 6000 after 1000th thermal cycle

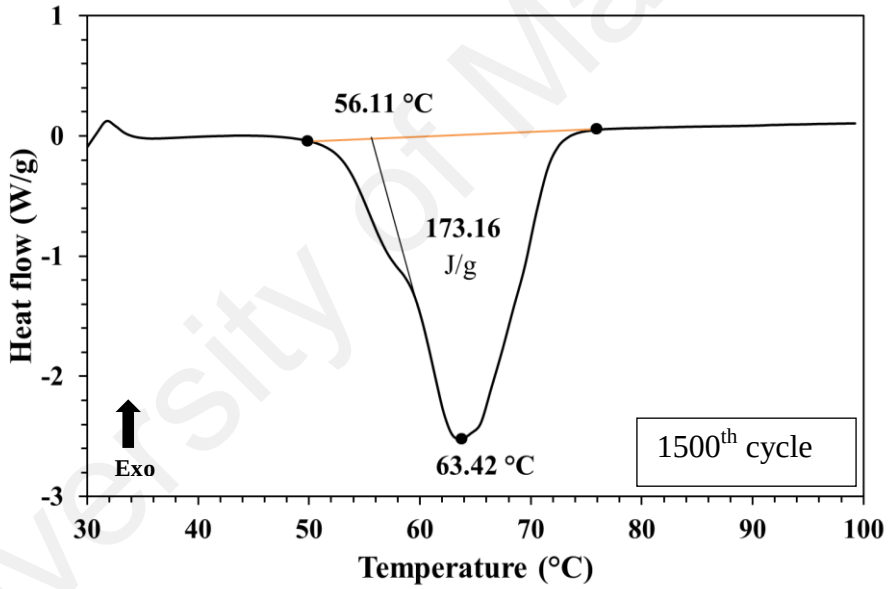

Figure 3.24 DSC curve of PEG 6000 after 1500th thermal cycle

On the contrary, a regular variation in the latent heat of fusion was observed between the 0th and 1500th cycle. A major reduction in the latent heat of fusion was observed after the first 100 melt-freeze cycles, which was approximately 13% in comparison to that of fresh PEG at 0th cycle. A further reduction of almost 19%, 22%,

and 25% in the latent heat of fusion with respect to the fresh PEG was observed after the 500th, 1000th, and 1500th cycles, respectively. It can be stated that in comparison to the first 100 thermal cycles, the measured drop in the latent heat of fusion in the next 400 cycles (between 100 and 500) was approximately 7% and, a drop of 4% was observed between the 500th and 1000th cycle. This reduction slightly dropped after the 1000th cycles and between the 1000th and 1500th cycles, a reduction of 3% in the latent heat of fusion was seen. For a clear comparison of all of the DSC curves during the entire thermal cycle test, Figure 3.25 can be referred where the overlapping of all obtained curves are presented.

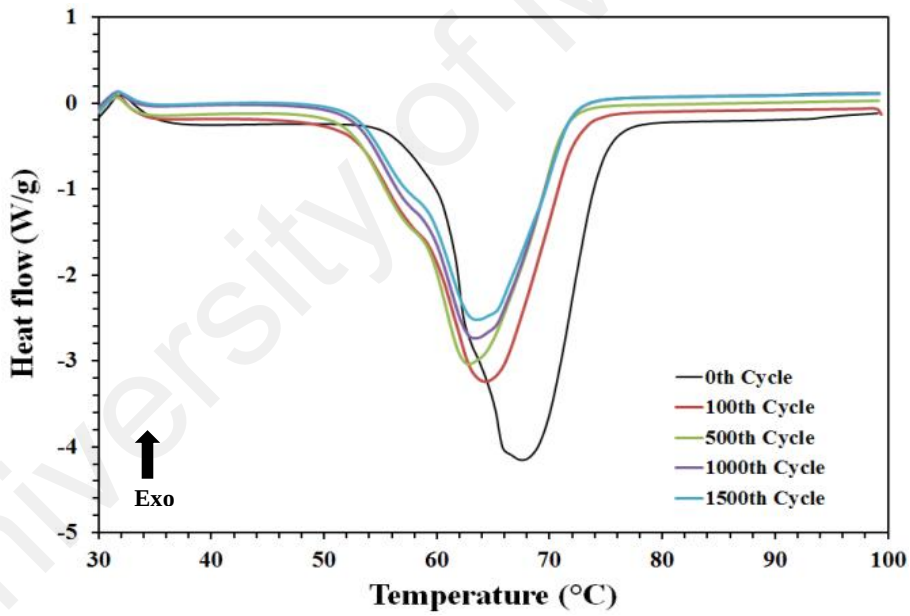

Figure 3.25 DSC curves of PEG 6000 during thermal cycle test

Table 3.2 Melting temperatures, T_m (°C) of the PCMs after repeated thermal cycles

No. of test cycles	PCM			
	Paraffin	**Palmitic acid**	**Myristic acid**	**PEG 6000**
0	52.90	62.21	54.03	59.90
100	52.18	61.86	53.12	56.13
500	49.63	62.50	56.12	55.96
1000	49.95	60.68	52.78	56.04
1500	50.33	60.45	52.96	56.11

Table 3.3 Latent heat of fusion, ΔH_f (J/g) of the PCMs after repeated thermal cycles

No. of test cycles	PCM			
	Paraffin	**Palmitic acid**	**Myristic acid**	**PEG 6000**
0	133.66	213.46	222.20	231.03
100	122.49	200.26	219.68	200.07
500	146.80	206.46	200.54	186.21
1000	125.06	178.04	220.23	179.13
1500	114.66	175.29	220.77	173.16

3.3.3 Chemical functional group analysis of O-PCMs

Tables 3.2 and 3.3 of Section 3.3.2 show the variations in the thermophysical properties of selected O-PCMs and the variations in the thermal properties can be clearly seen. There are two probable reasons for this variation; one is the impurities present in the PCM and another is due to the changes in the chemical structure of the material during

the cycle tests. To observe the changes in the compositional/functional group of the PCMs, the FT-IR spectroscopy was employed and the spectrum was taken of a fresh (uncycled) PCM and after 1500 thermal cycles for the wavenumbers between 4000 cm^{-1} and 400 cm^{-1}. This is presented in Figures 3.26 to Figure 3.29.

Figure 3.26 shows the FT-IR spectra of paraffin before and after the cycle tests. The peaks correspond to wavenumber 2918.18 and 2848.98 cm^{-1} are corresponding to the symmetrical stretching vibration of $–CH_3$ and $–CH_2$ groups in paraffin, which remains at the same position even after 1500 melt/freeze cycles. The C=O stretching vibration corresponds to wavenumber 1646 cm^{-1} of paraffin before and after the thermal cycle test show the same peak. The peak corresponds to wavenumber 1466 cm^{-1} signifies the deformation vibration of $–CH_3$ and $–CH_2$ group in paraffin. At wavenumber 1300 cm^{-1}, the in-plane bending vibration of the –OH group and at 943 cm^{-1}, to the out-plane bending vibration of the –OH group of paraffin has appeared. The symmetric peaks at 724 and 671 cm^{-1} correspond to the swinging vibration of the –OH functional group of paraffin before and after the thermal cycle test. A new peak at wavenumber 1103 cm^{-1} which appears in FT-IR spectra of paraffin after the thermal cycle test can be clearly seen. This new peak might be because of the impurities present in the PCM. The rest of the peaks fit into each other. This infers that the paraffin does not undergo any significant compositional/functional group changes during the cycle test and possesses a good thermal and chemical reliability for 1500 thermal cycles.

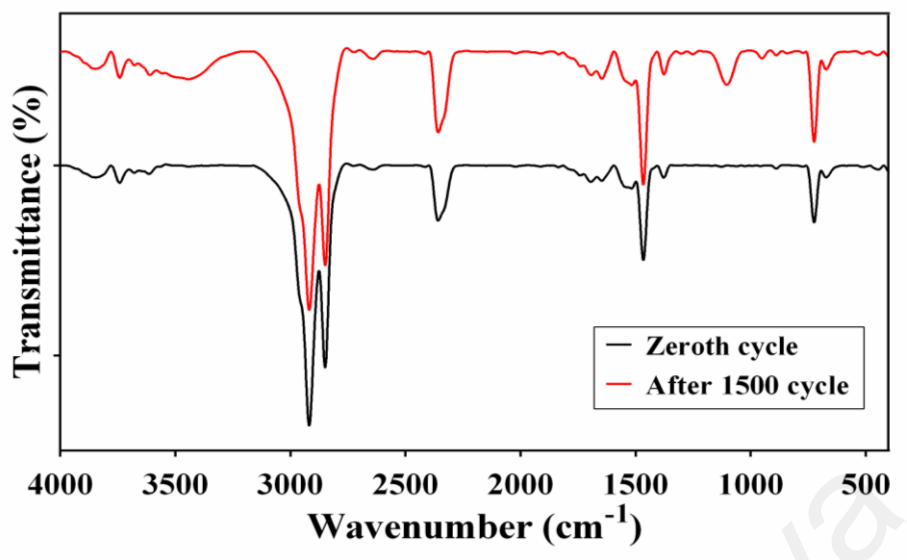

Figure 3.26 FT-IR spectra of uncycled (fresh) and cycled (1500 cycles) paraffin

The FT-IR spectra of palmitic acid before and after the cycle test are shown in Figure 3.27. The peaks at 2918.24 and 2850.20 represent the symmetrical stretching vibration of the $–CH_3$ and $–CH_2$ groups in PA, which take new positions after 1500 melt/freeze cycles at 2918.07 and at 2850.25, respectively. C=O stretching vibration is assigned by a peak seen at 1700 cm^{-1} which is the same, before and after the thermal cycle test. The peak at 1465 cm^{-1} signifies the deformation vibration of the $–CH_3$ and $–CH_2$ groups in the PA. The peak at 1300 cm^{-1} is corresponding to the in-plane bending vibration of the –OH group and the peak at 943 cm^{-1} is corresponding to the out-plane bending vibration of the –OH group of PA. The symmetric peaks at 722 and 678 cm^{-1} correspond to the swinging vibration of the –OH functional group of the PA before the thermal cycles and at 722 and 680 cm^{-1} after the thermal cycle test. A new peak at wavenumber 3500 cm^{-1} can be spotted after the thermal cycle test which might be due to the humidity absorption of PA from environment. Overall, palmitic acid has shown a good thermal and chemical reliability during the cycle test.

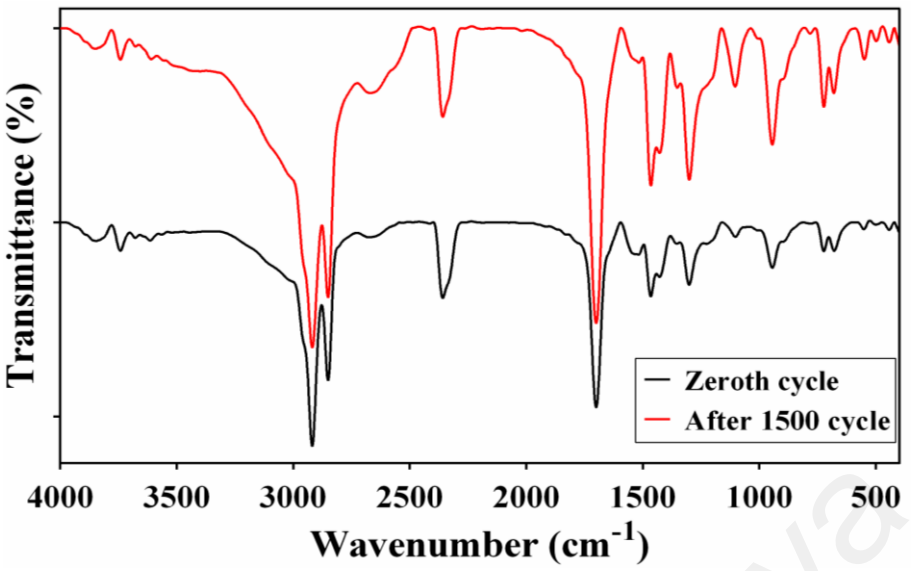

Figure 3.27 FTIR spectra of uncycled (fresh) and cycled (1500 cycles) palmitic acid

FT-IR spectrum of the fresh MA and after 1500 cycles wavenumbers between 4000 cm^{-1} and 400 cm^{-1} are shown in Figure 3.28. It can be seen in this Figure, that no new peak appears and no existing peak disappears in the PCM after 1500 cycles. So, the sole reason for this slight variation in the properties is the impurities present in the PCMs, which might be absorption of vaopurs from surrounding environment.

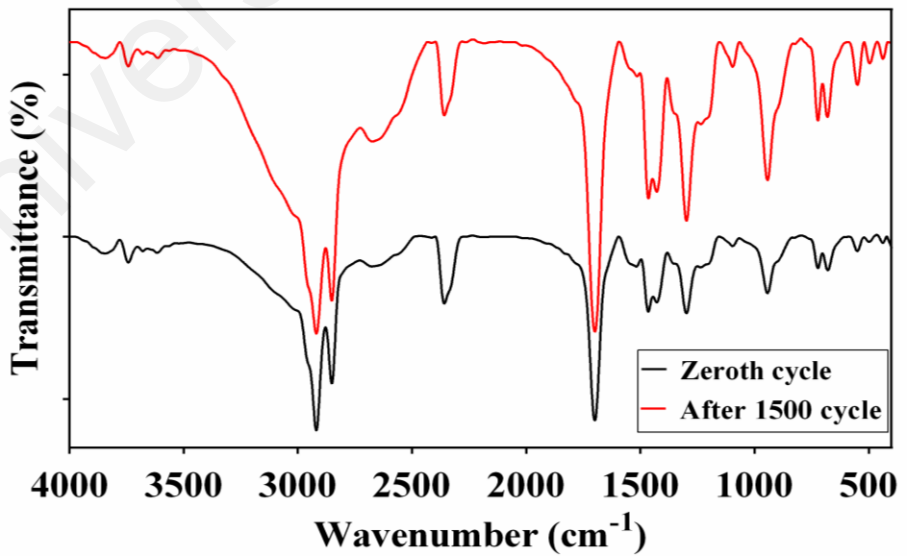

Figure 3.28 FTIT spectra of uncycled (fresh)and cycled (1500 cycles) myristic acid

Figure 3.29 shows the FT-IR spectrum of the uncycled (fresh) and cycled (1500 cycle) PEG 6000. As can be seen in the Figure, both curves are depicting a similar behavior at a particular frequency band and no peak shift is visible. It can be mentioned here that the PCM during the cycling process does not undergo any compositional/functional group changes. Therefore, it can be assumed that the variation in the thermal properties of the PCM with an increasing number of melting/freezing cycles may be due to the presence of impurities in the material.

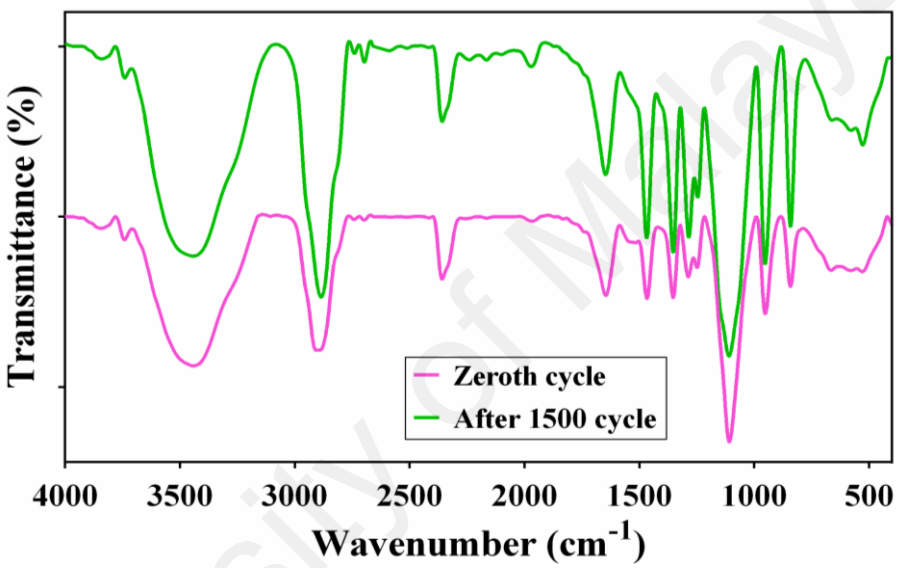

Figure 3.29 FT-IR spectra of PEG 6000 before and after thermal cycle test

3.4 Techno-economic analysis of O-PCMs

The techno-economic analysis of the PEG 6000 with the other five PCMs is discussed in this section. As per the available research papers, the thermal cycle test of different PCMs in the temperature range of 52-65 ˚C are given in Table 3.4. The comparison of the thermal properties and latent heat at the initial and after cycle test of previously tested PCMs in the temperature range of 52-65 °C are given in Table 3.4. Sharma et al. (2002) performed the cycle testing of stearic acid (M.P. - 63.0 ˚C), and paraffin wax (a) (M.P. - 53.0 ˚C) for 1500 thermal cycles. Shukla et al. (2008) conducted the accelerated

thermal cycles testing for paraffin wax (b) (M.P. 60-62 ˚C) and Sari (2003) considered palmitic acid (M.P. - 61.31˚C) and myristic acid (M.P. - 52.99 ˚C) for 1200 thermal cycle test. For a comparison of these PCMs for an economic analysis purpose, a temperature range of 52-65˚C has been considered and paraffin wax (a and b), stearic acid, myristic, and palmitic acid has been chosen for comparison with the PEG 6000 in the present study. As can be seen in the Table 3.4 and Ref (Sharma et al., 2002), the latent heat of fusion of fresh (uncycled) paraffin wax (a) is 184.0 J/g which was reduced to 136.0 J/g (by 26%) after the 1500 thermal cycles. Stearic acid (155.0 J/g) was also tested in the same study and showed a 21% reduction (155 to 123.0 J/g) in the latent heat of fusion after the 1500 thermal cycle test. Shukla et al. (2008) also tested the paraffin wax (b) of a melting temperature 60-62 ˚C for 600 melt/freeze cycles and reported a 16.15% reduction in the latent heat of fusion and -1.7% in melting temperature. It is important to mention here that paraffin (b) had lost 16.15 % of latent heat in just 600 thermal cycles and this loss in latent heat is expected to increase should it be selected for the 1500 thermal cycles. Another study for the cycle test of myristic and palmitic acid was carried out by Sari (2003). The results of this study showed a 11.3% reduction % in the latent heat of myristic acid and 13% in the case of palmitic acid after 1200 melt/freeze cycles. It is noteworthy here that the PCMs have been tested only for the 1200 thermal cycles by Sari (2003). So a further reduction in the latent heat of these PCMs is expected if these PCMs are tested for more number of thermal cycles. A variation of +3 °C in the melting temperature of paraffin and -1°C that of stearic acid during the cycle test have been reported in the Ref. (Sharma et al., 2002). A variation of +6.78 °C in the melting temperature of the myristic acid and 9.5% in the case of palmitic acid have been reported in the Ref. (Sarı, 2003).

In the present work, the PEG 6000 has been tested for 1500 melt/freeze cycles and a reduction of 25% in the latent heat of fusion and 3.79 °C in melting temperature have been observed. It can also be seen that the reduction in latent heat and melting temperature of PEG 6000 are lesser than in comparison to the other quoted PCMs in the Table 3.4. It is interesting to note that the latent heat of the PEG 6000 is 231.03 J/g which is 25%, 49%, 77.7%, 30.8%, and 16.7% higher than that of paraffin wax (a), stearic acid, paraffin wax (b), myristic acid, and palmitic acids, respectively. After the repeated 1500 melt/freeze cycles, the PEG 6000 has 173.16 J/g latent heat which is also higher than that of paraffin (a and b), stearic acid and close to that of myristic acid after the completion of the total cycle test by the other researchers. It can also be seen that the variation in the thermal properties of PEG-6000 remains within that of the variations of the PCMs tested by past researchers. The latent heat of PEG 6000 after 1500 thermal cycles is almost equal to that of the uncycled paraffin wax (a), palmitic acid and myristic acid and much higher than of stearic acid (almost 10%) and paraffin wax (b) (33%).

The variations in the latent heat of previously tested PCMs have shown an irregularity, while, in the case of PEG 6000, the variation in the latent heat has been a consistent value which makes it an attractive phase change material for thermal energy storage applications in the temperature range of 52-65 ˚C. The cost analysis is also given in Table 3.4 for the PCMs tested in the past studies and the PEG 6000. The cost of PEG 6000 was taken as an average from the bulk price quoted by various international chemical suppliers. The comparison shows that the cost of all PCMs is in the similar range so the suitability of the PCMs for different thermal energy storage

applications in this temperature range can be decided on the basis of their energy storage capacity and long term stability.

The results of this study can be very much helpful for predicting the life of thermal energy storage materials for their particular applications. Also, if it is assumed that a PCM undergoes approximately 300 melt/freeze cycles in a year excluding the cloudy and rainy days, these tested O-PCMs can be effectively used as thermal energy storage for five consecutive years. Also, it is recommended that all commercial grade PCMs should undergo an accelerated thermal cycle test before their use for thermal energy storage. It is because their thermophysical properties may vary from what is quoted by the companies when tested. These materials can be efficiently used as solar energy storage for low and medium temperature application such as solar water heaters and dryers.

Table 3.4: Comparative life cycle and techno-economic analysis of O-PCMs

PCM	**No. of Cycles**	**Latent heat (J/g)**		**Melting point (˚C)**		**Cost (USD/ kg)**	**Ref.**
		Initial*	**Final#**	**Initial***	**Final#**		
Paraffin wax (a)	1500	184	136	53.0	50.0	2.0	(Sharma et al., 2002)
Stearic acid	1500	155	123	63.0	64.0	1.6	(Sharma et al., 2002)
Paraffin wax (b)	600	130	109	58	59	1.5	(Shukla et al., 2008)
Myristic acid	1200	176.6	156.6	52.99	46.21	1.5	(Sarı, 2003)
Palmitic acid	1200	197.9	172.4	61.31	55.47	1.8	(Sarı, 2003)
Myristic acid	1500	222.20	220.77	54.03	52.96	1.5	Present work
Palmitic acid	1500	213.46	175.29	62.21	60.45	1.6	Present work
PEG 6000	1500	231.03	173.16	59.9	56.11	1.6	Present work

3.5 Summary

In this chapter, the variations in the thermophysical and chemical properties of the paraffin, palmitic acid, myristic acid, and PEG 6000 were investigated during accelerated thermal cycle test. Assuming that the minimum lifespan of the thermal energy storage is 5 years, repetitive 1500 thermal cycles were performed and the properties of the PCMs were measured at the 0^{th} cycle and after the 100^{th}, 500^{th}, 1000^{th}, and 1500^{th} thermal cycles using a differential scanning calorimeter. The following conclusions can be drawn from this study:

- The melting temperatures of paraffin, palmitic acid and myristic acid are found to be varied in the range of +0.72 to +3.27 ˚C, -0.29 to +1.76 ˚C, and -2 to +1.2 ˚C respectively, which is not a very significant variation and these PCMs are stable enough to be used as thermal energy storage materials.
- The latent heat of fusion of paraffin, palmitic acid and myristic acid are found to vary in the range of -9.8 to 14%, 3.28 to 18%, and 0.9 to 10% when compared with that of the pure PCM. Paraffin and palmitic acid show a slightly larger variation as compared to myristic acid which signifies that myristic acid is more stable.
- The variation in the melting temperature of PEG 6000 is found to be in the range of 3.77 to 3.86 ˚C and the variation in the latent heat of fusion of the material is between 13.4% and 25%. This variation is a bit higher than that of other PCMs, but is a potential PCM for solar thermal energy storage.
- FT-IR spectrum of paraffin and palmitic acid show new peaks at wavenumber 1103 cm^{-1} and 3500 cm^{-1}, which can be inferred as one of the reasons behind variation in the thermal properties of the materials.

- There are no peak shifts in the FT-IR spectra for myristic acid and PEG 6000 after 1500 repeated thermal cycles. This signifies their chemical stability. The thermal variation is purely due to impurities present in the materials.
- All selected O-PCMs have shown significant thermal and chemical stability with a mild variation in their melting temperature and the latent heat of fusion during repeated 1500 melt/freeze cycles.
- Accelerated thermal cycle test for potential phase change materials is strongly recommended to ensure their long term suitability for thermal energy storage.

CHAPTER 4: ENHANCEMENT IN HEAT TRANSFER OF ORGANIC PCM

4.1 Introduction

Previous studies and present accelerated thermal cycle tests (Chapter 3) have shown that the organic PCMs possess an extremely low thermal conductivity and this drawback limits their use in many domestic and industrial energy storage applications. A significant improvement can be achieved by simply dispersing the solid metal particles in micro or nano size in the organic PCMs. Adding the micro size particles, enhances the chances of sedimentation during the flow of the PCM while nano size particles do not exhibit such properties (Das et al., 2008). Also, due to the larger surface to volume ratio, the dispersion of nano particles of solid metal or metal oxide enhances the thermal conductivity and increases the heat transfer rate of the base PCM (Khodadadi & Hosseinizadeh, 2007; Sharma et al., 2014). A large variety of nanomaterials with unique thermophysical properties have been used in the past to enhance the thermal performance of the base PCM (Arico et al., 2005; Kannan et al., 2005). Section 2.3 shows that several studies have been conducted to enhance the thermal conductivity of organic PCMs in the past using nanoparticles of solid metal and metal oxides, however, there is still a need for more research to explore the effects of the various nanoparticles on the thermophysical properties of various PCMs. The reviewed literature shows that although the nano TiO_2 has been used to enhance the thermal properties of the aqueous solution, these nanoparticles have not been explored much with the organic PCMs.

In this chapter, the phase change behavior of the prepared novel composites of palmitic acid and solid nano-particles of titanium dioxide (TiO_2) for thermal energy storage will be investigated. The nano particles of TiO_2 are dispersed in the base PCM

(PA in the present study), in different weight fractions (0.5, 1.0, 3.0 and 5%) and their effect on the thermophysical properties of PA will be investigated.

4.2 Methodology

4.2.1 Materials

Palmitic acid with a melting temperature range of 60-62 °C, molecular weight of 256.43 g/mole, and purity of ≥ 98% was purchased from the R&M Chemical, UK. Nano-particles of titanium dioxide (TiO_2) anatase form of 21nm, and surfactant Sodium dodecyl benzene sulfonate (SDBS) were provided by Sigma–Aldrich, Germany. All the procured chemicals in the experiments were used without any further purification.

4.2.2 Preparation of composite materials

A well-established two-step method as shown in Figure 4.1 was adopted for the preparation of composite PCMs of palmitic acid and different weight fractions of TiO_2 nano-particles. Palmitic acid was considered as the base PCM and 0.5, 1.0, 3.0, and 5.0 wt% TiO_2 nano-particles as the supporting materials for thermal conductivity enhancement; and the prepared nano-enhanced organic phase change materials (NEOPCMs) were named as NEOPCM1, NEOPCM2, NEOPCM3, and NEOPCM4. While preparing the nanofluid, certain factors were kept in mind, i.e. uniform and stable dispersions, low agglomeration and no chemical reactions between the nano-materials and the base material. SDBS in the ratio of 1:1 wt% of TiO_2 was used as the capping agent (surfactant) for the uniform dispersions of nano-particles in palmitic acid. Uniform and stable dispersions of nano-particles help in faster melting/freezing rate of the PCM due to a higher thermal conductivity. In addition, for improving the nano-particle dispersions and minimizing the aggregation, the liquid NEOPCMs were

subjected to intensive ultrasonication using an ultrasonic vibrator (VCX 500, SONICS made) at a frequency of 40 kHz (Chandrasekar et al., 2010; Shao et al., 2016). Vibrational energy created at this frequency helps to disperse the nano-particles uniformly into the base liquid PCM. The residing time for 0.5, 1.0, 3.0, and 5.0 wt% nanofluids were set as 30, 35, 45, 60 minutes, respectively. A higher residing time may induce the defect in the nanofluid (Fan et al., 2015). During the entire sonication process, it was ensured that the temperature of the sonicator remains significantly above the melting temperature of palmitic acid to confirm its liquid state during the process.

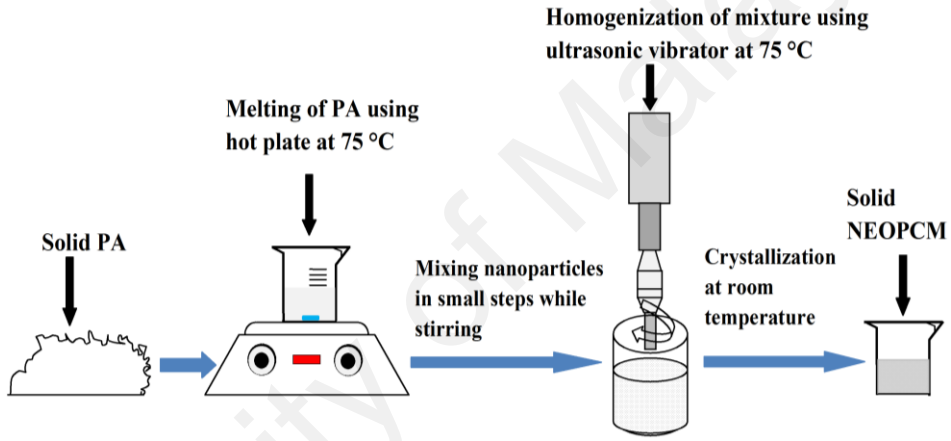

Figure 4.1 Preparation steps of PA/TiO_2 composites

4.2.3 Instruments

4.2.3.1 For preparation of composite PCMs

The adopted instruments for preparation of composite PCMs were:

- A hot plate with stirring facility C-MAG HS7 230V IKA 3581200 make having ceramic top that is kept in the Advanced Materials Laboratory, Department of Mechanical Engineering, University of Malaya.
- Ultrasonic probe sonicator SONICS 500 Watt, VCX 500 installed at the Department of Chemical Engineering, University of Malaya.

4.2.3.2 Chemical analysis of NEOPCMs

To ensure the uniform dispersion and to visualize the surface morphology of the composite PCM, a field emission scanning electron microscope (FESEM- CARL ZEISS- AURIGA 60) was used. In order to determine the changes in the compositional/functional groups during the cycle test, the Fourier Transform Infrared (FT-IR) spectroscope (Brand: Bruker, Model: IFS66v/S) was used between the wavenumbers of 4000 to 400 cm^{-1} with the spectral resolution of 2 cm^{-1}. Crystalloid phase of the NEOPCMs was investigated with an x-ray test conducted by an x-ray diffractometer (XRD: EMPYREAN, PANALYTICAL). Thermogravimetric analysis (TGA) curves depicting the thermal stability, and derivative thermogravimetry (DTG) curves depicting the rate of decomposition of composite PCM was obtained by Mettler Toledo TGA/STDA 851-Error ± 5 µg at a heating rate of 10°/min in the temperature range of 50-500 °C. FESEM, FT-IR, XRD, and TGA facilities were acquired at NANOCAT Lab, Institute of Postgraduate Studies, University of Malaya.

4.2.3.3 Thermal reliability test

The thermal reliability test of palmitic acid/TiO_2 composite NEOPCMs for 1500 thermal cycles was carried out using an accelerated thermal cycle tester as explained in the Section 3.2.3. The melting temperature of palmitic acid is nearly 62 °C so the temperature range of 40 to 80 °C was chosen in order to ensure that the material gets melted and solidified completely during the cycle test.

4.2.3.4 DSC analysis

The phase change temperature and latent heat of fusion of PA and NEOPCMs were measured by a differential scanning calorimeter; model METTLER TOLEDO 820C with an error of ± 0.25 °C. For a detailed description of this measurement, Section 3.2.4 can be referred.

4.2.3.5 Thermal conductivity measurement

The thermal conductivity of the pure PA and NEOPCMs was measured using the KD-2 pro, which is based on the hot wire technique and a well-established technique for such measurements. All the thermal conductivity measurements were taken when the materials were in a solid state and at a temperature of 30°C. For this measurement, the pure and composite PCMs were formed into a solid cylindrical form of 5.0 cm in length and 2.5 cm in diameter using a die and a hydraulic press at a pressure of 1.5 tonnes. Two holes of 1 mm diameter each were drilled on the flat surface of these cylindrical samples. The gap between these holes was kept equal to the distance between the probes of KD-2 pro. The temperature was maintained at a constant of 30 °C using a water bath. A time gap of 15 min was kept between two subsequent conductivity measurements in order to stabilize the temperature. Three measurements were recorded for each of the composites at this temperature and the average value was considered for reporting.

4.3 Results and discussion

4.3.1 Morphology of palmitic acid and NEOPCM

FESEM images, showing the micro-structural features of nano TiO_2 and NEOPCM4 in the solid state are shown in Figure 4.2. The spherical shape of the TiO_2 nano-particles can be seen in Figure 4.2 (a). The FESEM images show the uniform dispersion of TiO_2

nano-particles in palmitic acid (see Figure 4.2 (b and c)). This is due to the repulsive bond of the surfactant. Melting of the NEOPCM around the PA lump can be seen at some places due to the concentration of the electric beam on that particular location of the material, which makes it melt.

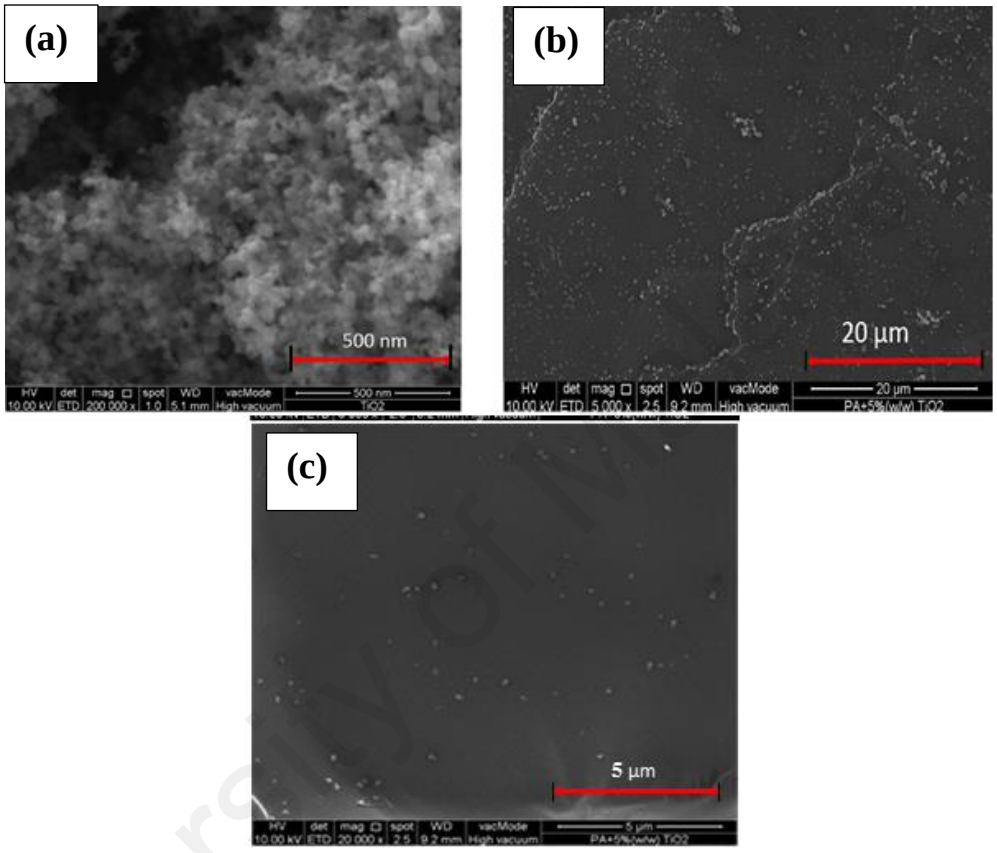

Figure 4.2 FESEM images of (a) TiO2, (b) NEPCM4 (5wt% TiO_2) at 5000 magnification, and (c) NEPCM4 at 20000 magnifications.

4.3.2 FT-IR analysis of palmitic acid and NEOPCMs

FT-IR curves of TiO_2 nano-particles, PA, and NEOPCM1-4 between wavenumbers of 400 and 4000 cm^{-1} are shown in Figure 4.3. The band at 648 cm^{-1} corresponds to the band stretching vibration of Ti-O. The band between 400 and 800 cm^{-1} represents the Ti-O vibrations. Two absorption peaks corresponding to 1642 and 3424 cm^{-1} are characteristic of the O-H bending of the hydroxyl group. The peaks at 2918 and 2850

represent the symmetrical stretching vibration of the $–CH_3$ and $–CH_2$ groups in PA. Nitrile stretch (C=N) appears at around wavenumber 2400 cm^{-1}. C=O stretching vibration is assigned by a peak seen at 1700 cm^{-1}. The deformation-vibration of $–CH_3$ and $–CH_2$ group in PA can be recognized at the peak of 1465 cm^{-1} . The peaks at 1300 cm^{-1} and 943 cm^{-1} are corresponding to the in-plane and out-plane bending vibration of the –OH group of PA. The symmetric peaks at 722 and 678 cm^{-1} correspond to the swinging vibration of the –OH functional group. FT-IR spectrum of NEPOCM1-4 shows neither any new peaks nor any significant peak shifts in the composite PCMs which signifies that only a physical interaction exists between PA, TiO_2 and SDBS. These spectra also do not show any chemical rearrangements of the functional group which implies that no chemical reaction has taken place between PA and TiO_2.

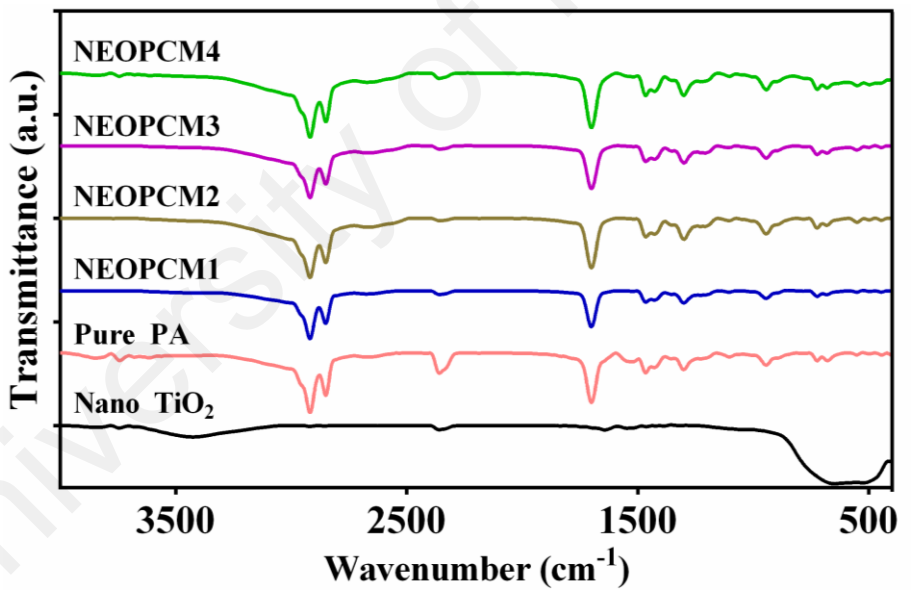

Figure 4.3 FT-IR Spectrum of pure PA, TiO_2, and NEOPCMs

4.3.3 XRD analysis of NEOPCMs

Figure 4.4 shows the XRD patterns of palmitic acid, TiO_2 nano-particles, and NEOPCM2-4. In the XRD pattern on TiO_2, the peaks at 25°, 38°, and 48° confirm the anatase form of the nano-particles. In the XRD pattern of pure PA, the peaks at around 2θ = 12°, 20°, 21.5°, 23°, and 30° are due to the given crystallization. The rest of the three curves represent the XRD patterns of NEOPCM 2-4. It can be found in these curves that the peaks at 12°, 21.5°, and 23° are caused by the palmitic acid, and peaks of the TiO_2 in the NEOPCM can be seen at 25° and 27.5°. The peak of TiO_2 at 25° can be seen in the NEOPCM clearly. The intensity of this peak in the NEOPCM is not significant when wheight fraction of nanoparticles is less than 1%, while it is clearly evident in the NEOPCM3 and NEOPCM4. The results of the XRD patterns indicate that during the preparation of the NEOPCMs, the crystal formation of PA did not change and the NEOPCM contains the peaks of both, PA and TiO_2.

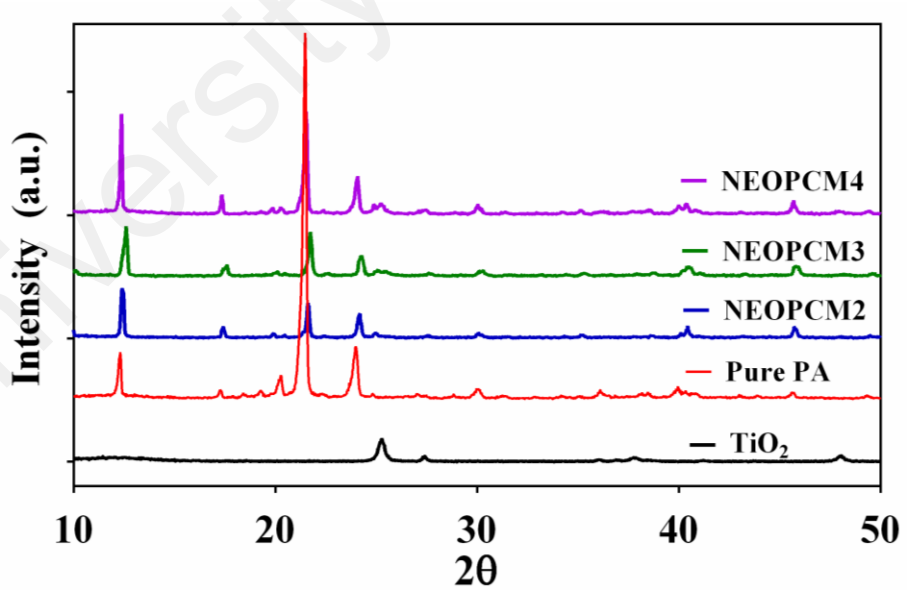

Figure 4.4 XRD patterns of pure PA, TiO_2, and NEOPCMs

4.3.4 Thermal energy storage properties

Upon increasing the temperature of the PA, the microstructure of the solid PA starts loosening up the compactness. When the temperature is further increased, the molecules of palmitic acid absorb the latent heat and change its phase to liquid, which is the result of the conversion of the absorbed energy into kinetic energy, which overcomes the intermolecular forces. Due to this conversion, the measurements of the latent heat and melting temperature of the material are of paramount importance. DSC analysis has been carried out for measuring the thermal energy storage properties of the pure PA and NEOPCMs of different TiO_2 nano-particle weight fractions.

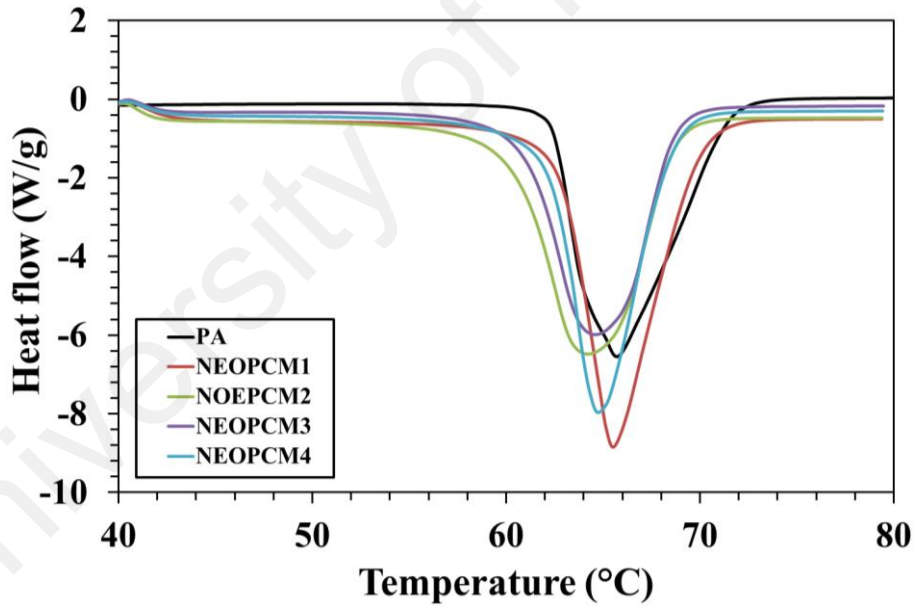

Figure 4.5 DSC measurement of PA and NEOPCMs

Figure 4.5 shows the DSC curves of pure palmitic acid and the four prepared NEOPCMs of 0.5, 1.0, 3.0, and 5.0 wt% nano TiO_2. The melting point was estimated by the tangent at the point of the highest slope on the face portion of the peak and the latent heat of fusion as the area under the curve. It can be clearly seen in the Figure that all

DSC curves of PA and all NEOPCMs are of similar shape. The measured values of the melting temperature, latent heat of fusion and calculated PCM percentage using Equation 4.1 are shown in Table 4.1.

$$\text{PCM} = \frac{\Delta H_{\text{NEOPCM}}}{\Delta H_{\text{O-PCM}}} \times 100\% \quad (4.1)$$

Table 4.1: DSC data of melting of PA and NEOPCMs

Sample name	**Melting temperature (°C)**	**Latent heat of fusion (kJ/kg)**	**PCM percentage (%)**
PA	62.21	213.46	100.0
NEOPCM1	62.47	209.02	98.0
NEOPCM2	60.16	202.9	95.0
NEOPCM3	60.75	184.43	86.4
NEOPCM4	61.59	180.03	84.3

As can be seen in Table 4.1, the melting temperature of the pue PA is 62.21 °C and that of NEOPCM4 is 61.59 °C, which implies that the phase change characteristics of pure PCM and NEOPCM are very close to each other. An irregular variation in the melting temperature was measured with an increasing nano-particle volume fraction. The melting temperature of the prepared composite PCMs is measured to be varied in the range of -0.26 and +2 °C and latent heat of fusion between 2% and 15.5%. The maximum reduction of +2 °C in the melting temperature of the NEOPCM is observed compared to O-PCM (PA in the present case), which is in the case of NEOPCM2. On the other hand, a regular degradation in the latent heat of fusion has been measured with an increasing nano-particle volume fraction. This decrease in the latent heat of the NEOPCMs is due to the changes in the physiochemical properties caused by the

dispersion of TiO_2 nano-particles, which was expected. Lowering the latent heat of fusion with the increase in the nano-particle wt% signifies that a lesser amount of heat is required to change the phase from solid to liquid which consequently reduces the melting/solidification of the O-PCMs. The maximum deviation of 15.5% of the latent heat of fusion is observed in the case of the NEOPCM4 in comparison with the pure PA, which is not very much significant for such a higher loading of the nano-particles. As can be seen in Table 4.1, as expected, the percentage of the PCM in the NEOPCMs decreases with the increase in the nano-particle mass fractions. The minimum PCM percentage is 84.3% for the high loading of 5 wt% nano-particles, which implies that the chances of the leaking of the O-PCM in the composite are less. A correlation is also developed to predict the latent heat of the NEOPCMs based on the curve fitting of the experimental data as a function of the weight fraction of nano-particles dispersed into the base PCM, as given below:

$$L_{NEOPCM} = L_{O-PCM}(0.99 - 0.03264 \times \emptyset) \quad (4.2)$$

Figure 4.6 shows the measured and calculated latent heat of fusion for the NEOPCMs. The latent heat of the NEOPCMs can be calculated using the composite theory (Wu et al., 2010):

$$L_{NEOPCM} = L_{O-PCM} \times \emptyset \quad (4.3)$$

where L_{NEOPCM} and L_{O-PCM} are the latent heat of fusion of the composite and pure O-PCM, respectively, and $\emptyset$ is the weight fraction of the nano-particles dispersed into the base O-PCM.

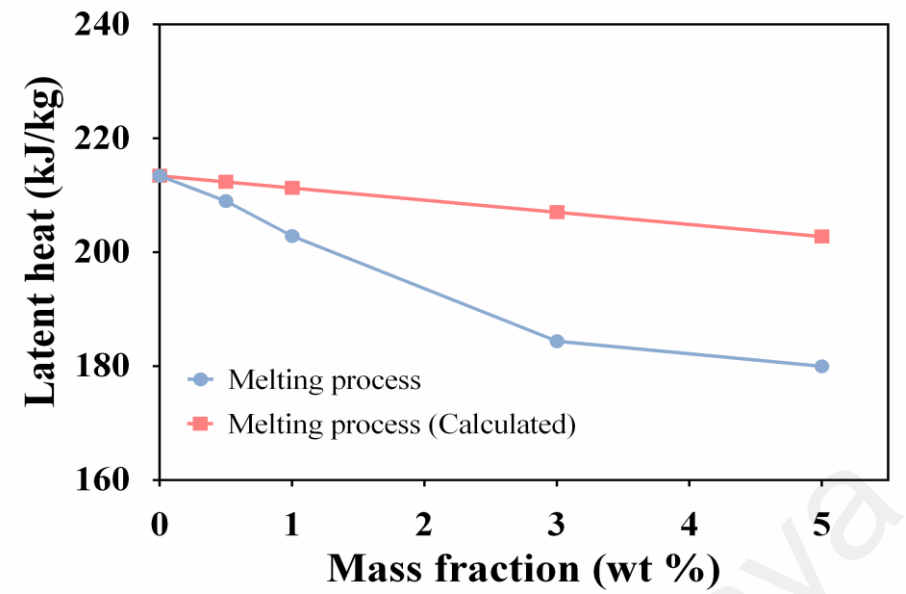

Figure 4.6 Effect of mass fraction of TiO_2 nanoparticles on the latent heat

As can be seen in the Figure 4.6, the measured latent heat of each composite is smaller than that of the calculated value and this deviation gets wider with the increase in the wt% of the nano-particles, which might be due to the surface morphology and structure of the material. Similar deviations in the measured and calculated values were found in the investigations of Wu et al. (2010), Wang et al. (2009), and Sari et al. (2009), which confirms the reliability of the current results.

4.3.5 Thermal stability

Thermal gravimetric analysis was carried out for the pure PA and NEOPCM1-NEOPCM4 to investigate their thermal stability. The TGA curves for the pure PA and NEOPCM4 are shown in Figure 4.7, while Figure 4.8 shows the DTG curve of these materials. The weight loss of the pure PA occurred between 202 and 282 °C and between 202 and 286 °C for NEOPCM4. Below 200 °C, the weight loss is around 4%, which can be attributed as the removal of the absorbed water. The charred residue

amount of the PA after 500 °C was determined to be less than 0.5% and it remained constant thereafter, so it can be considered that the pure PA completely degraded at 282 °C, which can be understood as the complete breakage of the polymer chains into monomers. In the case of NEOPCM4, which is the composite PCM of the high nano-particle concentration (5 wt%) in the present study, the charred amount of residue after 500 °C was around 4.5% and this remained constant thereafter. So, the maximum degradation of the NEOPCM4 occurred at around 286 °C which is close to that of the pure PCM. This minor delay in the degradation may be due to the fact that the addition of nano-particles in the pure PCM serves as a thermal retardant against the temperature, which results in the delay in the decomposition. So, it can be understood from the TGA and DTG (Figure 4.8) curves that the dispersion of nano-particles in the pure PA has improved the stability of this PCM. Since, no decompositions of the material have been noticed until 200 °C, the pure PA and NEOPCMs can be effectively used for the cooling/heating applications of buildings and solar thermal energy storage applications.

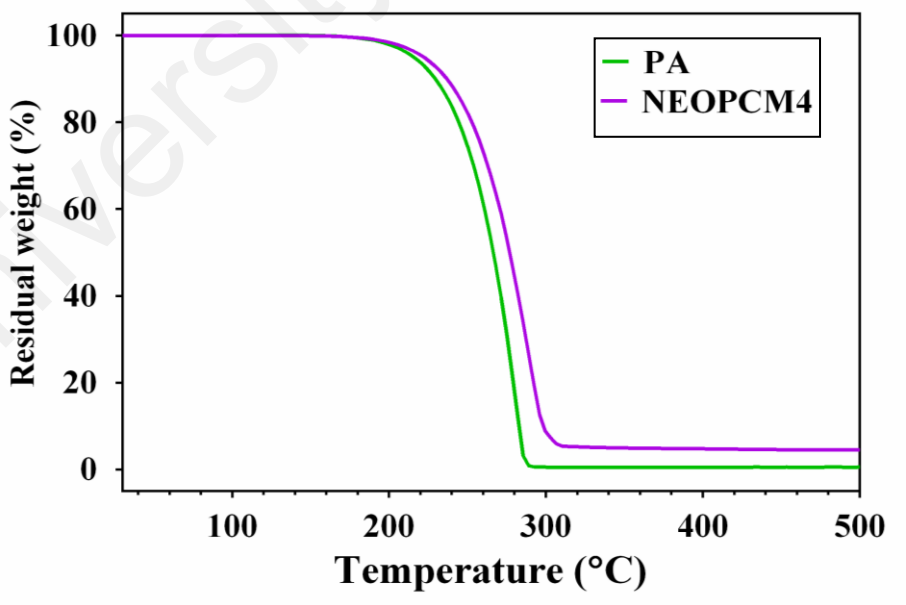

Figure 4.7 TGA curves of PA and NEOPCM4

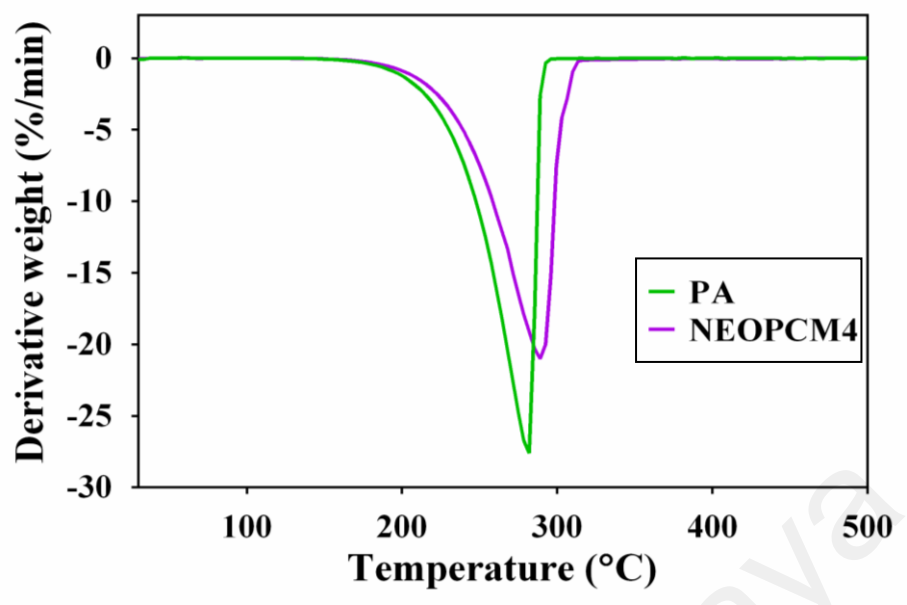

Figure 4.8 DTG curves of PA and NEOPCM4

4.3.6 Thermal reliability

An accelerated thermal cycle test was performed using our in-house (University of Malaya) designed test rig to investigate the reliability of NEOPCMs after a large number of repetitive melt/freeze cycles. The 1500 melt/freeze cycles for NEOPCM3 were performed and the melting temperature and the latent heat of fusion were obtained using the DSC after 100, 500, 1000, and 1500 cycles.

The DSC curves and FT-IR spectrum of pure PA before and after the thermal cycle test are shown in Figure 4.9 (a and b). The DSC curves obtained and the thermal properties measured of the NEOPCM3 during the cycle test are shown in Figure 4.9 and Table 4.2 respectively. As can be seen in the Figure, the latent heat of fusion of the pure PA after 1500 melt/freeze cycles has degraded by 17.88 % and the melting temperature has changed by an amount of +1.76 °C. This degradation in the thermal properties is mainly due to two reasons, one is due to the impurities present in the material and another is due to the changes in their chemical structure. To identify the changes in the

chemical structure, the FT-IR spectrum of the PA was taken before and after the thermal cycle test and the curves are presented in Figure 4.9 (b). It is clearly visible in the Figure that an absorption peak has been created in the pure PA after the cycle test at around 3500 cm^{-1}, whereas, along with the impurities being present in the material, this can be inferred as a possible reason for the degradation of the material properties.

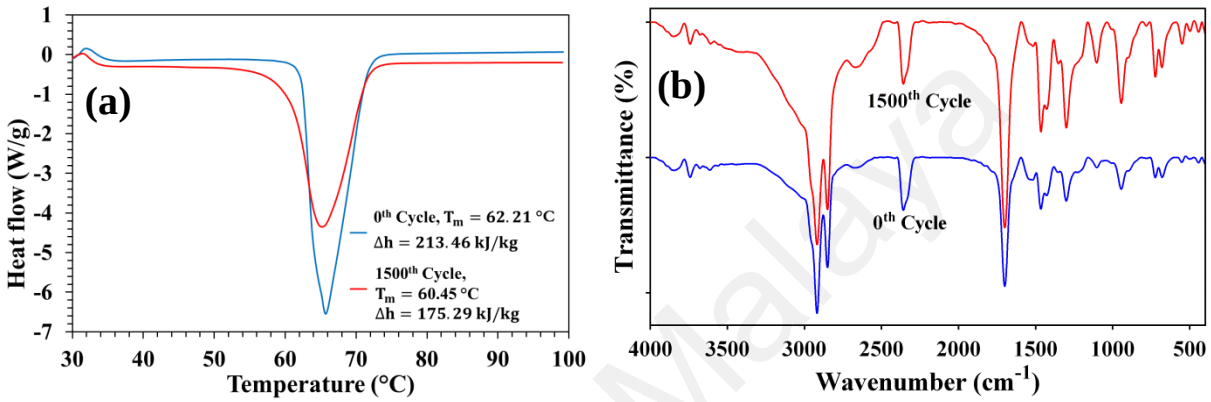

Figure 4.9 (a) Melting DSC curves (b) FT-IR spectrum of pure PA before and after the thermal cycle test

Figure 4.10 shows the DSC curves and FT-IR spectrums of NEOPCM3 before and after the cycle test. As can be seen in the Table 4.1, the maximum jump in the reduction of latent heat of fusion was observed in NEOPCM3, so this composite sample was selected for thermal reliability test. The Table 4.2 shows that during the thermal cycle test, the melting temperature of NEOPCM3 after the 100^{th}, 500^{th}, 1000^{th}, and 1500^{th} thermal cycles changed by 0.26, -2.05, -1.46, and -0.62 ˚C, respectively. In comparison with the pure PA, a variation of -2.0%, -0.26%, -1.42%, and -2.54% in the latent heat of fusion was observed after the 100^{th}, 500^{th}, 1000^{th}, and 1500^{th} cycles, respectively. It can be understood by looking at the variations in the melting temperatures and the latent heat of fusion that the changes are not significant even after a large number of melt/freeze cycles. The depreciation in the latent heat of fusion of

NEOPCM3 is within the acceptable level of the LHTES applications (Sharma et al., 2016). So, if 300 melt/freeze cycles are considered in a calendar year, these NEOPCMs can be effectively used for five consecutive years for thermal energy storage in many domestic and industrial applications.

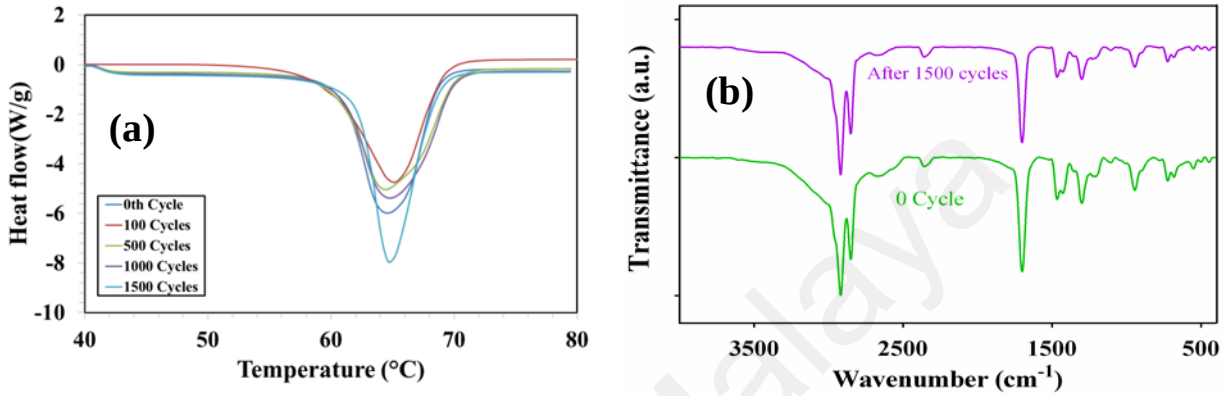

Figure 4.10 (a) Melting DSC curves (b) FT-IR spectrum of NEOPCM3 before and after thermal cycle test

Table 4.2.Thermal properties of NEOPCM3 before and after the thermal cycle test

No. of test cycles	Melting temperature (°C)	Latent heat of fusion (kJ/kg)
0	60.75	184.43
100	60.47	181.52
500	60.16	182.99
1000	61.02	184.02
1500	60.59	180.03

To study the changes in the compositional/functional group of the NEOPCMs during the cycle tests, the FT-IR spectrum of NEOPCM3 before and after the cycle test was obtained and is shown in Figure 4.10 (b). As can be seen in the spectrum, no new peak has appeared after the 1500 melt/freeze cycles and no old peak has disappeared,

which signifies that the accelerated thermal cycle test has not affected the chemical structure of the NEOPCM. Accordingly, the PA/TiO_2 composite O-PCMs show the stable chemical and thermal properties after such a large number of thermal cycles.

Figures 4.9 and 4.10 shows that the dispersion of the nano TiO_2 enhances the thermal and chemical stability of the pure PA significantly. The addition of the 3% TiO_2 decreases the degradation in the latent heat from 17.88% to 2.4% and melting temperature from 1.76 °C to 0.16 °C. This enhanced chemical and thermal stability of the PA/TiO_2 composite makes them highly suitable for effective solar thermal energy storage.

4.3.7 Thermal conductivity

The energy storage and its discharge rate of the phase change materials is very much dependent on their thermal conductivity (Wu et al., 2010). Higher thermal conductivity increases the heat transfer rate, which in turn increases the melting and solidification process and this leads to a lesser solidification/melting time. In the present study, the TiO_2 nano-particles of 21nm average size, dispersed in different wt% into the liquid PA. The thermal conductivity of the prepared NEOPCMs was measured in the solid state at a temperature of 30 °C, which is below melting point using KD-2 Pro. This equipment is based on the hot wire method. It is a well-known fact, that if the thermal conductivity is measured at different temperatures, the enhancement in the value of thermal conductivity is not very much significant (Sharma et al., 2015) so keeping this in mind, the conductivity has been measured at one particular temperature. The values of the measured thermal conductivity against the wt% of nano-particles are presented in Figure 4.11(a). As can be seen, the thermal conductivity consistently increases with the increase in the weight fraction of the nano-particles. The addition of a very small

amount of nano-particles (0.5 weight%, NEOPCM1) increases the thermal conductivity by 12.7%. The enhancement in the thermal conductivity was 20.6%, 46.6%, and 80% in the case of the NEOPCM2, NEOPCM3, and NEOPCM4, respectively. This enhancement shows that the thermal conductivity of NEOPCMs is directly proportional to the nano-particle wt%. The nonlinear behavior of the thermal conductivity enhancement is mainly due to the agglomeration caused by a higher percentage of the TiO_2 nano-particles in the PA (Harikrishnan et al., 2013). The enhancement of the thermal conductivity also ascertains the lesser melting and solidification time of NEOPCMs compared to pure PA. Supercooling effect in the case of the NEOPCMs is also diminished due to the fact that the TiO_2 nano-particles dispersed into palmitic acid act as a nucleating agent, which helps in achieving the congruent melting and solidification of the NEOPCMs (Harikrishnan et al., 2013). Additionally, Figure 4.11 (b) shows the thermal conductivity ratio ($=\frac{k}{k_0}$), where *k* is the thermal conductivity of the NEOPCM and k_0 is that of pure palmitic acid. The value of this ratio is greater than 1 for all NEOPCMs, which also signifies the enhanced thermal conductivity of all composite PCMs. A correlation to predict the thermal conductivity of NEOPCMs as a function of loading of the nano-particles has been developed on the basis of the best fit curve of the experimental data and is given below:

$$k_{NEOPCM} = k_{O-PCM}(1 + 1.48 \times \emptyset) \quad (4.4)$$

Where k_{NEOPCM} is the thermal conductivity of composite PCMs, k_{O-PCM} is the conductivity of pure O-PCM, and $\emptyset$ is the weight fraction of TiO_2 nano-particles.

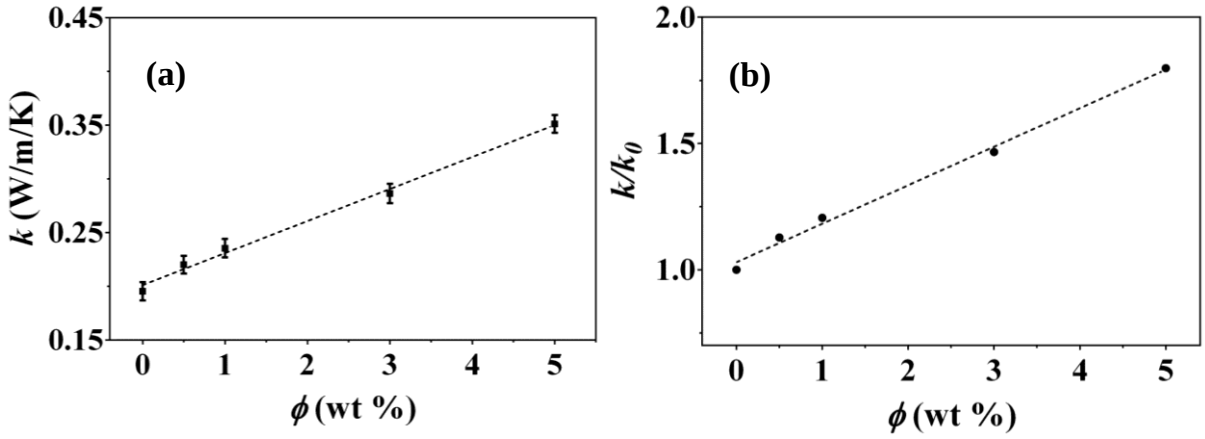

Figure 4.11 (a) Thermal conductivity and (b) conductivity ratio of PA and NEOPCM1-NEOPCM4

4.3.8 Summary and comparison of thermal conductivity with previous studies

Table 4.3 shows the thermal conductivity and the latent heat of fusion of nano enhanced PCMs prepared in previous studies based on the dispersion of the nano-particles of metal oxides such as Al_2O_3, CuO, SiO_2, ZnO, Fe_2O_3, and TiO_2 and the results are compared with the findings of the current study. Wang et al. (2014) prepared the nanocomposites of paraffin and nano TiO_2 and reported a 13% enhancement in the thermal conductivity with a dispersion of 7% at the cost of 9% reduction in the latent heat. In another study, Harikrishnan et al. (2014) prepared the mixture of stearic acid and lauric, and the nano TiO_2 was mixed together. A dispersion of 1% TiO_2 enhanced the thermal conductivity by approximately 42% and a 2% reduction in the latent heat of fusion. In their another work, Harikrishnan et al. (2013) prepared a NEPCM of stearic acid and nano TiO_2 and they reported that the addition of the 0.3% nano TiO_2 enhanced the thermal conductivity by approximately 63%. In a recent study, Motahar et al. (2014a) dispersed the nano TiO_2 into organic PCM n-octadecane and found that the dispersion of the 5% nanoparticles enhances the thermal conductivity by 26.6%. An addition of 4% of Fe_2O_3, Al_2O_3, ZnO and SiO_2 have also shown enhanced thermal conductivity of paraffin by 87.5%, 135%, 90%, and 90% respectively (Babapoor &

Karimi, 2015). The present study shows an increment of approximately 80% in thermal conductivity when the TiO_2 nano-particles dispersion of 5%. This can be considered as a significant enhancement when compared with the existing NEPCMs. Furthermore, it can be seen in Table 4.3 that the latent heat of the pure PA is higher than that of the many PCMs which shows the suitability of this organic candidates in many domestic and commercial energy storage applications. In addition, the thermal reliability results also ensure the long term use of these NEOPCMs.

Table 4.3 Comparison of thermal conductivity and the latent heat of fusion of NEOPCMswith previous similar composites

Composite	**Thermal Conductivity (W/mK)**		**Latent heat (kJ/kg)**		**Ref**
	Base PCM	**NEPCM**	**Base PCM**	**NEPCM**	
Paraffin/7% TiO_2	0.22	0.25	165	150	(Wang et al., 2014)
(SA+LA)/1% TiO_2	0.19	0.27	176.98	173.22	(Harikrishnan et al., 2014)
n-octadecane/5% TiO_2	0.45	0.57	-	-	(Motahar et al., 2014a)
Paraffin/4% Fe_2O_3	0.4	0.75	212	105	(Babapoor & Karimi, 2015)
Paraffin/4% Al_2O_3		0.94		200	
Paraffin/4% ZnO		0.76		182	
Paraffin/4% SiO_2		0.76		200	
Paraffin/5% γ-Al_2O_3	0.22	0.275	142.2	134.1	(Wang et al., 2010)
Paraffin/5% CuO	0.25	0.2663	-	-	(Jesumathy et al., 2012)
Paraffin/10% Al_2O_3	0.13	0.138	243.1	212.3	(Ho & Gao, 2009)
Palmitic acid/5% TiO_2	0.19	0.35	213.46	180.03	Present study

4.4 Summary

This experimental study was conducted on the preparation and characterization of palmitic acid/TiO_2 nano-enhanced organic phase change materials. The TiO_2 nano-particles in 0.5, 1.0, 3.0, and 5.0 wt% were dispersed into liquid palmitic acid (PA) and the effect of its weight fraction on the thermo-physical properties of the NEOPCMs were measured using the DSC and thermal conductivity apparatus. The results of this study can be summarized as below:

- The FESEM and XRD images confirm the uniform dispersion of the nano-particles and the FT-IR spectrum show that the TiO_2 nano-particles are in chemical compatibility with the PA and the interaction between the base O-PCM and nano-particles is purely physical.
- DSC results of the NEOPCMs do not exhibit any significant changes in the melting temperature (maximum 3.3% deviation). A variation of about 15.5% is found for the latent heat of fusion. These finding show that this composite PCM has great potential to be used as thermal energy storage materials.
- The accelerated thermal cycle test of the NEOPCM showed that the prepared composite material does not lose its thermal and chemical properties even after a large number of melt/freeze cycles. During the cycle test, the deviation in the melting temperature was found to be in the range of -0.4 to +0.98% and in the latent heat of fusion +0.2 to 2.4%.
- Addition of nanoparticles of TiO_2 improves the chemical and thermal stability of the pure PA.

- Thermal conductivity was found to be increasing with the increase of the loading of the nano-particles. An 80% enhancement in thermal conductivity was seen in the case of the NEOPCM4 compared to pure PA. The prepared composites have shown the enhanced thermal properties without significantly affecting the thermal energy storage capacity, so, these NEOPCMs can be used as potential candidates for solar energy storage applications.

CHAPTER 5: MATHEMATICAL MODELING FOR ENHANCED SOLIDIFICATION IN AN ENCLOSURE

5.1 Introduction

Understanding of the results of the thermal cycle tests and of composite nano enhanced organic PCMs has led to the understanding that the dispersion of the nano particles of metal or metal oxides enhances the thermal conductivity significantly which in turn increases the heat transfer rate of PCMs. During the charging (melting) process, the PCM remains in a liquid state and it becomes essential to store it in a leak proof container. The shape of the container affect the heat transfer process within the PCM significantly (Verma et al., 2008). The behavior of the melting/freezing phenomenon in the PCM can be very well predicted using analytical or numerical methods. A parametric investigation of solidification phenomenon of nanofluid flled in the trapezoidal cavity has been carried out using ANSYS Fluent. The FLUENT has a specific model to simulate and predict the phase front interface during melting/freezing process and crystal growth. This computational fluid dynamics (CFD) software has shown its capability in predicting the melt/freeze phenomenon very accurately in previous studies The effect of nanoparticle concentration, trapezoidal wall, cold wall temperature and Grashof number on the total solidification time has been investigated in this chapter.

5.2 Methodology

5.2.1 Geometry

A two-dimensional (2D) trapezoidal cavity of 100 mm^2 internal area, as shown in Figure 5.1, is considered in this study. The length (L) of the cavity is 10 mm and the height (H) is varied in such a way that the internal area of the cavity remains constant at

100 mm^2. Three types of trapezoidal cavities are formed based on three different angles such as θ = 2.72°, 5.42° and 7.69°. Details of these geometries are given in Table 5.1.

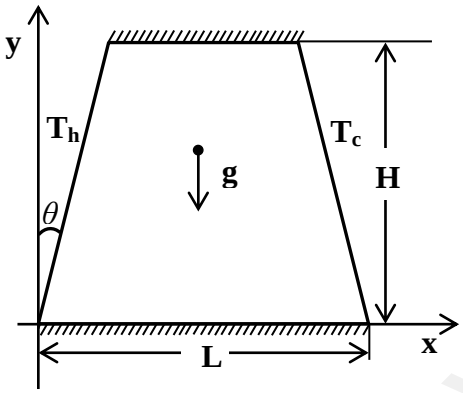

Figure 5.1 Sketch of the two dimensional trapezoidal cavity

Table 5.1 Configuration of tested trapezoidal geometries

Tested cavity	Length (L), mm	Height (H), mm	Inclination angle (θ)
Square cavity	10	10	0°
Cavity 1	10	10.52	2.72°
Cavity 2	10	11.20	5.42°
Cavity 3	10	11.91	7.69°

5.2.2 Boundary conditions

The horizontal walls are assumed to be insulated, non-conducting, and impermeable to heat transfer. The mathematical relations given in the following section are identical to the work of Khanafer et al. (2003) and Khodadadi & Hosseinizadeh (2007), thus they can be used to benchmark our numerical model by comparing our findings with theirs. The left and right inclined walls are kept at constant temperatures of T_h = 283.15 K and

T_c = 273.15 K, respectively. The nanofluid in the cavity is considered to be Newtonian, laminar, and incompressible. Thermo-physical properties of the nanofluids are assumed to be constant in the case of water-Cu nanofluid, whereas the density variation in the buoyancy force is handled by the Boussinesq approximation. In the case of paraffin-Cu nanofluid, the thermophysical properties have been considered temperature dependent and discussed in the following sections. The user defined functions (UDF) for accommodating the variation in the thermophysical properties with the temperature were written using language C and appended in the prepared ANSYS Fluent numerical model. The nanoparticles are assumed to have a uniform shape and size (10 nm diameter). The left lower corner of the cavity is the origin of a coordinate system. Gravity acts in the negative y-direction, i.e., $g_x = 0$ and $g_y = -g$.

The initial and boundary conditions for the present investigation are as follows:

At the left inclined wall, $u = v = 0, T = T_h,$ at $x = 0$ and $0 \le y \le H$

At the right inclined wall, $u = v = 0, T = T_c$ at $x = L$ and $0 \le y \le H$

At horizontal surfaces, $u = v = \frac{\partial T}{\partial y} = 0,$ at $y = 0, H$ and $0 \le x \le L$

Table 5.2 Thermo-physical properties of the base fluid (water) and the Cu nanoparticles

Property	**Copper nanoparticles**	**Base fluid (water)**
$\rho\ [kg = m^3]$	8954	997.1
$\mu\ [Pa\ s]$	-	8.9×10^{-4}
$c_p [J/kg\ K]$	383	4179
$k\ [W/m\ K]$	400	0.6
$\beta\ [1/K]$	1.67×10^{-5}	2.1×10^{-4}
$L\ [J/kg]$	-	3.35×10^5
Pr	-	6.2
Ste	-	0.125
$d_p [m]$	10^{-9}	-

5.2.3 Governing equations

The continuity, momentum, and energy equations can be written as follows:

Continuity

$$\frac{\partial u}{\partial x}+\frac{\partial v}{\partial y}=0, \tag{5.1}$$

X-momentum

$$\frac{\partial u}{\partial t}+u\frac{\partial u}{\partial x}+v\frac{\partial u}{\partial y}=\frac{1}{\rho_{nf}}\left(-\frac{\partial p}{\partial x}+\mu_{nf}\nabla^2 u+\left(\rho\beta\right)_{nf} g_x\left(T-T_C\right)\right)+S_x, \tag{5.2}$$

Y-momentum

$$\frac{\partial v}{\partial t}+u\frac{\partial v}{\partial x}+v\frac{\partial v}{\partial y}=\frac{1}{\rho_{nf}}\left(-\frac{\partial p}{\partial y}+\mu_{nf}\nabla^2 v+\left(\rho\beta\right)_{nf} g_y\left(T-T_C\right)\right)+S_y, \tag{5.3}$$

Energy equation

$$\frac{\partial T}{\partial t}+u\frac{\partial T}{\partial x}+v\frac{\partial T}{\partial y}=\frac{\partial}{\partial x}\left[\frac{(k_{nfo}+k_d)}{(\rho c_p)_{nf}}\frac{\partial T}{\partial x}\right]+\frac{\partial}{\partial y}\left[\frac{(k_{nfo}+k_d)}{(\rho c_p)_{nf}}\frac{\partial T}{\partial y}\right]-S_h, \tag{5.4}$$

The density of the nanofluid is given by:

$$\rho_{nf}=\left(1-\phi\right)\rho_f+\phi\rho_s, \tag{5.5}$$

The viscosity of nanofluid is given by Brinkman (1952):

$$\mu_{nf}=\frac{\mu_f}{(1-\phi)^{2.5}}, \tag{5.6}$$

The heat capacitance of the nanofluid and part of the Boussinesq are:

$$(\rho c_p)_{nf} = (1-\phi)(\rho c_p)_f + \phi(\rho c_p)_s \tag{5.7}$$

$$(\rho\beta)_{nf} = (1-\phi)(\rho\beta)_f + \phi(\rho\beta)_s \tag{5.8}$$

The latent heat of the nanofluid is evaluated using

$$(\rho L_h)_{nf} = (1-\phi)(\rho L_h)_f \tag{5.9}$$

The thermal conductivity of the quiescent (subscript 0) nanofluid is given as (Wasp, 1977):

$$\frac{k_{nfo}}{k_f} = \frac{k_s + 2k_f - 2\phi(k_f - k_s)}{k_s + 2k_f + 2\phi(k_f - k_s)} \tag{5.10}$$

The effective thermal conductivity of the nanofluid is:

$$k_{eff} = k_{nf\,0} + k_d, \tag{5.11}$$

Where k_d is the thermal conductivity enhancement term due to the thermal dispersion and is given as (Amiri & Vafai, 1994):

$$k_d = C(\rho c_p)_{nf}\sqrt{u^2+v^2}\,\phi d_p. \tag{5.12}$$

The constant *C* is obtained from work of Wakao and Kaguei (1982).

In Eqs. (2)-(4), *S* is the source terms which are given by:

$$S_x = A(f)u, \quad S_y = A(f)v,$$
$$S_h = \frac{\partial[(\rho L f)_{nf}]}{\partial t} \tag{5.13}$$

where $A(f) = \frac{M(1-f)^2}{f^3+\varepsilon}$ causes the gradual change in velocity from a finite value in the liquid to zero in the solid in the computational cells. Here $\varepsilon = 0.001$, a small computational constant used to avoid division by zero and M (10^5 in the current investigation) is the mushy zone constant reflecting the morphology of the melting/solidification.

The sensible enthalpy h, and total enthalpy, H_e is written as:

$$h = h_c + \int_{T_c}^{T} C_{p,nf}\, dT \tag{5.14}$$

$$H_e = h + fL_h \tag{5.15}$$

where fL_h is latent heat which varies between zero for solid to L_h for liquid, and f is given by:

$$f = \begin{cases} 0 \quad if \quad T < T_s \\ \dfrac{T - T_s}{T_l - T_s} \quad if \quad T_s < T < T_l \\ 1 \quad if \quad T > T_l \end{cases} \tag{5.16}$$

Where T_s and T_l are the solidus and liquidus temperatures, respectively.

The calculation of the Nusselt number is an effective way to represent the heat transfer rate of a nanofluid. A local Nusselt number (Nu_L) is calculated with the following equation:

$$Nu_L = \frac{k_{nf}}{k_f} \frac{H}{\Delta T} \frac{\partial T}{\partial n}\bigg|_w \tag{5.17}$$

An average Nusselt number is calculated by integrating the local Nusselt number:

$$Nu_{ave} = \frac{1}{S_i}\int_0^S Nu_L ds \tag{5.18}$$

Where s is the distance along the inclined wall and S_i is the length of the inclined wall.

5.2.4 Simulation cases

A total of sixty two CFD simulations as shown in Table 5.3 were carried out for validation and to study the effect of various parameters, such as the inclination angle of a trapezoidal section, nanoparticle volume fraction, and wall temperature difference on the total solidification time of the nanofluid. Case 1 CFD model, which is based on a rectangular cavity of 8.89 cm × 6.35 cm filled with solid gallium, is used to investigate the propagation of the melt front of gallium. Case 2 is based on the solidification of water filled in a trapezoidal cavity and is used to investigate the temperature distribution at a certain height of the cavity. Eight simulations, i.e., Cases 3-10 are based on a square cavity of 1 cm length, filled with nanofluid, and these cases are used to validate the U-velocity at the vertical mid plane and the temperature profiles at the horizontal mid plane for Gr = 10^4 and 10^5 against such results from Khanafer et al. (2003). The remaining cases are based on a trapezoidal cavity. Thirteen simulations, i.e., Cases 11-23, were used to investigate the effect of the nanoparticle volume fraction, ϕ, inclination angle, θ, and temperature difference, ΔT on the total solidification time of the nanofluid in a trapezoidal cavity. Three simulation cases (24-26) are used to investigate the effect of Gr on the mode of heat transfer. Cases 27-62 (thirty six simulations) are used to calculate an average Nusselt number along the hot wall of the trapezoidal cavity for various values of Gr, θ, and ϕ.

Table 5.3 Simulation cases

Sim.* cases	Inclination angle, θ °	Material	ΔT (°C)	*Gr*	Remarks
1 (square cavity)	0	Solid gallium	9.7	-	Used to validate the phase front of Gau and Viskanta (1986), Brent et al. (1988), and Khodadadi et al. (2007)
2 (trapezoidal cavity)	-	Pure water	-	-	Used to validate the temperature profile of solidifying water in the cavity (Duggirala et al., 2006)
3-10 (square cavity)	0	0, 0.1, and 0.2 Cu-H_2O nanofluid	-	10^4 10^5	Used to validate the temperature profile and U-velocity results of Khanafer et al. (2003)
11-13 (trapezoidal cavity)	2.72	0, 0.1, and 0.2 Cu-H_2O nanofluid	10	-	To study the effect of nanoparticle volume fraction on solidification of nanofluid
14-16 (trapezoidal cavity)	2.72 5.42 7.69	0.2 Cu-H_2O nanofluid	10	-	To study the effect of inclination angles on solidification of nanofluid
17-19 (trapezoidal cavity)	2.72 5.42 7.69	0.2 Cu-H_2O nanofluid	10	-	To study the phase front propagation in trapezoidal cavity
20-23 (trapezoidal cavity)	2.72	0.2 Cu-H_2O nanofluid	10 20 30 55 110	-	To study the effects of temperature difference on the solidification
24-26 (trapezoidal cavity)	2.72	0.2 Cu-H_2O nanofluid	-	10^5 10^6 10^7	To study the effect of conduction or convection dominated heat transfer
27-62 (trapezoidal cavity)	2.72 5.42 7.69	0, 0.1, and 0.2 Cu-H_2O nanofluid	-	10^3 10^4 10^5	To compute the values of average Nusselt number

*Simulation

5.2.5 Mesh independency test

Structured and uniform square grid spacing for x and y-direction, as shown in Figure 5.2, is used for all the numerical simulation cases reported here. The grid independence study is carried out from coarse to fine grid using five different uniform grids 50 × 50, 80 × 80, 120 × 120, 150 × 150, and 200 × 200. The complete solidification time for all grids are numerically computed and shown in Table 5.4. Between the grid size of 50 × 50 and 120 × 120, the fluctuation in results is as high as 4% but increasing the grid size beyond 120 × 120 reduces the variation substantially down (to 1%), so the grid size of 120 × 120 is considered in the present study with the finer grid on the side walls.

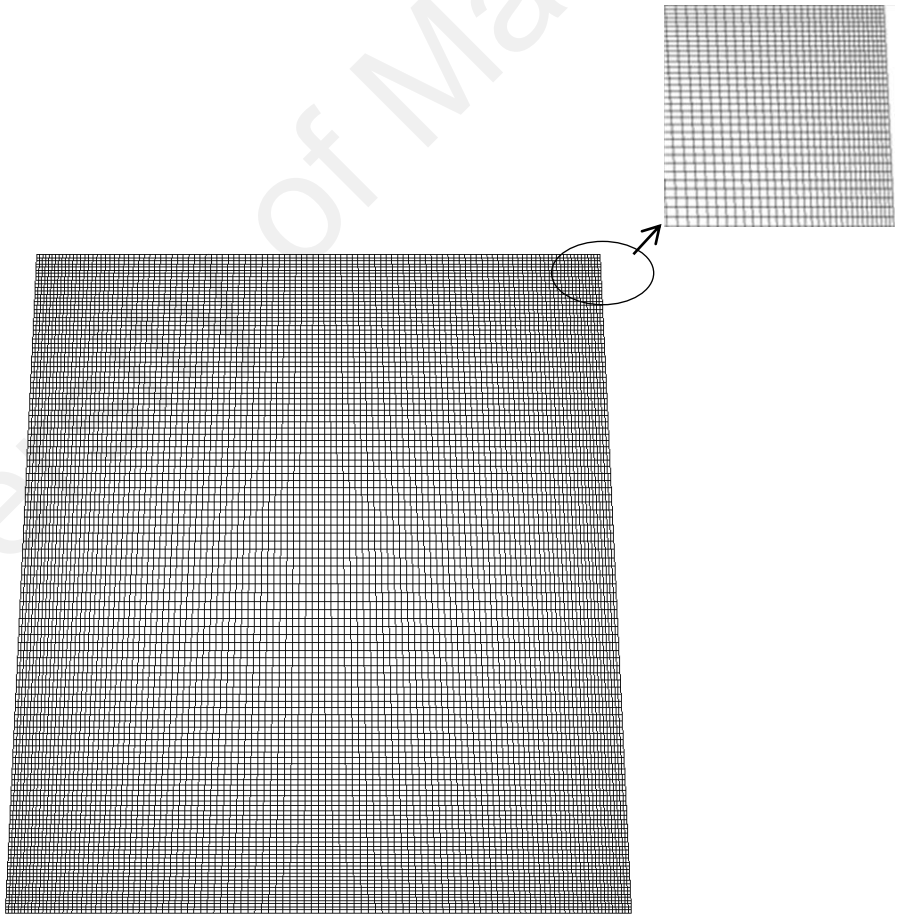

Figure 5.2 Meshed trapezoidal cavity

Table 5.4 Mesh independency test

Sr. No.	Inclination angle	Mesh size	Total solidification time (s)	Deviation (%)
1.	2.72^{o}	50 × 50	1292	-
2.	2.72^{o}	80 × 80	1304	0.92
3.	2.72^{o}	120 × 120	1360	4.118
4.	2.72^{o}	160 × 160	1378	1.306
5.	2.72^{o}	200 × 200	1392	1.006

5.2.6 Numerical methods

The Semi-Implicit Method for Pressure-Linked Equations (SIMPLE) method within the commercial CFD package ANSYS Fluent (13.0., 2011) is used to solve the governing Eqs. 5.1 – 5.4. The Enthalpy-porosity approach is used for the phase change region inside the PCM, by which the porosity in each cell is set equal to the liquid fraction in that cell. The Quadratic upstream interpolation for convective kinematics (QUICK) differencing scheme is used for solving the momentum and energy equations, whereas the Pressure Staggering Option (PRESTO) scheme is used for pressure correction equations. In the enthalpy method, the solution is based on a fixed grid and governing equations are modified such that they are valid for both phases. Also, the mushy zone constant (M) is set to 10^5 kg/m^{3}s. The time step size used for all the simulations in this study is 0.5 s and number of iterations for each time step are 800. The under-relaxation factor of all the components, such as velocity components, pressure correction, thermal energy etc. is kept at 0.3. Convergence criteria are set at 10^{-6} for continuity and momentum and 10^{-8} for thermal energy.

Numerical simulations of solidification begin with the steady state natural convection within the trapezoidal cavity filled with nanofluid (Cu-H_2O). At t = 0s, the left wall of the cavity is kept at 10°C higher than that of the solidification point of water (273.15 K) and the right wall is held at the solidification temperature. The nanofluid is maintained at uniform temperature 273.15 K throughout the cavity at t = 0s. Then, the temperatures of both inclined walls are lowered by an equal amount (10°C). Consequently, solidification of nanofluid begins at the right wall and the solid-liquid interface travels towards the left until the complete solidification of the nanofluid within cavity is calculated. This phenomenon is discussed below.

5.2.7 Selection of nano enhanced phase change materials

This particular study has been divided in two sections. One belongs to the organic PCM based nano-enhanced phase change material and another is the inorganic PCM based nano-enhanced phase change material. Paraffin is chosen as organic PCM and water as inorganic. Cu nanoparticles of 20 nm are chosen as dispersant in both PCMs and their effects on thermo-physical properties are determined. The data for the thermophysical properties of the nano enhanced organic PCMs are limited in the literature, so a preliminary analysis for determining the effect of nanoparticles on the thermal performance of organic PCM and effect of trapezoidal cavity on the solidification of paraffin based nanofluid is carried out. Then using the same methodology, a detailed parametric study is carried out to investigate the effect of various pertinent parameters such as nanoparticle volume fraction, cold wall temperature, Grashof number, inclined walls of trapezoidal cavity etc. on the heat transfer mechanism during solidification of Cu-water nanofluid filled inside a trapezoidal cavity.

5.3 Results and discussion

5.3.1 Validation of the numerical model

The results of the Case 1 CFD model are compared with those of an experimental study of Gau and Viskanta (1986), numerical predictions by Brent et al. (1988) and Khodadadi and Hosseinizadeh (2007) of the melting of solid gallium in a two-dimensional rectangular cavity (height, L_y = 6.35 cm; width, L_x = 8.9 cm) in Figure 5.3. The horizontal walls are adiabatic and vertical walls have different but constant temperatures. A uniform internal temperature at the melting point of gallium, 302.95 K is set to the cavity. At t = 0s, the temperature of the left vertical wall is suddenly raised to a prescribed temperature above the melting point, resulting in the melting of the gallium. The values of the governing dimensionless numbers and aspect ratio are listed in Table 5.5. The melt front is plotted at different times, i.e., 2, 6, 10 and 17 minutes, in Figure 5.3. It is evident from this Figure that a reasonably good agreement exists between the computed and experimental melt front positions with a small discrepancy between the measured and calculated results. This discrepancy between the predicted phase front of the present CFD model and the experimental results may be due to the sub-cooling of approximately 2 °C in the solid (Gong et al., 1999). In addition, at specific times, e.g., 2 min, 6 min and 10 min, our results are relatively much closer to that of the experiment than the numerical prediction of Khodadadi et al. (2007).

Table 5.5 Parameters used in the validation of melting of gallium

AR	Aspect ratio	0.714
Ra	Rayleigh number	3×10^5
Pr	Prandtl number	0.021
Ste	Stefan number	0.040

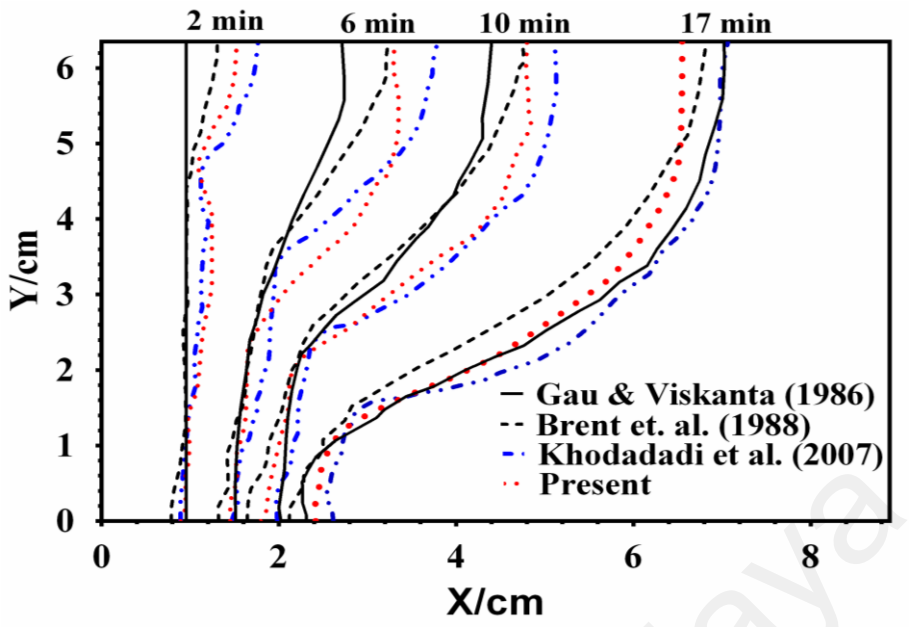

Figure 5.3 Progress of the melting phase front with time: Comparison among the prediction of Khodadadi et al. (2007) Brent et al. (1988), experimental data of Gau and Viskanta (1986), and present work.

To benchmark our model for solidification of water based PCMs, the results of the numerical study (Case 2) have been compared with the experimental data as reported by Duggirala et al. (2006) and presented in Figure 5.4. To validate the current numerical model, a 2-D trapezoidal cavity with a bottom and top width of 65 mm and 165 mm respectively and a height of 130 mm was used. This cavity was completely filled with pure water and the initial temperature was kept at 0 °C. Top and bottom wall were made insulated and both inclined walls were kept at -30 °C. As soon as the simulation was started, solidification began immediately. The temperature profile at a distance of 37 mm from the bottom wall and t = 72 min was plotted and compared with the experimental data available in literature. Numerical prediction is in good agreement with the experimental data.

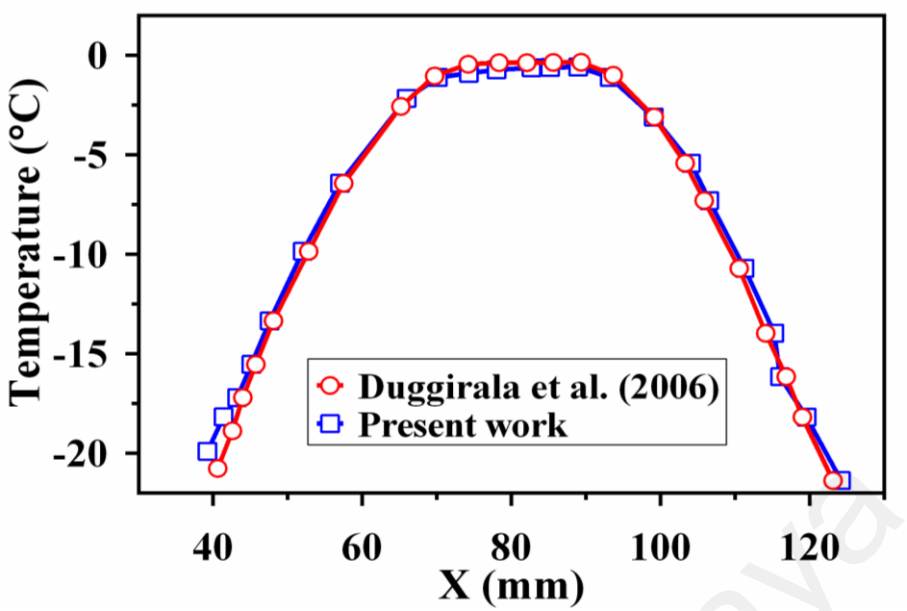

Figure 5.4 Comparison of the temperature profile at y = 37 mm in the pure water between the experimental data of Duggirala et al. (2006) and present work.

The results from Case 3-10 CFD models, which are based on a square cavity of 1 cm, have been checked against numerical results reported by Khanafer et al. (2003). Figure 5.5(a), and 5.5(b) show the U-velocity distribution at the vertical mid plane for $Gr = 10^4$ and 10^5, respectively based on nanoparticle volume fractions of 0, 0.1, and 0.2. Figure 5.5(c) shows the temperature distribution at the horizontal mid plane of the differential heated square cavity of height 1 cm filled with nanofluid of nanoparticle volume fraction 0.2, for $Gr = 10^4$ and 10^5. In general, for all of the nanoparticle volume fractions, the well-established trend of the horizontal velocity is seen exhibiting an accelerated flow near the top and bottom horizontal walls and a weak flow near the center of the cavity which shows the nanofluid behaves like a base fluid (water) near the center. Overall, the CFD results for all nanoparticle volume fractions are close to those from the literature (Khanafer et al., 2003). In particular, the results for the water (ϕ=0) for the both Grashof numbers have an excellent agreement. However, small discrepancies can be seen for ϕ =0.1 and ϕ =0.2 especially at the peaks. Figure 5.5(c) shows the temperature distribution at the horizontal mid plane for $Gr = 10^4$ and 10^5

based on nanoparticle volume fraction of 0.2. The temperature distribution of the CFD models is consistent with that of Khanafer et al. (2003) for both *Gr*. All of the above comparisons were used to validate our CFD models.

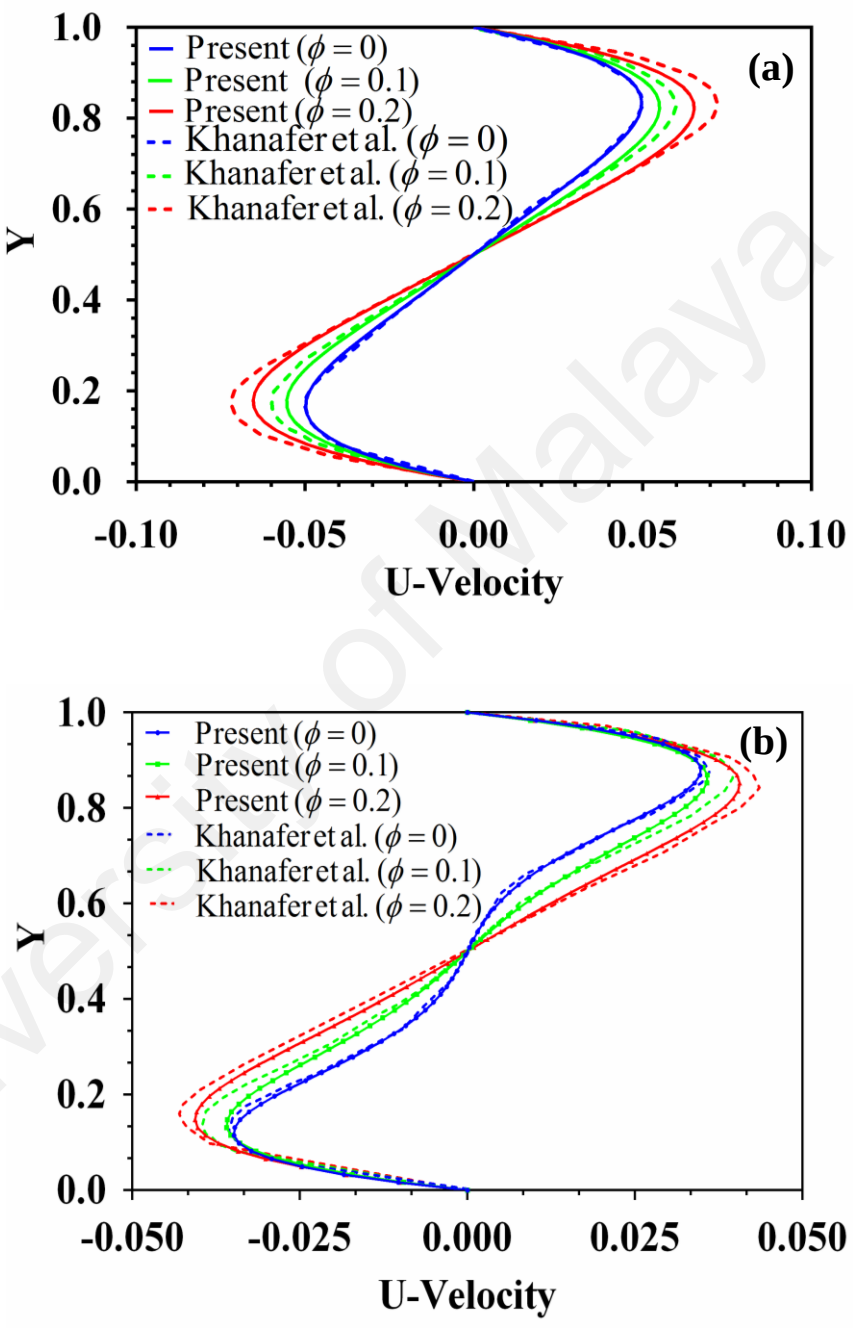

Figure 5.5 Comparison of the U-velocity along the vertical mid plane of the cavity between present work and those of Khanafer et al. (2003) for (a) $Gr = 10^4$, and (b) $Gr = 10^5$, and (c) comparison of temperature on the mid plane for $\phi = 0.2$.

Figure 5.5 continued…

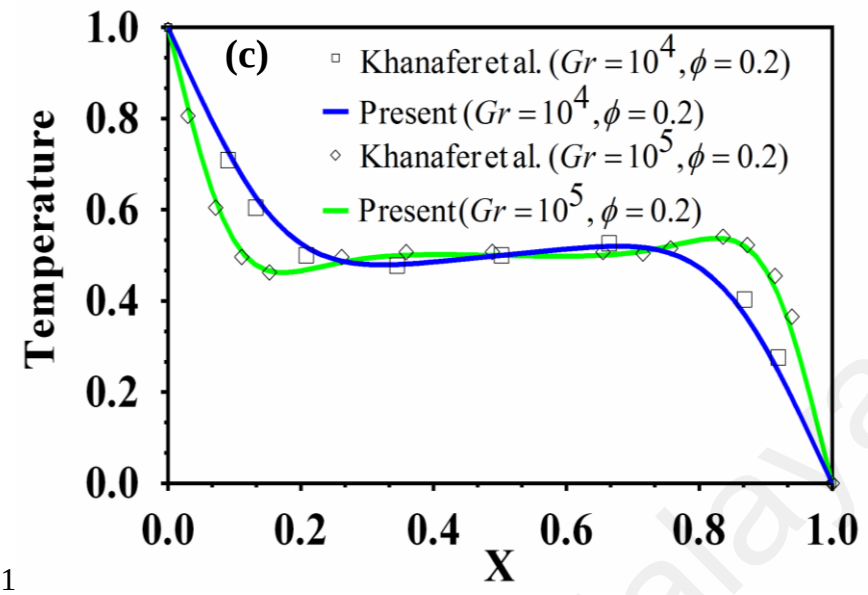

1

Figure 5.5 Comparison of the U-velocity along the vertical mid plane of the cavity between present work and those of Khanafer et al. (2003) for (a) $Gr = 10^4$, and (b) $Gr = 10^5$, and (c) comparison of temperature on the mid plane for $\phi = 0.2$.

Table 5.6 shows the comparison of variation of average Nusselt number (Nu_{avg}) given in Eq. (18) with the Grashof number along the hot wall to validate the present results with those reported by Khanafer et al. (2003), Ho et al. (2008), and Das and Ohal (2009) for a square cavity filled with pure water. A good agreement is obtained between the present and benchmark solutions.

Table 5.6 Comparison of the average Nusselt number for square cavity where $Pr = 6.2$ (water) for $\phi = 0.0$

Literature	$Gr_{bf} = 10^3$	$Gr_{bf} = 10^4$	$Gr_{bf} = 10^5$
Present	1.9377	4.1093	8.2521
Khanafer et al. (2003)	1.9806	4.0653	8.3444
Ho et al. (2008)	Not applicable	3.9494	7.8258
Das and Ohal (2009)	2.3097	4.6512	9.3662

5.3.2 Solidification of paraffin-Cu nanoparticles nanofluid filled in trapezoidal cavity

A nanofluid of liquid paraffin and copper nanoparticles was considered to be filled up in a trapezoidal cavity and a parametric investigation was carried out to study the effect of the trapezoidal cavity and Cu nanoparticle concentration on the total solidification time of the paraffin based nanofluid. The thermo physical properties of paraffin wax and Cu nanoparticles are given in the Table 5.7. As can be seen in the Table, the solidus and liquidus temperature of paraffin are different, and this difference defines the phase transition from solid to liquid state.

Table 5.7 Thermophysical properties of paraffin and Cu nanoparticles

Property	**Paraffin wax**	**Cu**
Density (kg/m^3)	$\frac{750}{0.001\,(T-319.15)+1}$	8954
Specific heat (J/kgK)	2890	383
Thermal conductivity (W/mK)	0.21 if $T < T_{solidus}$	400
	0.12 if $T > T_{liquidus}$	-
Viscosity (Ns/m^2)	$0.001 \exp\left(-4.25 + \frac{1790}{T}\right)$	-
Latent heat (J/Kg)	173,400	-
Thermal expansion coefficient (1/K)	-	1.67×10^{-5}
Solidus temperature (K)	319	-
Liquidus temperature (K)	321	-

5.3.2.1 Effect of trapezoidal cavity of the total solidification time

To study the effect of trapezoidal cavity on the total solidification time of Cu nanoparticle enhanced paraffin, the three different inclination angle of side walls θ as discussed in the Section 5.3.1 and temperature difference of 10 K are considered in the present study and the results of trapezoidal cavity are compared with that of square cavity and shown in Figure 5.6. This parametric investigation is carried out considering that the nanofluid has 10% concentration of Cu nanoparticles dispersed into liquid paraffin. It can be noted that the internal area of these selected cavity geometry is same i.e. 10 mm^2. As can be seen in the Figure that, the total solidification time of the nanofluid decreases with the increase of angle of the side walls. A total reduction of 22% in the solidification time is observed when the inclination angle is 7.69° compared to that of square cavity (θ = 0°). This reduction is because of the surface area normal to the direction of heat transfer increases with increase of θ.

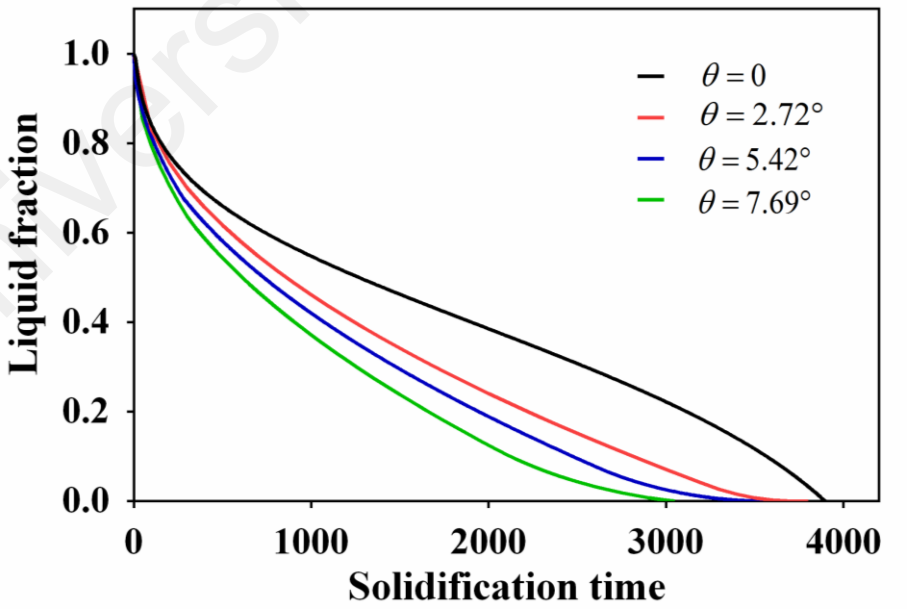

Figure 5.6 Liquid fraction in trapezoidal cavity filled with nanofluid of 10% Cu nanoparticled

5.3.2.2 Effect of nanoparticle volume fraction on the total solidification time of paraffin based nanofluid

To study the effect of Cu nanoparticle concentration on the solidification time of liquid paraffin, the nanoparticles were considered to be dispersed in volume fractions of 0%, 10%, and 20%. For the nanofluid with 10% nanoparticles dispersed, the total solidification time was observed to be 40 % less than that of in case of pure paraffin. And this solidification time was reduced by 53% in case of 20% nanofluid.

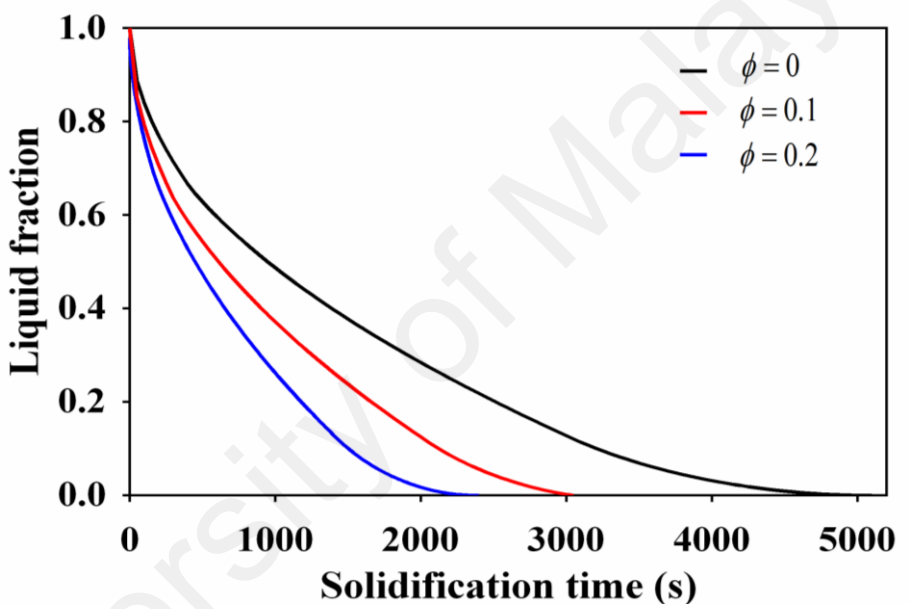

Figure 5.7 Liquid fraction in trapezoidal cavity of θ = 7.69° filled with paraffin and different concentration of Cu nanoparticles

5.3.3 Solidification of water-Cu nanoparticles nanofluid filled in trapezoidal cavity

This section discusses the heat transfer phenomenon during the solidification of the Cu-water nanofluid filled in the trapezoidal cavity of different inclination angle of the side walls. The three different concentrations of Cu nanoparticles 0%, 10%, and 20% are considered for a detailed parametric investigation to assess the feasibility of such geometry for PCM containment. The effect of the nanoparticle concentration (ϕ),

inclination angle of side walls (θ), and the temperature difference between hot and cold walls (ΔT) have been investigated. In addition, the average values of the Nusselt number, Nu_{ave} calculated for various values of Grashof number (Gr_{bf}), ϕ, and θ along the hot wall of trapezoidal cavities have been calculated and discussed.

5.3.3.1 Effect of nanoparticle volume fraction on solidification time

The vertical walls of the square cavity were inclined to form a trapezoidal cavity in such a way that the internal area remains constant for all inclination angles. Solidification was studied for three different angles, θ = 2.72°, 5.42°, and 7.69°. For θ = 2.72 °, the reduction in solidification time is almost 8% and then it further increases with inclination.

The dependency of the solidification time on the dispersed copper nanoparticle volume fractions (ϕ = 0, 0.1, and 0.2), in the base fluid (H_2O) filled in a trapezoidal cavity of θ = 2.72° is investigated in Cases 11-13 CFD models. Note that, the internal area (10 mm^2) of the trapezoidal cavity is kept equal to the square cavity used by Khodadadi et al. (2007). The solidification time for Cases 11-13 and those from the literature are presented in Figure 5.8. The increase of the nanoparticle volume fractions decreases the solidification time of the nanofluids for all cases. For example, the total solidification time of the trapezoidal cavity (θ=2.72°) for ϕ=0 and 0.2 are about 2700s and 1300s, respectively. In general, the last 30% of the fluids needs about a half of the total solidification time before it completely solidifies and this is true for all cases. A possible reason for the reduction in solidification time with the dispersion of the solid nanoparticles is that, when there is a higher heat transfer rate of NEPCM, the crystal grows rapidly. It may also be due to the fact that less energy per unit mass of nanofluid is required to solidify it because of the lower latent heat of fusion.

Now, compare the trapezoidal cavity with the square cavity. The nanofluid requires less time to solidify completely in the trapezoidal cavity than in the square cavity. The solidification time in the trapezoidal cavity of θ = 2.72° filled with pure water is almost 10% less than that of water filled in a square cavity, while this time is approximately 5% and 8% less for the trapezoidal cavity of θ = 2.72° filled with nanoparticle volume fractions of 0.1 and 0.2 respectively. This enhancement of the heat transfer may be due to a higher surface area normal to the direction of heat transfer in the trapezoidal cavity than that in the square one. In other words, the length of the side walls of the trapezoidal cavity is higher than that of the side vertical walls of the square cavity.

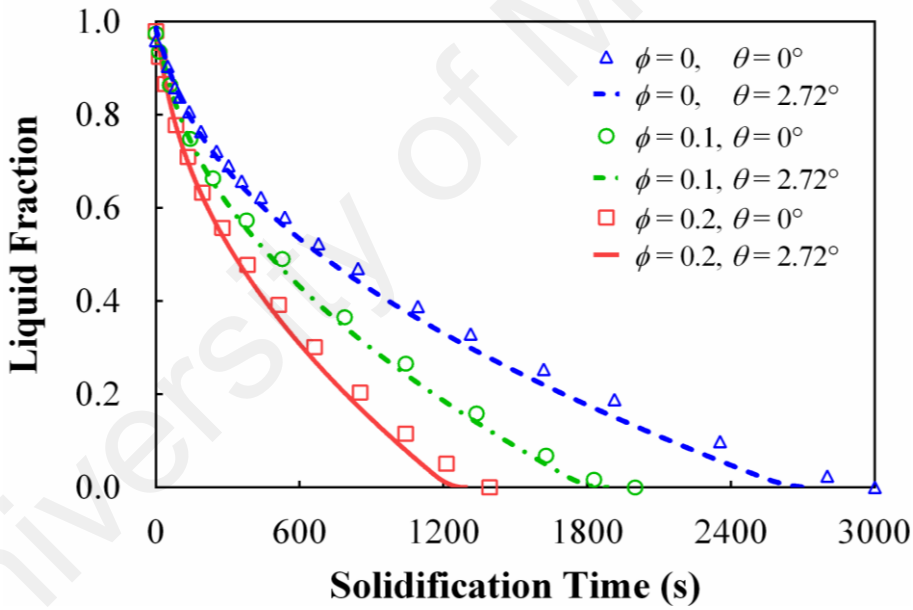

Figure 5.8 Effect of nanoparticle volume fraction on solidification time of nanofluid within the square and trapezoidal cavity of θ = 2.72°.

5.3.3.2 Effect of inclination angles

Figure 5.9 shows the effect of the inclination angle of the side walls, θ, on the solidification time for Cases 14-16, which are based on θ = 2.72°, 5.42° and 7.69°, ϕ = 0.2 and the temperature difference of 10 K. For a comparison, the total solidification

time of the nanofluid (ϕ = 0.2) under the same temperature difference in a square cavity is included in the Figure. Note that the internal area of the trapezoidal cavities of these cases and that of the square cavity were kept constant and equal to 10 mm^2. The solidification time of the nanofluid within the trapezoidal cavities decreases with the increase of θ. The total solidification time for the trapezoidal cavity of θ = 7.69° filled with nanofluid (ϕ = 0.2) is approximately 140s (11.3%) less than that for the square cavity. This may be because of the surface area that is normal to the direction of heat transfer increases with increase of θ, resulting in the enhanced heat transfer rate.

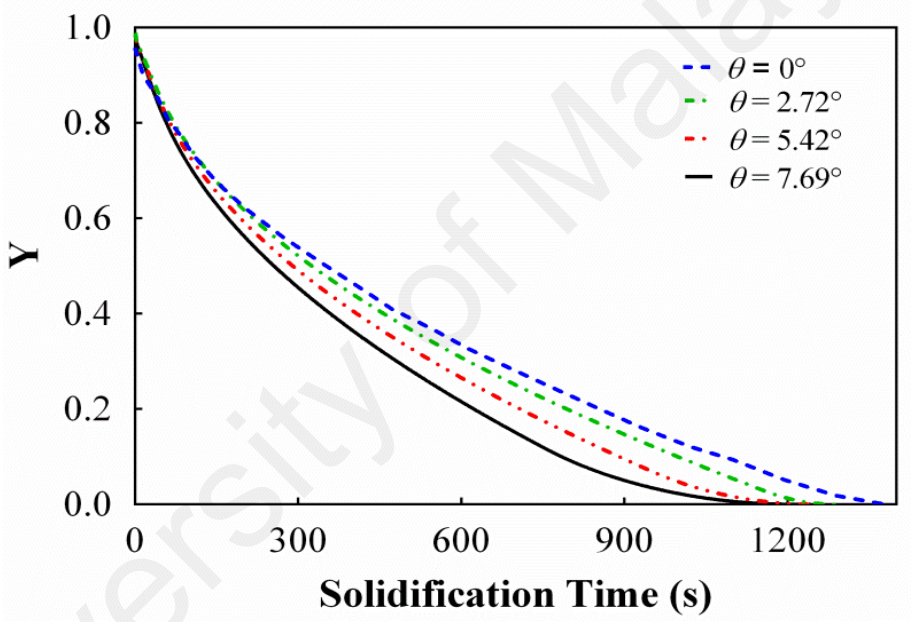

Figure 5.9 Effects of inclination angles on solidification time of nanofluid within a trapezoidal cavity at ΔT = 10° C and ϕ = 0.2

The heat transfer phenomenon for solidification consists of both conduction and convection energy transfer. To understand this phenomenon in the solidification of the nanofluid, the propagation of the solid-liquid interface for Cases 17, 18 and 19 are shown in Figure 5.10a, 5.10b and 5.10c, respectively at 10s, 100s, 300s, 600s, 900s and 1200s. In general, the higher the inclination angle of side walls, the quicker the phase front moves. For example, at 900s, the phase front has reached near the extreme left

corner of the cavity for the case of θ =7.69° (Figure 5.10c). However, this is not the same for the case of θ =2.72° (Figure 5.10a) where the phase front is yet to reach the left inclined side wall. The Figure also shows the apparent difference in phase velocities for all inclination angles and the solid-liquid interface is parallel to the cold wall which means the heat transfer in all these cases is consistently conduction dominated.

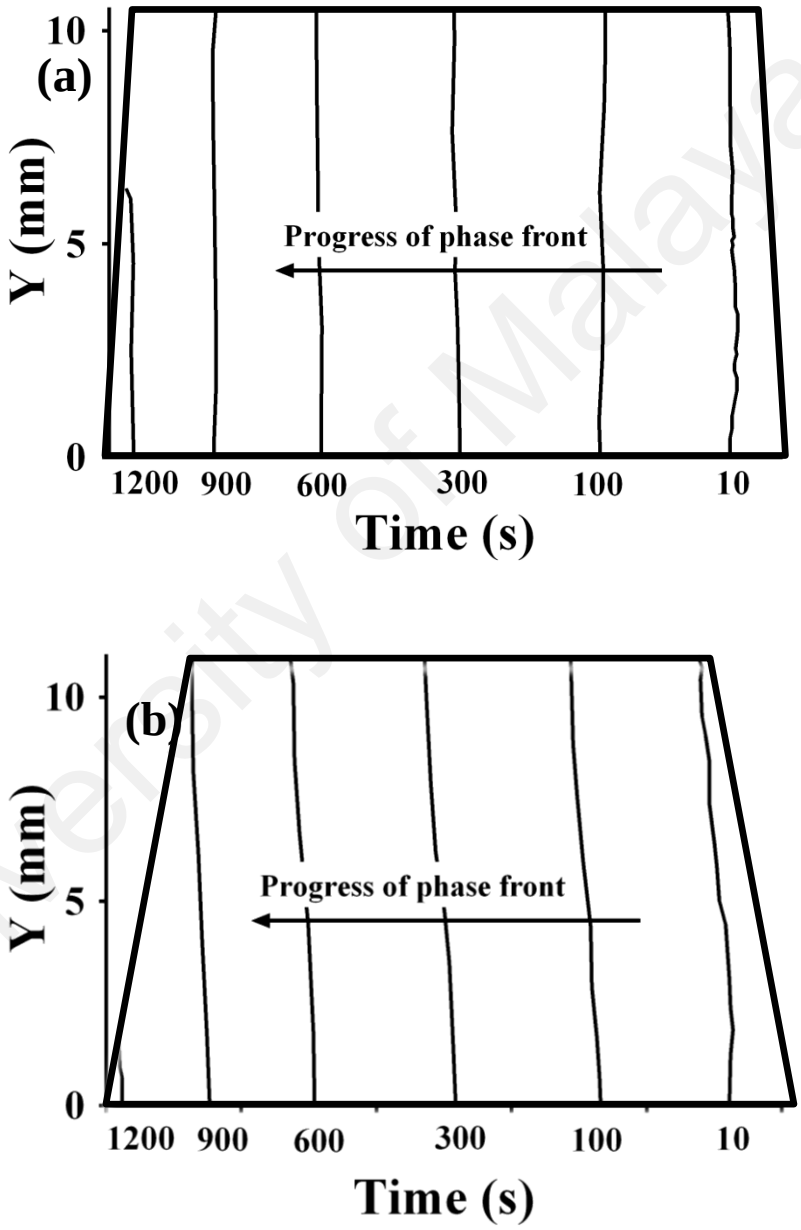

Figure 5.10 Solid – liquid interface position at different time during solidification process for temperature difference of 10°C and ϕ = 0.2. (a) θ = 2.72°

Figure 5.9 continued…

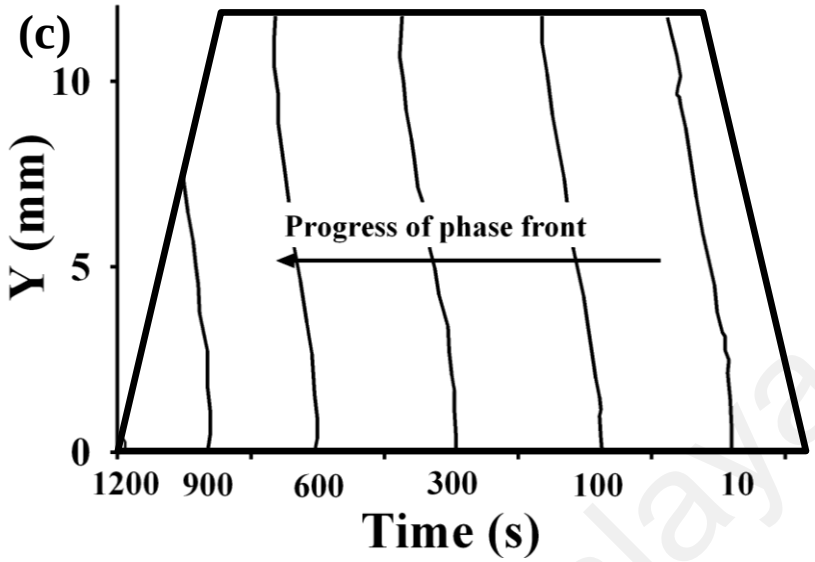

Figure 5.10 Solid – liquid interface position at different time during solidification process for temperature difference of 10°C and ϕ = 0.2. (a) θ = 2.72°, (b) θ = 5.42° and (c) θ = 7.69°.

Velocity vectors at a certain time during the solidification of pure water (ϕ = 0) are shown in Figure 5.11. Figure 5.11 (a) shows the velocity vectors at 200s for three inclination angles (θ = 2.72°, 5.42°, and 7.69°). The Figure shows that for a particular ΔT, the strength of circulation diminishes with increase in θ. This is due to the decrease in the vertical velocity with increase in θ. Instantaneous velocity vectors during the solidification of pure water filled in a cavity with θ = 7.69° are presented in Figure 5.11 (b). In the early time step of 50 s, two vortices nearly equal in size formed in the CW and CCW directions. As the solidification progresses this dual vortex structure persists but because the solid-liquid interface moves towards the left, both vortices shrink in covered space and their strength decays.

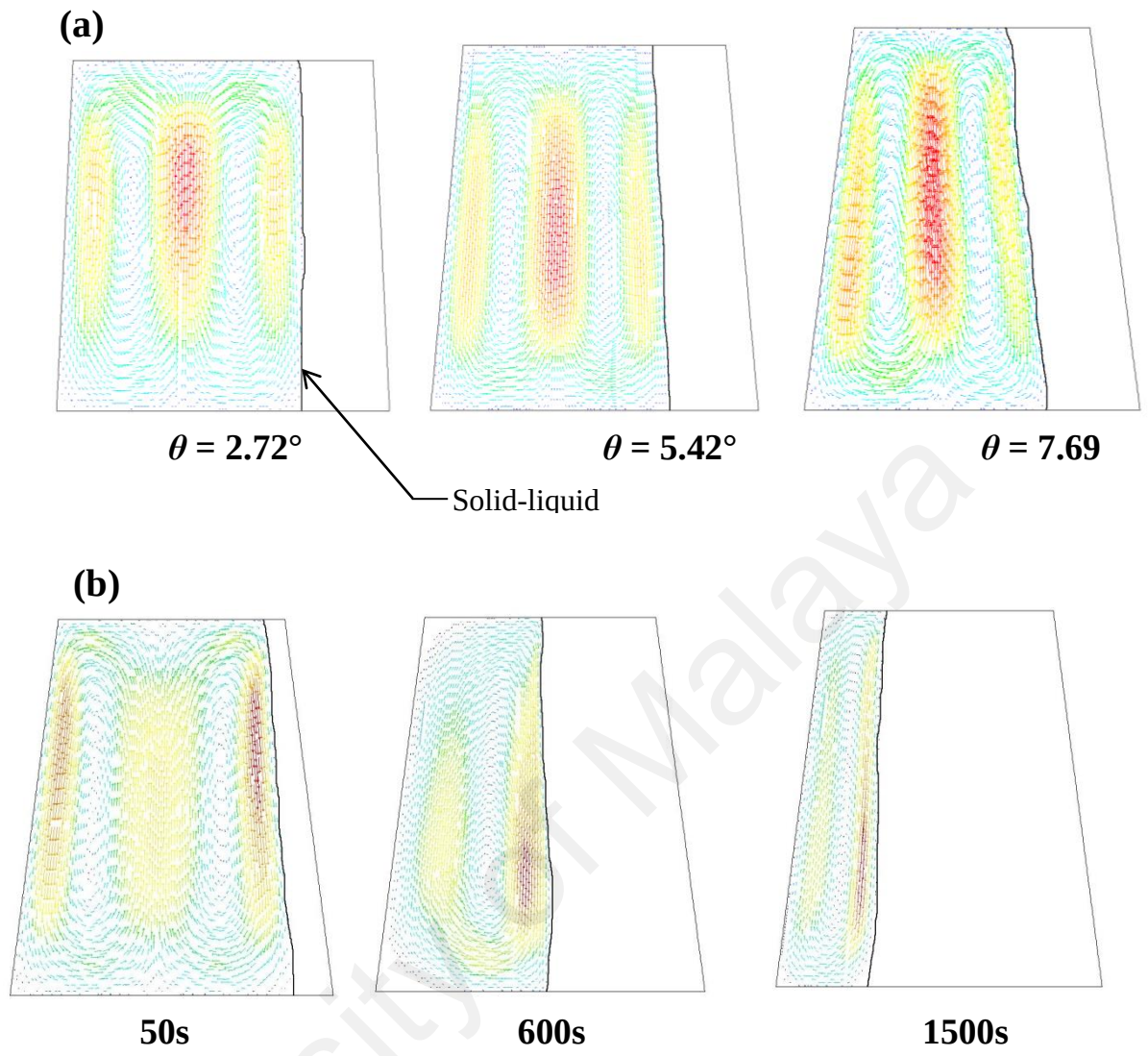

Figure 5.11 Velocity field for pure water (ϕ = 0), and temperature difference ΔT = 10 °C (a) at t = 200s, (b) for θ = 7.69 °

5.3.3.3 Effects of temperature difference and Grashof number

The variation of the liquid fraction against the solidification time of Cases 20-23, which are based on ϕ = 0.2 at five different temperature differences, ΔT = 10°, 20°, 30°, 55° and 110° in the trapezoidal cavity with inclination angle, θ = 2.72^{o} is shown in Figure 5.12. The increasing temperature difference consistently decreases the solidification time. Similar to the low temperature difference, the phase front moves parallel to the

cold wall for a large temperature difference of 110 °C as well, which signifies that conduction still dominates the heat transfer phenomenon as shown in Figure 5.13.

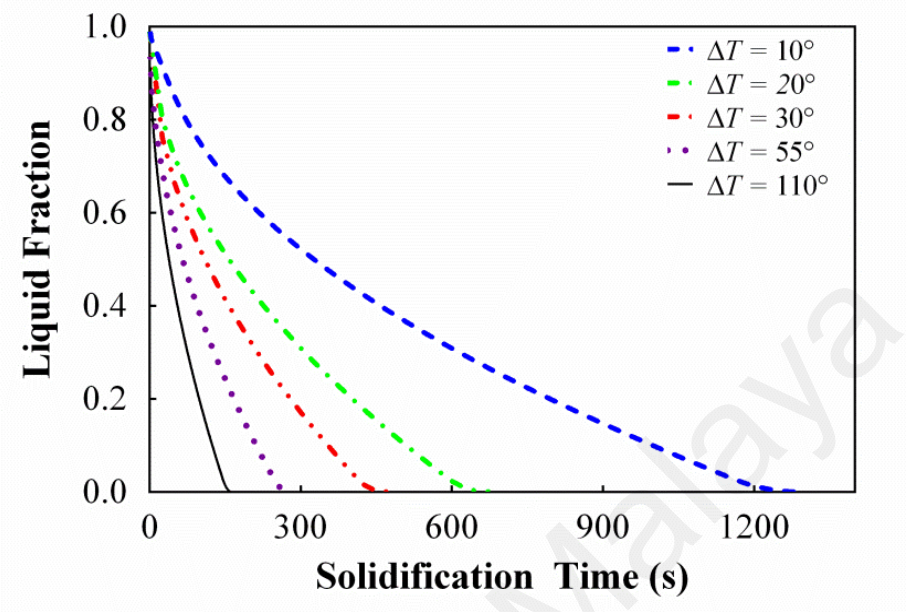

Figure 5.12 Effect of temperature difference on the solidification of nanofluid of nanoparticle volume fraction 0.2 inside cavity of θ = 2.72°.

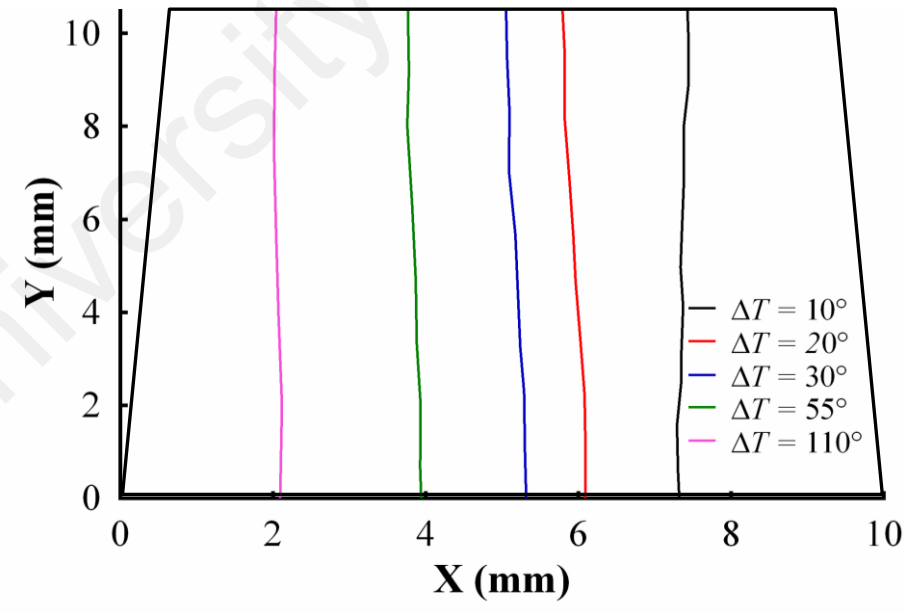

Figure 5.13 Effect of temperature difference on the solid-liquid interface at 100s during solidification of nanofluid of nanoparticle volume fraction 0.2 inside cavity of θ = 2.72°.

To study the effect of natural convection on heat transfer, the *Gr* is varied from 10^5 to 10^7 (Cases 24-26) and the results are shown in Figure 5.14. The Figure shows the solid-liquid interface at two different times (100s and 300s) during solidification for all three Grashof numbers. For $Gr \leq 10^5$ the solid-liquid interface is almost parallel to the cold wall and moves towards hot wall with uniform velocity until complete solidification from which conduction dominated heat flow can be inferred. As the *Gr* increases (10^6, and 10^7), buoyancy force increases within the liquid which causes the interface to deflect and rapid solidification appears in the lower half of the cavity compared to the upper half which indicates the natural convection dominated heat flow.

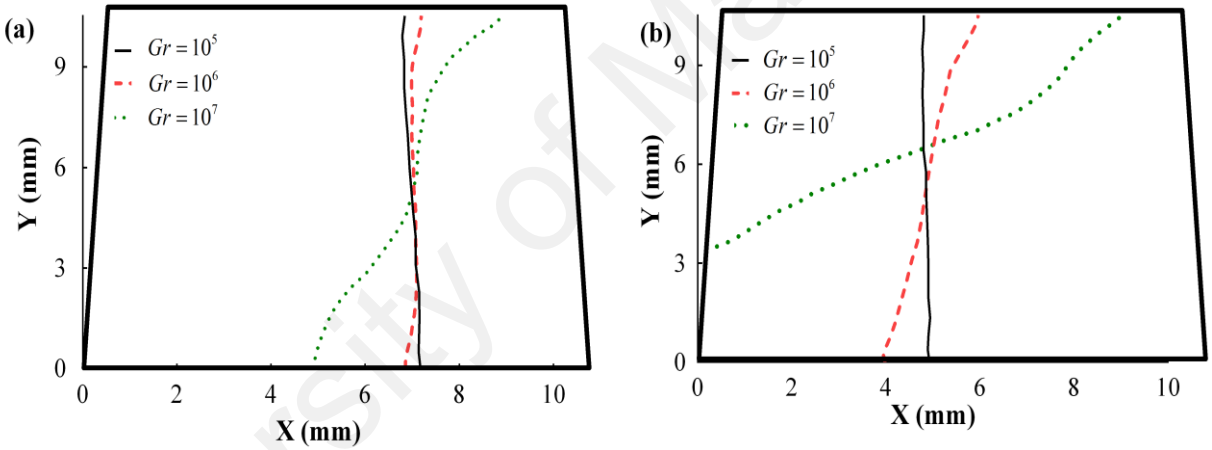

Figure 5.14 Solid – liquid interface position for ϕ = 0.2 and θ = 2.72° at (a) 100s, and (b) 300s.

5.3.3.4 Effect of Grashof number on Nusselt number

Figure 5.15 shows the variation of the average Nusselt number along the hot wall for Cases 27 - 62 where the Grashof number (*Gr*) is varied from 10^3 to 10^5, cavity inclination angles (θ) from 0^o to 7.69^o and nanoparticle volume fractions (ϕ) from 0 to 0.2. *Pr* = 6.2 are used in all these cases. The Nusselt number depends strongly on the inclination angle and it increases with the increasing angle. In general, the Nusselt number increases with an increase of the nanoparticle volume fractions and this occurs

for all Grashof numbers because the thermal conductivity of the nanofluid enhances with the void fraction. For low Grashof numbers ($<10^3$ and 10^4), the increase in the Nusselt number versus the angles is small because of the dominant conductive heat transfer but as we increase the Grashof number ($\geq 10^5$), the buoyancy-driven heat transfer dominates and a higher difference in Nusselt number versus the angle can be seen. It should be noted that the trend in the Figure for the average Nusselt number along the hot wall against the inclination angle would be downward if the Nusselt number is based on the effective thermal conductivity k_{eff}.

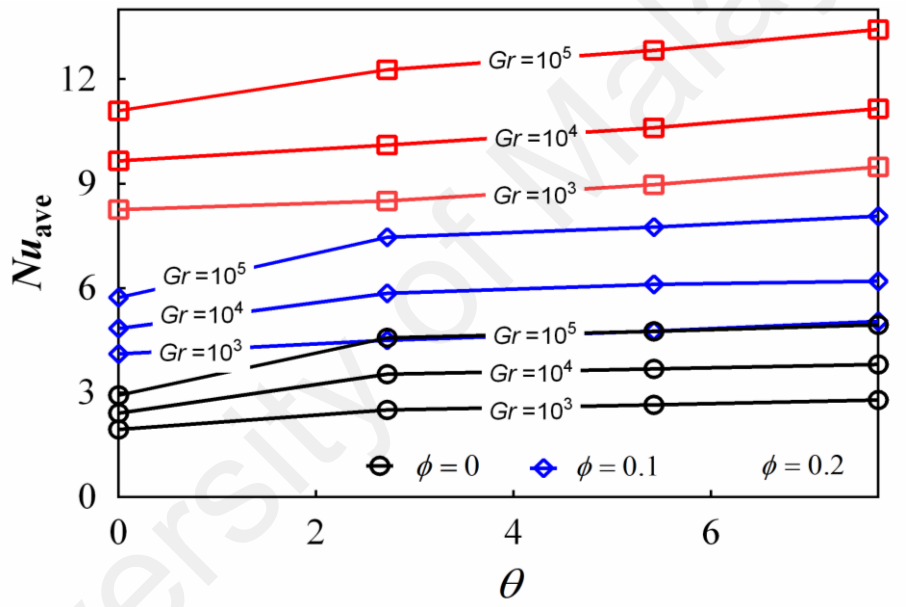

Figure 5.15 Effect of Grashof number, nanoparticle volume fraction and inclination angle on average Nusselt number for *Pr* = 6.2.

5.4 Summary

The solidification process of the nano-enhanced organic and inorganic phase change materials in the isosceles trapezoidal cavities has been studied using CFD. Various nanoparticle volume concentrations, inclination angles, and Grashof numbers have been considered to study their effect on the heat transfer. This study has the following conclusions:

- The heat transfer performance of NEPCM is significantly enhanced with the use of a trapezoidal cavity when compared to a square cavity having the same internal area.
- For the temperature difference of 10° C, and a small inclination angle (2.72°) in the side walls of square cavity decreases the solidification time of nanofluid of 20% nanoparticle volume fraction by approximately 7% while increasing the inclination angle to 5.42° and 7.69°, it reduces by 11% and 11.5% respectively. In short, the solidification time reduces with an increase of the inclination angle.
- NEPCM as used in the current study shows great ability to store/release the thermal energy in comparison to conventional PCMs. Increasing nanoparticle volume fraction decreases the solidification time.
- The heat transfer rate greatly depends upon the temperature difference and increasing temperature difference increases the heat transfer rate for all values of nanoparticle volume fractions and inclination angles but, the mode of heat transfer remains conduction.
- The mode of heat transfer depends on the value of the Grashof number. For low values of Gr ($\leq 10^5$), conduction is the main heat transfer mechanism while for higher values of Gr ($> 10^5$), heat transfer takes place majorly by convection.

CHAPTER 6: CONCLUSIONS AND FUTURE WORKS

6.1 Conclusions

The performance of four organic phase change materials during an accelerated thermal cycle test was investigated experimentally to assess their thermal energy storage capabilities. The changes in their thermal properties during the cycle test were monitored using the differential scanning calorimeter (DSC) and the changes in the compositional/functional group were studied using the Fourier transformation and infrared spectrometer (FT-IR). The results of this study and understating obtained from the literature review were used to prepare a novel nano-enhanced composite of an organic PCM and nano titanium dioxide (TiO_2) of various mass fractions. In addition, a novel geometry was also proposed for containing the PCMs for practical use. The output of this research can be summarized as follows:

The results of the accelerated thermal cycle test of paraffin, palmitic acid, myristic acid, and polyethylene glycol (PEG 6000) show that the organic PCMs are more stable than inorganic PCMs when they undergo a large number of melt/freeze cycles. In this study, a new organic PCM viz. polyethylene glycol (PEG) of molecular weight 6000 was also tested for a 1500 melt/freeze cycles and the variations in thermal and chemical properties were monitored. The results show that PEG 6000 is a potential candidate for low temperature solar thermal energy storage applications. The variations in the thermal properties of all four PCMs were not very much significant and this makes them highly suitable for many industrial and domestic energy storage devices. Also, the FT-IR results show that these PCMs do not lose their compositional/functional group for the 1500 thermal cycle test, which makes them chemically stable for long term use.

Dispersion of nanoparticles in the base PCM is a well-established way to enhance the thermal conductivity of organic PCMs. Nano particles of titanium dioxide (TiO_2) were dispersed in liquid palmitic acid (PA) in various mass fractions and the thermal properties of these composites were measured. It was observed that the thermal conductivity of palmitic acid increases with the increase in the mass fraction of nanoparticles at the slight expense of the latent heat of fusion. It was also observed that the addition of nano TiO_2 makes PA more stable thermally and chemically in comparison to the base PA. The XRD and FESEM images show the uniform dispersion and FT-IR spectra of composite PCMs exhibit the chemical compatibility of PA and nano TiO_2. The accelerated thermal cycle test of the nano enhanced organic PCM reveals the thermal reliability of the composite, which show the potential of energy storage capacity of these materials.

A novel trapezoidal geometry for encapsulation of organic/inorganic PCMs was also proposed and a detailed parametric study was carried out numerically using the CFD technique. The effect of the geometry aspect ratio in terms of the inclination angle of the geometry wall, cold wall temperature, nanoparticle mass fraction, Grashof number, etc. were investigated and discussed. The results of this study revealed that the geometry shape plays a very important role in improving the heat transfer process during the solidification/melting of PCMs. Trapezoidal geometry has shown the expedited heat transfer process which resulted in a reduced solidification time of the PCM. Grashof number was found to be an important factor for deciding the conduction and/or convection driven heat transfer process. This particular geometry can be very much suitable for solar water heating systems and mold casting processes.

6.2 Future works

This study mainly concentrated on the investigation of the thermal energy storage properties of organic and nano enhanced organic phase change materials. An accelerated thermal cycle test of paraffin, fatty acid and poly ethylene glycol was conducted and their thermal and chemical properties were investigated during the cycle test. This study can be extended by testing these materials for a longer number of thermal cycles. Glycols are the potential thermal energy storage materials, so new glycols and their eutectics can be tested for a large number thermal cycles in the future.

Another potential concept which can be investigated in the future is the use of a mixture of different nanoparticles as a dispersant for enhancing the thermal conductivity of organic PCMs. The major issue with nano composite PCMs is the leakage when they are in the liquid state. To avoid this issue, they need to be encapsulated properly to be prepared in form stable phase change materials which can also be investigated in the future. TiO_2 of micro size and other metal or metal oxides of micro size can be used to prepare form stable materials. Form stable phase change materials provide as advantage of not being encapsulated and avoid the requirement of encapsulation materials.

The shape of the container for holding the PCMs plays an important role as well. A careful selection of enclosure geometry can affect the heat transfer process in PCMs significantly. A trapezoidal shape for containing the PCMs has been investigated numerically in this study, which can further be extended for other irregular geometry too. A trapezoidal cavity with inbuilt fins inside can also be investigated as fins are able to enhance the heat transfer rate greatly. The numerical study of the solidification/melting phenomenon can be made more realistic by considering variable thermal properties of PCMs.

REFERENCES

13.0., ANSYS Fluent. (2011). User's Guide. *ANSYS Inc., USA*.

Abdollahzadeh, Jamalabadi MY, & Park, Jae Hyun. (2014). Effects of Brownian motion on freezing of PCM containing nanoparticles. *Thermal Science*(00), 94-94.

Abhat, A. (1983). Low temperature latent heat thermal energy storage: Heat storage materials. *Solar Energy, 30*(4), 313-332.

Abhat., A., Heine., D., Heinisch., M., Malatidis., A.N., & Neuer., G. (1981). Development of a modular heat exchanger with integrated latent heat energy store *Report no. BMFT FBT 81-050*. Institut fuer Kemtechnik und Energiewandlung e.V., Stuttgart, Germany,.

Agyenim, Francis, Hewitt, Neil, Eames, Philip, & Smyth, Mervyn. (2010). A review of materials, heat transfer and phase change problem formulation for latent heat thermal energy storage systems (LHTESS). *Renewable and Sustainable Energy Reviews, 14*(2), 615-628.

Ahmad, Maha, Bontemps, André, Sallée, Hébert, & Quenard, Daniel. (2006). Experimental investigation and computer simulation of thermal behaviour of wallboards containing a phase change material. *Energy and Buildings, 38*(4), 357-366.

Al-Hinti, I., Al-Ghandoor, A., Maaly, A., Abu Naqeera, I., Al-Khateeb, Z., & Al-Sheikh, O. (2010). Experimental investigation on the use of water-phase change material storage in conventional solar water heating systems. *Energy Conversion and Management, 51*(8), 1735-1740.

Ali Memon, Shazim, Yiu Lo, Tommy, Shi, Xian, Barbhuiya, Salim, & Cui, Hongzhi. (2013). Preparation, characterization and thermal properties of Lauryl alcohol/Kaolin as novel form-stable composite phase change material for thermal energy storage in buildings. *Applied Thermal Engineering, 59*(1–2), 336-347.

Alkan, Cemil. (2006). Enthalpy of melting and solidification of sulfonated paraffins as phase change materials for thermal energy storage. *Thermochimica Acta, 451*(1–2), 126-130.

Alkan, Cemil, Sarı, Ahmet, Karaipekli, Ali, & Uzun, Orhan. (2009). Preparation, characterization, and thermal properties of microencapsulated phase change material for thermal energy storage. *Solar Energy Materials and Solar Cells, 93*(1), 143-147.

Alkilani, Mahmud M., Sopian, K., Alghoul, M. A., Sohif, M., & Ruslan, M. H. (2011). Review of solar air collectors with thermal storage units. *Renewable and Sustainable Energy Reviews, 15*(3), 1476-1490.

Amin, NAM, Bruno, Frank, & Belusko, Martin. (2014). Effective thermal conductivity for melting in PCM encapsulated in a sphere. *Applied Energy, 122*, 280-287.

Amiri, A., & Vafai, K. (1994). Analysis of dispersion effects and non-thermal equilibrium, non-Darcian, variable porosity incompressible flow through porous media. *International Journal of Heat and Mass Transfer, 37*(6), 939-954.

Arasu, A. Valan, & Mujumdar, Arun S. (2012). Numerical study on melting of paraffin wax with Al2O3 in a square enclosure. *International Communications in Heat and Mass Transfer, 39*(1), 8-16.

Arico, Antonino Salvatore, Bruce, Peter, Scrosati, Bruno, Tarascon, Jean-Marie, & Van Schalkwijk, Walter. (2005). Nanostructured materials for advanced energy conversion and storage devices. *Nature materials, 4*(5), 366-377.

Assis, E., Katsman, L., Ziskind, G., & Letan, R. (2007). Numerical and experimental study of melting in a spherical shell. *International Journal of Heat and Mass Transfer, 50*(9–10), 1790-1804.

Athienitis, A. K., & Chen, Y. (2000). The effect of solar radiation on dynamic thermal performance of floor heating systems. *Solar Energy, 69*(3), 229-237.

Athienitis, A. K., Liu, C., Hawes, D., Banu, D., & Feldman, D. (1997). Investigation of the thermal performance of a passive solar test-room with wall latent heat storage. *Building and Environment, 32*(5), 405-410.

Atkinson, C. M. L., Larkin, J. A., & Richardson, M. J. (1969). Enthalpy changes in molten n-alkanes and polyethylene. *The Journal of Chemical Thermodynamics, 1*(5), 435-440.

Babapoor, Aziz, & Karimi, Gholamreza. (2015). Thermal properties measurement and heat storage analysis of paraffinnanoparticles composites phase change material: Comparison and optimization. *Applied Thermal Engineering, 90*, 945-951.

Bal, Lalit M., Satya, Santosh, & Naik, S. N. (2010). Solar dryer with thermal energy storage systems for drying agricultural food products: A review. *Renewable and Sustainable Energy Reviews, 14*(8), 2298-2314.

Bal, Lalit M., Satya, Santosh, Naik, S. N., & Meda, Venkatesh. (2011). Review of solar dryers with latent heat storage systems for agricultural products. *Renewable and Sustainable Energy Reviews, 15*(1), 876-880.

Bansal, N. K., & Buddhi, D. (1992). An analytical study of a latent heat storage system in a cylinder. *Energy Conversion and Management, 33*(4), 235-242.

Barry, Edward J. (1940). Solar water heater: US Patent 2,213,894.

Biswas, Kaushik, Lu, Jue, Soroushian, Parviz, & Shrestha, Som. (2014). Combined experimental and numerical evaluation of a prototype nano-PCM enhanced wallboard. *Applied Energy*(0).

Bouadila, Salwa, Fteïti, Mehdi, Oueslati, Mohamed Mehdi, Guizani, Amenallah, & Farhat, Abdelhamid. (2014). Enhancement of latent heat storage in a rectangular cavity: Solar water heater case study. *Energy Conversion and Management, 78*(0), 904-912.

Brent, A. D., Voller, V. R., & Reid, K. J. (1988). Enthalpy-porosity technique for modeling convection-diffusion phase change: application to the melting of a pure metal

Numerical Heat Transfer, 13(3), 297-318.

Brinkman, H.C. (1952). The Viscosity of concentrated suspensions and solutions the viscosity of concentrated suspensions and solutions. *J. Chem. Phys., 20*, 571-581.

Buddhi, D, Sawhney, RL, Sehgal, PN, & Bansal, NK. (1987). A simplification of the differential thermal analysis method to determine the latent heat of fusion of phase change materials. *Journal of Physics D: Applied Physics, 20*(12), 1601.

Buddhi., D., & Sawhney., R.L. (1994). In: Proceedings of thermal energy storage and energy conversion;.

Burchill, S. (1983). Smectite-polymer interactions in aqueous systems. *Clay Minerals, 18*(4), 373-397.

Butler, JL, & Troeger, JM. (1981). Drying peanuts using solar energy stored in a rock bed.

Cabeza, L. F., Castell, A., Barreneche, C., de Gracia, A., & Fernández, A. I. (2011). Materials used as PCM in thermal energy storage in buildings: A review. *Renewable and Sustainable Energy Reviews, 15*(3), 1675-1695.

Cabeza, L. F., Mehling, H., Hiebler, S., & Ziegler, F. (2002). Heat transfer enhancement in water when used as PCM in thermal energy storage. *Applied Thermal Engineering, 22*(10), 1141-1151.

Chaabane, Monia, Mhiri, Hatem, & Bournot, Philippe. (2014). Thermal performance of an integrated collector storage solar water heater (ICSSWH) with phase change materials (PCM). *Energy Conversion and Management, 78*(0), 897-903.

Chandrasekar, M., Suresh, S., & Chandra Bose, A. (2010). Experimental investigations and theoretical determination of thermal conductivity and viscosity of Al2O3/water nanofluid. *Experimental Thermal and Fluid Science, 34*(2), 210-216.

Chandrasekaran, P., Cheralathan, M., Kumaresan, V., & Velraj, R. (2014). Enhanced heat transfer characteristics of water based copper oxide nanofluid PCM (phase change material) in a spherical capsule during solidification for energy efficient cool thermal storage system. *Energy*(0).

Charvát, Pavel, Klimeš, Lubomír, & Ostrý, Milan. (2014). Numerical and experimental investigation of a PCM-based thermal storage unit for solar air systems. *Energy and Buildings, 68, Part A*(0), 488-497.

Chen, Changzhong, Wang, Linge, & Huang, Yong. (2011). Electrospun phase change fibers based on polyethylene glycol/cellulose acetate blends. *Applied Energy, 88*(9), 3133-3139.

Chen, Yin-Ju, Nguyen, Duc-Dung, Shen, Ming-Yuan, Yip, Ming-Chuen, & Tai, Nyan-Hwa. (2013). Thermal characterizations of the graphite nanosheets reinforced paraffin phase-change composites. *Composites Part A: Applied Science and Manufacturing, 44*, 40-46.

Chihara, Shoichi, Isaki, Tsutomu, Kakiuchi, Hiroyuki, & Yamazaki, Masanori. (1998). Heat storage material composition: Google Patents.

Cho, Jeong-Sook, Kwon, Aehwa, & Cho, Chang-Gi. (2002). Microencapsulation of octadecane as a phase-change material by interfacial polymerization in an emulsion system. *Colloid and Polymer Science, 280*(3), 260-266.

Choi, Da Hee, Lee, Juhyuk, Hong, Hiki, & Kang, Yong Tae. (2014). Thermal conductivity and heat transfer performance enhancement of phase change materials (PCM) containing carbon additives for heat storage application. *International Journal of Refrigeration, 42*, 112-120.

Choi, J. K., Lee, J. G., Kim, J. H., & Yang, H. S. (2001). Preparation of microcapsules containing phase change materials as heat transfer media by in-situ polymerization. *Journal of Industrial and Engineering Chemistry, 7*(6), 358-362.

Choi, S.U.S., & Eastman, J.A. (1995). *Enhancing thermal conductivity of fluids with nanoparticles*.

Constantinescu, M., Dumitrache, L., Constantinescu, D., Anghel, E. M., Popa, V. T., Stoica, A., & Olteanu, M. (2010). Latent heat nano composite building materials. *European Polymer Journal, 46*(12), 2247-2254.

Cui, Yanbin, Liu, Caihong, Hu, Shan, & Yu, Xun. (2011). The experimental exploration of carbon nanofiber and carbon nanotube additives on thermal behavior of phase change materials. *Solar Energy Materials and Solar Cells, 95*(4), 1208-1212.

D.V. Hale, M.J. Hoover, & O'Niell, M.J. (1971). *Phase Change Materials Hand-book.* AL: NASA CR-61363, Marshal Space Flight Center.

Das, M.K., & Ohal, P.S. (2009). Natural convection heat transfer augmentation in a partially heated and partially cooled square cavity utilizing nanofluids,. *International Journal of Numerical Methods for Heat & Fluid Flow, 19*(3/4), 411-311.

Das, S.K, Choi, S.U.S, Yu, W, & Pradeep, R. (2008). *Nanofluids: Science and Technology, .* Hoboken, NJ.

Delgado, Mónica, Lázaro, Ana, Mazo, Javier, & Zalba, Belén. (2012). Review on phase change material emulsions and microencapsulated phase change material slurries: Materials, heat transfer studies and applications. *Renewable and Sustainable Energy Reviews, 16*(1), 253-273.

Demirbas, M. Fatih. (2006). Thermal Energy Storage and Phase Change Materials: An Overview. *Energy Sources, Part B: Economics, Planning, and Policy, 1*(1), 85-95.

Desgrosseilliers, Louis, Whitman, Catherine A., Groulx, Dominic, & White, Mary Anne. (2013). Dodecanoic acid as a promising phase-change material for thermal energy storage. *Applied Thermal Engineering, 53*(1), 37-41.

Dimaano, Maria Natalia R., & Watanabe, Takayuki. (2002). The capric–lauric acid and pentadecane combination as phase change material for cooling applications. *Applied Thermal Engineering, 22*(4), 365-377.

Dincer, I., & Rosen, M.A. (2002). *Thermal energy storage, Systems and Aplications*. Chichester (England): John Wiley & Sons.

Duggirala, R. K., Lin, C. X., & Ghenai, C. (2006). Investigation of double-diffusive convection during the solidification of a binary mixture (NH4Cl–H2O) in a trapezoidal cavity. *Experiments in Fluids, 40*(6), 918-927.

Durupt, N., Aoulmi, A., Bouroukba, M., & Rogalski, M. (1995). Heat capacities of liquid polycyclic aromatic hydrocarbons. *Thermochimica Acta, 260*(0), 87-94.

Dutil, Yvan, Rousse, Daniel R., Salah, Nizar Ben, Lassue, Stéphane, & Zalewski, Laurent. (2011). A review on phase-change materials: Mathematical modeling and simulations. *Renewable and Sustainable Energy Reviews, 15*(1), 112-130.

Elefsiniotis, A, Becker, Th, & Schmid, U. (2014). Thermoelectric Energy Harvesting Using Phase Change Materials (PCMs) in High Temperature Environments in Aircraft. *Journal of Electronic Materials, 43*(6), 1809-1814.

Elsayed, Moustafa M, Taha, Ibrahim S, & Sabbagh, Jaffar A. (1994). *Design of solar thermal systems*: Scientific Publishing Center, King Abdulaziz University.

Enibe, S. O. (2002). Performance of a natural circulation solar air heating system with phase change material energy storage. *Renewable Energy, 27*(1), 69-86.

Enibe, S. O. (2003). Thermal analysis of a natural circulation solar air heater with phase change material energy storage. *Renewable Energy, 28*(14), 2269-2299.

Entrop, A. G., Brouwers, H. J. H., & Reinders, A. H. M. E. (2011). Experimental research on the use of micro-encapsulated Phase Change Materials to store solar

energy in concrete floors and to save energy in Dutch houses. *Solar Energy, 85*(5), 1007-1020.

Ettouney, Hisham, El-Dessouky, Hisham, & Al-Ali, Amani. (2005). Heat transfer during phase change of paraffin wax stored in spherical shells. *Journal of solar energy engineering, 127*(3), 357-365.

Faghri, Amir, & Zhang, Tuwen. (2006). *Transport phenomena in multiphase systems*. London, UK: Elsevier Inc.

Fan, Li-Wu, Fang, Xin, Wang, Xiao, Zeng, Yi, Xiao, Yu-Qi, Yu, Zi-Tao, . . . Cen, Ke-Fa. (2013). Effects of various carbon nanofillers on the thermal conductivity and energy storage properties of paraffin-based nanocomposite phase change materials. *Applied Energy, 110*(0), 163-172.

Fan, Li. Wu, Zhu, Zi. Qin, Zeng, Yi, Xiao, Yu. Qi, Liu, Xue. Ling, Wu, Yu. Yue, . . . Cen, Ke. Fa. (2015). Transient performance of a PCM-based heat sink with high aspect-ratio carbon nanofillers. *Applied Thermal Engineering, 75*, 532-540.

Fan, Liwu, & Khodadadi, J. M. (2011). Thermal conductivity enhancement of phase change materials for thermal energy storage: A review. *Renewable and Sustainable Energy Reviews, 15*(1), 24-46.

Fang, Xin, Fan, Li-Wu, Ding, Qing, Wang, Xiao, Yao, Xiao-Li, Hou, Jian-Feng, . . . Cen, Ke-Fa. (2013). Increased thermal conductivity of eicosane-based composite phase change materials in the presence of graphene nanoplatelets. *Energy & Fuels, 27*(7), 4041-4047.

Farid, Mohammed M., Khudhair, Amar M., Razack, Siddique Ali K., & Al-Hallaj, Said. (2004). A review on phase change energy storage: materials and applications. *Energy Conversion and Management, 45*(9–10), 1597-1615.

Farrell, Anthony J., Norton, Brian, & Kennedy, David M. (2006). Corrosive effects of salt hydrate phase change materials used with aluminium and copper. *Journal of Materials Processing Technology, 175*(1–3), 198-205.

Fath, Hassan ES. (1995). Thermal performance of a simple design solar air heater with built-in thermal energy storage system. *Energy Conversion and Management, 36*(10), 989-997.

Fauzi, Hadi, Metselaar, Hendrik S. C., Mahlia, T. M. I., Silakhori, Mahyar, & Nur, Hadi. (2013). Phase change material: Optimizing the thermal properties and thermal conductivity of myristic acid/palmitic acid eutectic mixture with acid-based surfactants. *Applied Thermal Engineering, 60*(1–2), 261-265.

Fazilati, Mohammad Ali, & Alemrajabi, Ali Akbar. (2013). Phase change material for enhancing solar water heater, an experimental approach. *Energy Conversion and Management, 71*(0), 138-145.

Feldman, D., Banu, D., & Hawes, D. (1995a). Low chain esters of stearic acid as phase change materials for thermal energy storage in buildings. *Solar Energy Materials and Solar Cells, 36*(3), 311-322.

Feldman, D., Banu, D., Hawes, D., & Ghanbari, E. (1991). Obtaining an energy storing building material by direct incorporation of an organic phase change material in gypsum wallboard. *Solar Energy Materials, 22*(2–3), 231-242.

Feldman, D., Banu, D., & Hawes, D. W. (1995b). Development and application of organic phase change mixtures in thermal storage gypsum wallboard. *Solar Energy Materials and Solar Cells, 36*(2), 147-157.

Feldman, D., Shapiro, M. M., Banu, D., & Fuks, C. J. (1989). Fatty acids and their mixtures as phase-change materials for thermal energy storage. *Solar Energy Materials, 18*(3–4), 201-216.

Feng, Li Li, Tong, Jing Jing, & Wang, Chong Yun. (2013). Preparation and Thermal Propertites of Polyethylene Glycol/Silica Hollow Nanospheres Composite as Shape-Stabilized Phase Change Materials. *Advanced Materials Research, 773*, 534-537.

Finke, H. L., Gross, M. E., Waddington, Guy, & Huffman, H. M. (1954). Low-temperature Thermal Data for the Nine Normal Paraffin Hydrocarbons from Octane to Hexadecane. *Journal of the American Chemical Society, 76*(2), 333-341.

Flejtuch, Kinga. (2004). Badanie przemian fazowych wybranych układów polieterów pod kątem akumulacji energii cieplnej.

Fukai, Jun, Hamada, Yuichi, Morozumi, Yoshio, & Miyatake, Osamu. (2002). Effect of carbon-fiber brushes on conductive heat transfer in phase change materials. *International Journal of Heat and Mass Transfer, 45*(24), 4781-4792.

Fukai, Jun, Kanou, Makoto, Kodama, Yoshikazu, & Miyatake, Osamu. (2000). Thermal conductivity enhancement of energy storage media using carbon fibers. *Energy Conversion and Management, 41*(14), 1543-1556.

Gau, C., & Viskanta, R. (1986). Melting and Solidification of a Pure Metal on a Vertical Wall. *Journal of Heat Transfer, 108*(1), 174-181.

George, A. (1989). *Handbook of thermal design*: McGraw Hill Book Co.

Goli, Pradyumna, Legedza, Stanislav, Dhar, Aditya, Salgado, Ruben, Renteria, Jacqueline, & Balandin, Alexander A. (2014). Graphene-enhanced hybrid phase change materials for thermal management of Li-ion batteries. *Journal of Power Sources, 248*, 37-43.

Gong, Zhen-Xiang, Devahastin, Sakamon, & Mujumdar, Arun S. (1999). Enhanced heat transfer in free convection-dominated melting in a rectangular cavity with an isothermal vertical wall. *Applied Thermal Engineering, 19*(12), 1237-1251.

Harikrishnan, S., Deenadhayalan, M., & Kalaiselvam, S. (2014). Experimental investigation of solidification and melting characteristics of composite PCMs for building heating application. *Energy Conversion and Management, 86*, 864-872.

Harikrishnan, S., Magesh, S., & Kalaiselvam, S. (2013). Preparation and thermal energy storage behaviour of stearic acid–TiO2 nanofluids as a phase change material for solar heating systems. *Thermochimica Acta, 565*, 137-145.

Hasan, A., & Sayigh, A. A. (1994). Some fatty acids as phase-change thermal energy storage materials. *Renewable Energy, 4*(1), 69-76.

Hasnain, S. M. (1998). Review on sustainable thermal energy storage technologies, Part I: heat storage materials and techniques. *Energy Conversion and Management, 39*(11), 1127-1138.

Hasnain, S.M. (1990). Latent heat thermal energy storage for solar heating applications. *PhD Thesis. University of Leeds*.

Hawes, D. W., Feldman, D., & Banu, D. (1993). Latent heat storage in building materials. *Energy and Buildings, 20*(1), 77-86.

Hawes, DW, Banu, D, & Feldman, D. (1992). The stability of phase change materials in concrete. *Solar energy materials and solar cells, 27*(2), 103-118.

Himran, Syukri, Suwono, Aryadi, & Mansoori, G. Ali. (1994). Characterization of Alkanes and Paraffin Waxes for Application as Phase Change Energy Storage Medium. *Energy Sources, 16*(1), 117-128.

Ho, C. J., Chen, M. W., & Li, Z. W. (2008). Numerical simulation of natural convection of nanofluid in a square enclosure: Effects due to uncertainties of viscosity and thermal conductivity. *International Journal of Heat and Mass Transfer, 51*(17–18), 4506-4516.

Ho, Ching Jenq, & Gao, JY. (2009). Preparation and thermophysical properties of nanoparticle-in-paraffin emulsion as phase change material. *International Communications in Heat and Mass Transfer, 36*(5), 467-470.

Hong, Hiki, Kim, Sun Kuk, & Kim, Yong-Shik. (2004). Accuracy improvement of T-history method for measuring heat of fusion of various materials. *International Journal of Refrigeration, 27*(4), 360-366.

Hormansdorfer, Gerd. (1989). Latent heat storage material and use thereof: Google Patents.

Hosseinizadeh, S. F., Darzi, A. A. Rabienataj, & Tan, F. L. (2012). Numerical investigations of unconstrained melting of nano-enhanced phase change material (NEPCM) inside a spherical container. *International Journal of Thermal Sciences, 51*(0), 77-83.

HP Garg, SC Mullick, & Bhargava, AK. (1985). *Solar thermal energy storage*: Dordrecht: Reidel Publishing Company.

Hwang, Yi-Jeong, Lee, Young-Ho, Oh, Chul, Jun, Young-Doo, & Oh, Seong-Geun. (2006). Preparation and characterization of PEG-grafted silica particles using emulsion. *Journal of Industrial and Engineering Chemistry, 12*(3), 380-386.

Ip, KCW., & Gates, JR. (2000). Thermal storage for sustainable dwellings. Maastricht, The Netherlands.

Ismail, K. A. R., Alves, C. L. F., & Modesto, M. S. (2001). Numerical and experimental study on the solidification of PCM around a vertical axially finned isothermal cylinder. *Applied Thermal Engineering, 21*(1), 53-77.

Jegadheeswaran, S., & Pohekar, Sanjay D. (2009). Performance enhancement in latent heat thermal storage system: A review. *Renewable and Sustainable Energy Reviews, 13*(9), 2225-2244.

Jeon, Jisoo, Lee, Jung-Hun, Seo, Jungki, Jeong, Su-Gwang, & Kim, Sumin. (2013). Application of PCM thermal energy storage system to reduce building energy consumption. *Journal of Thermal Analysis and Calorimetry, 111*(1), 279-288.

Jesumathy, Stella, Udayakumar, M, & Suresh, S. (2012). Experimental study of enhanced heat transfer by addition of CuO nanoparticle. *Heat and Mass Transfer, 48*(6), 965-978.

Jiang, Yanjiao, Hussain, Hazrat, & Kressler, Joerg. (2014). Poly (vinyl alcohol) Cryogel Formation Using Biocompatible Ice Nucleating Agents. *Macromolecular Materials and Engineering*.

Jiao, Changmei, Ji, Baohua, & Fang, Dong. (2012). Preparation and properties of lauric acid–stearic acid/expanded perlite composite as phase change materials for thermal energy storage. *Materials Letters, 67*(1), 352-354.

Jurinak, J. J., & Abdel-Khalik, S. I. (1978). Properties optimization for phase-change energy storage in air-based solar heating systems. *Solar Energy, 21*(5), 377-383.

Jurinak, J. J., & Abdel-Khalik, S. I. (1979a). On the performance of air-based solar heating systems utilizing phase-change energy storage. *Energy, 4*(4), 503-522.

Jurinak, J. J., & Abdel-Khalik, S. I. (1979b). Sizing phase-change energy storage units for air-based solar heating systems. *Solar Energy, 22*(4), 355-359.

Kaizawa, Akihide, Maruoka, Nobuhiro, Kawai, Atsushi, Kamano, Hiroomi, Jozuka, Tetsuji, Senda, Takeshi, & Akiyama, Tomohiro. (2008). Thermophysical and heat transfer properties of phase change material candidate for waste heat transportation system. *Heat and Mass Transfer, 44*(7), 763-769.

Kakiuchi, H, Yamazaki, M, Yabe, M, Chihara, S, Terunuma, T, Sakata, Y, & Usami, T. (1998). A study of erythritol as phase change material. *IEA Annex, 10*, 11-13.

Kannan, Ruben Y, Salacinski, Henryk J, Butler, Peter E, & Seifalian, Alexander M. (2005). Polyhedral oligomeric silsesquioxane nanocomposites: the next generation material for biomedical applications. *Accounts of chemical research, 38*(11), 879-884.

Karaıpeklı, A., Sarı, A., & Kaygusuz, K. (2009). Thermal Properties and Thermal Reliability of Capric Acid/Stearic Acid Mixture for Latent Heat Thermal Energy Storage. *Energy Sources, Part A: Recovery, Utilization, and Environmental Effects, 31*(3), 199-207.

Karaipekli, Ali, & Sarı, Ahmet. (2010). Preparation, thermal properties and thermal reliability of eutectic mixtures of fatty acids/expanded vermiculite as novel form-stable composites for energy storage. *Journal of Industrial and Engineering Chemistry, 16*(5), 767-773.

Karthikeyan, S., Ravikumar Solomon, G., Kumaresan, V., & Velraj, R. (2014). Parametric studies on packed bed storage unit filled with PCM encapsulated spherical containers for low temperature solar air heating applications. *Energy Conversion and Management, 78*(0), 74-80.

Kaygusuz, Kamıl. (2000). Experimental and theoretical investigation of a solar heating system with heat pump. *Renewable Energy, 21*(1), 79-102.

Ke, Huizhen, Li, Dawei, Zhang, Huidan, Wang, Xiaoling, Cai, Yibing, Huang, Fenglin, & Wei, Qufu. (2013). Electrospun form-stable phase change composite nanofibers consisting of capric acid-based binary fatty acid eutectics and polyethylene terephthalate. *Fibers and Polymers, 14*(1), 89-99.

Kenisarin, Murat M. (2010). High-temperature phase change materials for thermal energy storage. *Renewable and Sustainable Energy Reviews, 14*(3), 955-970.

Kenisarin, Murat, & Mahkamov, Khamid. (2007). Solar energy storage using phase change materials. *Renewable and Sustainable Energy Reviews, 11*(9), 1913-1965.

Kenisarin, Murat, & Mahkamov, Khamid. (2016). Salt hydrates as latent heat storage materials:Thermophysical properties and costs. *Solar Energy Materials and Solar Cells, 145, Part 3*, 255-286.

Khalifa, Abdul Jabbar N., Suffer, Kadhim H., & Mahmoud, Mahmoud Sh. (2013). A storage domestic solar hot water system with a back layer of phase change material. *Experimental Thermal and Fluid Science, 44*(0), 174-181.

Khanafer, Khalil, Vafai, Kambiz, & Lightstone, Marilyn. (2003). Buoyancy-driven heat transfer enhancement in a two-dimensional enclosure utilizing nanofluids. *International Journal of Heat and Mass Transfer, 46*(19), 3639-3653.

Khateeb, Siddique A., Farid, Mohammed M., Selman, J. Robert, & Al-Hallaj, Said. (2004). Design and simulation of a lithium-ion battery with a phase change

material thermal management system for an electric scooter. *Journal of Power Sources, 128*(2), 292-307.

Khodadadi, J. M., & Hosseinizadeh, S. F. (2007). Nanoparticle-enhanced phase change materials (NEPCM) with great potential for improved thermal energy storage. *International Communications in Heat and Mass Transfer, 34*(5), 534-543.

Khudhair, Amar M., & Farid, Mohammed M. (2004). A review on energy conservation in building applications with thermal storage by latent heat using phase change materials. *Energy Conversion and Management, 45*(2), 263-275.

Kim, KH, Kim, HK, Park, CW, Peck, JH, & Kang, CD. (2011). Experimental Study on Melting/solidification of adjoining Two Different PCMs in a Concentric Vertical Cylinder. *Proceedings of the KSME*, 130-135.

Konuklu, Yeliz, Unal, Murat, & Paksoy, Halime O. (2014). Microencapsulation of caprylic acid with different wall materials as phase change material for thermal energy storage. *Solar Energy Materials and Solar Cells, 120*, 536-542.

Kuznik, Frédéric, David, Damien, Johannes, Kevyn, & Roux, Jean-Jacques. (2011). A review on phase change materials integrated in building walls. *Renewable and Sustainable Energy Reviews, 15*(1), 379-391.

Kuznik, Frédéric, & Virgone, Joseph. (2009). Experimental assessment of a phase change material for wall building use. *Applied Energy, 86*(10), 2038-2046.

Kuznik, Frédéric, Virgone, Joseph, & Johannes, Kevyn. (2011). In-situ study of thermal comfort enhancement in a renovated building equipped with phase change material wallboard. *Renewable Energy, 36*(5), 1458-1462.

Lane, G.A. (1983). *Solar Heat Storage:Latent Heat Materials, Vol. I* (Vol. I). Florida: CRC Press, Inc.

Lane, G.A. (1986). *Solar Heat Storage:Latent Heat Materials, Vol. II, Technology*. Florida: CRC Press.

Lane, George A. (1980). Low temperature heat storage with phase change materials. *International Journal of Ambient Energy, 1*(3), 155-168.

Li, Hairong, Jiang, Ming, Li, Qi, Li, Denian, Chen, Zongyi, Hu, Waping, . . . Xie, Haian. (2013). Aqueous preparation of polyethylene glycol/sulfonated graphene phase change composite with enhanced thermal performance. *Energy Conversion and Management, 75*, 482-487.

Li, Min. (2013). A nano-graphite/paraffin phase change material with high thermal conductivity. *Applied Energy, 106*(0), 25-30.

Li, Wei, Zhang, Rong, Jiang, Nan, Tang, Xiao-fen, Shi, Hai-feng, Zhang, Xing-xiang, . . . Zhang, Ningxin. (2013). Composite macrocapsule of phase change materials/expanded graphite for thermal energy storage. *Energy, 57*, 607-614.

Li, Z, Sun, WG, Wang, G, & Wu, ZG. (2014). Experimental and numerical study on the effective thermal conductivity of paraffin/expanded graphite composite. *Solar Energy Materials and Solar Cells, 128*, 447-455.

Lin, Kunping, Zhang, Yinping, Xu, Xu, Di, Hongfa, Yang, Rui, & Qin, Penghua. (2005). Experimental study of under-floor electric heating system with shape-stabilized PCM plates. *Energy and Buildings, 37*(3), 215-220.

Liu, Cheng, Yuan, Yanping, Zhang, Nan, Cao, Xiaoling, & Yang, Xiaojiao. (2014). A novel PCM of lauric–myristic–stearic acid/expanded graphite composite for thermal energy storage. *Materials Letters, 120*(0), 43-46.

Liu, Ming, Saman, Wasim, & Bruno, Frank. (2012). Review on storage materials and thermal performance enhancement techniques for high temperature phase change thermal storage systems. *Renewable and Sustainable Energy Reviews, 16*(4), 2118-2132.

Lopez, Jérôme, Caceres, Gustavo, Palomo Del Barrio, Elena, & Jomaa, Wahbi. (2010). Confined melting in deformable porous media: A first attempt to explain the graphite/salt composites behaviour. *International Journal of Heat and Mass Transfer, 53*(5–6), 1195-1207.

Lorsch, H.G. , Kauffman, K.W. , & Denton, J.C. . (1976). Thermal energy storage for heating and air conditioning, future energy production system. *Heat and Mass Transfer, 1*, 69-85.

Lorsch, Harold G, Kauffman, Kenneth W, & Denton, Jesse C. (1975). Thermal energy storage for solar heating and off-peak air conditioning. *Energy conversion, 15*(1), 1-8.

M. Zábranský, V. Růžička, V. Major, & Domalski., E.S. (1996). Heat capacity of liquids: critical review and recommended values. *Journal of Physical and Chemical Reference Data*.

Ma, Biao, Adhikari, Sanjeev, Chang, Yujiao, Ren, Junping, Liu, Jiang, & You, Zhanping. (2013). Preparation of composite shape-stabilized phase change materials for highway pavements. *Construction and Building Materials, 42*, 114-121.

Mahdaoui, M, Kousksou, T, Blancher, S, Ait Msaad, A, El Rhafiki, T, & Mouqallid, M. (2014). A numerical analysis of solid–liquid phase change heat transfer around a horizontal cylinder. *Applied Mathematical Modelling, 38*(3), 1101-1110.

Mahfuz, M. H., Anisur, M. R., Kibria, M. A., Saidur, R., & Metselaar, I. H. S. C. (2014). Performance investigation of thermal energy storage system with Phase Change Material (PCM) for solar water heating application. *International Communications in Heat and Mass Transfer, 57*(0), 132-139.

Mathur, Sharad, & Moudgil, Brij Mohan. (1997). Adsorption mechanism (s) of poly (ethylene oxide) on oxide surfaces. *Journal of colloid and interface science, 196*(1), 92-98.

Mazman, Muhsin, Cabeza, Luisa F., Mehling, Harald, Nogues, Miquel, Evliya, Hunay, & Paksoy, Halime Ö. (2009). Utilization of phase change materials in solar domestic hot water systems. *Renewable Energy, 34*(6), 1639-1643.

Mehling, Herald, & Cabeza, Luisa F. (2008). *Heat and cold storage with PCM: An up to date introduction into basics and applications*. Berlin Heidelberg: Springer-Verlag.

Mehrali, Mohammad, Latibari, Sara Tahan, Mehrali, Mehdi, Metselaar, Hendrik Simon Cornelis, & Silakhori, Mahyar. (2013). Shape-stabilized phase change materials with high thermal conductivity based on paraffin/graphene oxide composite. *Energy Conversion and Management, 67*, 275-282.

Memon, Shazim Ali, Lo, Tommy Yiu, Barbhuiya, S. A., & Xu, Weiting. (2013). Development of form-stable composite phase change material by incorporation of dodecyl alcohol into ground granulated blast furnace slag. *Energy and Buildings, 62*(0), 360-367.

Meng, Qinghao, & Hu, Jinlian. (2008). A poly(ethylene glycol)-based smart phase change material. *Solar Energy Materials and Solar Cells, 92*(10), 1260-1268.

Meng, Xin, Zhang, Huanzhi, Sun, Lixian, Xu, Fen, Jiao, Qingzhu, Zhao, Ziming, . . . Liu, Yingliang. (2013). Preparation and thermal properties of fatty acids/CNTs composite as shape-stabilized phase change materials. *Journal of Thermal Analysis and Calorimetry, 111*(1), 377-384.

Messerly, John F., Guthrie, George B., Todd, Samuel S., & Finke, Herman L. (1967). Low-temperature thermal data for pentane, n-heptadecane, and n-octadecane. Revised thermodynamic functions for the n-alkanes, C5-C18. *Journal of Chemical & Engineering Data, 12*(3), 338-346.

Mettawee, Eman-Bellah S., & Assassa, Ghazy M. R. (2006). Experimental study of a compact PCM solar collector. *Energy, 31*(14), 2958-2968.

Mills, Andrew, Farid, Mohammed, Selman, J. R., & Al-Hallaj, Said. (2006). Thermal conductivity enhancement of phase change materials using a graphite matrix. *Applied Thermal Engineering, 26*(14–15), 1652-1661.

Moeini Sedeh, Mahmoud, & Khodadadi, J. M. (2013). Thermal conductivity improvement of phase change materials/graphite foam composites. *Carbon, 60*(0), 117-128.

Morrison, D. J., & Abdel-Khalik, S. I. (1978). Effects of phase-change energy storage on the performance of air-based and liquid-based solar heating systems. *Solar Energy, 20*(1), 57-67.

Motahar, Sadegh, Nikkam, Nader, Alemrajabi, Ali A, Khodabandeh, Rahmatollah, Toprak, Muhammet S, & Muhammed, Mamoun. (2014a). Experimental investigation on thermal and rheological properties of n-octadecane with dispersed TiO 2 nanoparticles. *International Communications in Heat and Mass Transfer, 59*, 68-74.

Motahar, Sadegh, Nikkam, Nader, Alemrajabi, Ali A, Khodabandeh, Rahmatollah, Toprak, Muhammet S, & Muhammed, Mamoun. (2014b). A novel phase change material containing mesoporous silica nanoparticles for thermal storage: a study on thermal conductivity and viscosity. *International Communications in Heat and Mass Transfer, 56*, 114-120.

Neeper, D. A. (2000). Thermal dynamics of wallboard with latent heat storage. *Solar Energy, 68*(5), 393-403.

Nkwetta, Dan Nchelatebe, & Haghighat, Fariborz. (2014). Thermal energy storage with phase change material—A state-of-the art review. *Sustainable Cities and Society, 10*(0), 87-100.

Nkwetta, Dan Nchelatebe, Vouillamoz, Pierre-Edouard, Haghighat, Fariborz, El-Mankibi, Mohamed, Moreau, Alain, & Daoud, Ahmed. (2014). Impact of phase change materials types and positioning on hot water tank thermal performance: Using measured water demand profile. *Applied Thermal Engineering, 67*(1–2), 460-468.

Oliver, Alicia. (2012). Thermal characterization of gypsum boards with PCM included: Thermal energy storage in buildings through latent heat. *Energy and Buildings, 48*(0), 1-7.

Ona, Erwin P, Zhang, Xuemei, Kyaw, Kyaw, Watanabe, Fujio, Matsuda, Hitoki, Kakiuchi, Hiroyuki, . . . Chihara, Shouichi. (2001). Relaxation of Supercooling of Erythritol for Latent Heat Storage. *Journal of chemical engineering of Japan, 34*(3), 376-382.

Pan, Lin, Tao, Quanhong, Zhang, Shudong, Wang, Shuangshuang, Zhang, Jian, Wang, Suhua, . . . Zhang, Zhongping. (2012). Preparation, characterization and thermal properties of micro-encapsulated phase change materials. *Solar Energy Materials and Solar Cells, 98*(0), 66-70.

Paris, Jean, Falardeau, Michel, & Villeneuve, CÉCile. (1993). Thermal Storage by Latent Heat: A Viable Option for Energy Conservation in Buildings. *Energy Sources, 15*(1), 85-93.

Parks, George S., Moore, George E., Renquist, Melvin L., Naylor, Benjamin F., McClaine, Leslie A., Fujii, Paul S., & Hatton, John A. (1949). Thermal Data on Organic Compounds. XXV. Some Heat Capacity, Entropy and Free Energy Data for Nine Hydrocarbons of High Molecular Weight. *Journal of the American Chemical Society, 71*(10), 3386-3389.

Parks, George S., West, Theo J., Naylor, Benjamin F., Fujii, Paul S., & McClaine, Leslie A. (1946). Thermal Data on Organic Compounds. XXIII. Modern Combustion Data for Fourteen Hydrocarbons and Five Polyhydroxy Alcohols. *Journal of the American Chemical Society, 68*(12), 2524-2527.

Peck, Jong Hyeon, Kim, Jae-Jun, Kang, Chaedong, & Hong, Hiki. (2006). A study of accurate latent heat measurement for a PCM with a low melting temperature using T-history method. *International journal of refrigeration, 29*(7), 1225-1232.

Pielichowska, K., Głowinkowski, S., Lekki, J., Biniaś, D., Pielichowski, K., & Jenczyk, J. (2008). PEO/fatty acid blends for thermal energy storage materials. Structural/morphological features and hydrogen interactions. *European Polymer Journal, 44*(10), 3344-3360.

Pielichowska, Kinga, & Pielichowski, Krzysztof. (2014). Phase change materials for thermal energy storage. *Progress in Materials Science, 65*(0), 67-123.

Pielichowski, Krzysztof, & Flejtuch, Kinga. (2003a). Binary blends of polyethers with fatty acids: a thermal characterization of the phase transitions. *Journal of applied polymer science, 90*(3), 861-870.

Pielichowski, Krzysztof, & Flejtuch, Kinga. (2003b). Differential Scanning Calorimetry Study of Blends of Poly(ethylene glycol) with Selected Fatty Acids. *Macromolecular Materials and Engineering, 288*(3), 259-264.

Pielichowski, Krzysztof, & Flejtuch, Kinga. (2005). Recent developments in polymeric phase change materials for energy storage: poly (ethylene oxide)/stearic acid blends. *Polymers for advanced technologies, 16*(2-3), 127-132.

Porisini, Fernanda Coen. (1988). Salt hydrates used for latent heat storage: corrosion of metals and reliability of thermal performance. *Solar Energy, 41*(2), 193-197.

Prakash, J., Garg, H. P., & Datta, G. (1985). A solar water heater with a built-in latent heat storage. *Energy Conversion and Management, 25*(1), 51-56.

Py, Xavier, Olives, Régis, & Mauran, Sylvain. (2001). Paraffin/porous-graphite-matrix composite as a high and constant power thermal storage material. *International Journal of Heat and Mass Transfer, 44*(14), 2727-2737.

Rathod, Manish K., & Banerjee, Jyotirmay. (2013). Thermal stability of phase change materials used in latent heat energy storage systems: A review. *Renewable and Sustainable Energy Reviews, 18*(0), 246-258.

Regin, A. Felix, Solanki, S. C., & Saini, J. S. (2008). Heat transfer characteristics of thermal energy storage system using PCM capsules: A review. *Renewable and Sustainable Energy Reviews, 12*(9), 2438-2458.

Reyes, Alejandro, Mahn, Andrea, & Vásquez, Francisco. (2014). Mushrooms dehydration in a hybrid-solar dryer, using a phase change material. *Energy Conversion and Management, 83*(0), 241-248.

Rozanna, D., Chuah, T. G., Salmiah, A., Choong, Thomas S. Y., & Sa'ari, M. (2005). Fatty Acids as Phase Change Materials (PCMs) for Thermal Energy Storage: A Review. *International Journal of Green Energy, 1*(4), 495-513.

Sadhishkumar, S, & Balusamy, T. (2014). Performance improvement in solar water heating systems—A review. *Renewable and Sustainable Energy Reviews, 37*, 191-198.

Salyer, Ival O. (2000). Water heating unit with integral thermal energy storage: Google Patents.

Sari, Ahmet. (2005). Eutectic mixtures of some fatty acids for low temperature solar heating applications: Thermal properties and thermal reliability. *Applied Thermal Engineering, 25*(14), 2100-2107.

Sarı, Ahmet. (2003). Thermal reliability test of some fatty acids as PCMs used for solar thermal latent heat storage applications. *Energy Conversion and Management, 44*(14), 2277-2287.

Sarı, Ahmet. (2014). Composites of polyethylene glycol (PEG600) with gypsum and natural clay as new kinds of building PCMs for low temperature-thermal energy storage. *Energy and Buildings, 69*(0), 184-192.

Sarı, Ahmet, Alkan, Cemil, Karaipekli, Ali, & Uzun, Orhan. (2009). Microencapsulated n-octacosane as phase change material for thermal energy storage. *Solar Energy, 83*(10), 1757-1763.

Sarı, Ahmet, & Karaipekli, Ali. (2007). Thermal conductivity and latent heat thermal energy storage characteristics of paraffin/expanded graphite composite as phase change material. *Applied Thermal Engineering, 27*(8–9), 1271-1277.

Sarı, Ahmet, Karaipekli, Ali, & Alkan, Cemil. (2009). Preparation, characterization and thermal properties of lauric acid/expanded perlite as novel form-stable composite phase change material. *Chemical Engineering Journal, 155*(3), 899-904.

Sari, Ahmet, & Kaygusuz, Kamil. (2001). Thermal performance of myristic acid as a phase change material for energy storage application. *Renewable Energy, 24*(2), 303-317.

Sari, Ahmet, & Kaygusuz, Kamil. (2002a). Thermal performance of a eutectic mixture of lauric and stearic acids as PCM encapsulated in the annulus of two concentric pipes. *Solar Energy, 72*(6), 493-504.

Sari, Ahmet, & Kaygusuz, Kamil. (2002b). Thermal performance of palmitic acid as a phase change energy storage material. *Energy Conversion and Management, 43*(6), 863-876.

Sari, Ahmet, & Kaygusuz, Kamil. (2006). Thermal Energy Storage Characteristics of Myristic and Stearic Acids Eutectic Mixture for Low Temperature Heating Applications1. *Chinese Journal of Chemical Engineering, 14*(2), 270-275.

Sari, Ahmet, & Kaygusuz, Kamİl. (2001). Thermal energy storage system using stearic acid as a phase change material. *Solar Energy, 71*(6), 365-376.

Sari, Ahmet, Sari, Hayati, & Önal, Adem. (2004). Thermal properties and thermal reliability of eutectic mixtures of some fatty acids as latent heat storage materials. *Energy conversion and management, 45*(3), 365-376.

Sarier, Nihal, & Onder, Emel. (2012). Organic phase change materials and their textile applications: An overview. *Thermochimica Acta, 540*(0), 7-60.

Shabtay, Yoram L, & Black, John RH. (2014). Compact Hot Water Storage Systems Combining Copper Tube with High Conductivity Graphite and Phase Change Materials. *Energy Procedia, 48*, 423-430.

Shalaby, S. M., & Bek, M. A. (2014). Experimental investigation of a novel indirect solar dryer implementing PCM as energy storage medium. *Energy Conversion and Management, 83*(0), 1-8.

Shalaby, S. M., Bek, M. A., & El-Sebaii, A. A. (2014). Solar dryers with PCM as energy storage medium: A review. *Renewable and Sustainable Energy Reviews, 33*(0), 110-116.

Shao, Jingjing, Darkwa, Jo, & Kokogiannakis, Georgios. (2016). Development of a novel phase change material emulsion for cooling systems. *Renewable Energy, 87, Part 1*, 509-516.

Sharma, Atul, Sharma, S. D., & Buddhi, D. (2002). Accelerated thermal cycle test of acetamide, stearic acid and paraffin wax for solar thermal latent heat storage applications. *Energy Conversion and Management, 43*(14), 1923-1930.

Sharma, Atul, Shukla, A., Chen, C. R., & Dwivedi, S. (2013). Development of phase change materials for building applications. *Energy and Buildings, 64*(0), 403-407.

Sharma, Atul, Tyagi, V. V., Chen, C. R., & Buddhi, D. (2009). Review on thermal energy storage with phase change materials and applications. *Renewable and Sustainable Energy Reviews, 13*(2), 318-345.

Sharma, R. K., Ganesan, P., Sahu, J. N., Metselaar, H. S. C., & Mahlia, T. M. I. (2014). Numerical study for enhancement of solidification of phase change materials using trapezoidal cavity. *Powder Technology, 268*(0), 38-47.

Sharma, R. K., Ganesan, P., Tyagi, V. V., & Mahlia, T. M. I. (2016). Accelerated thermal cycle and chemical stability testing of polyethylene glycol (PEG) 6000 for solar thermal energy storage. *Solar Energy Materials and Solar Cells, 147*, 235-239.

Sharma, R. K., Ganesan, P., Tyagi, V. V., Metselaar, H. S. C., & Sandaran, S. C. (2015). Developments in organic solid–liquid phase change materials and their applications in thermal energy storage. *Energy Conversion and Management, 95*, 193-228.

Sharma, S. D., Kitano, H., & Sagara, K. (2004). Phase Change Materials for Low Temperature Solar Thermal Applications: Research Reports of Faculty of Engineering-Mie University.

Sharma, SD, Buddhi, D, & Sawhney, RL. (1999). Accelerated thermal cycle test of latent heat-storage materials. *Solar Energy, 66*(6), 483-490.

Shilei, Lv, Neng, Zhu, & Guohui, Feng. (2006). Eutectic mixtures of capric acid and lauric acid applied in building wallboards for heat energy storage. *Energy and Buildings, 38*(6), 708-711.

Shukla, A, Buddhi, D, Sharma, SD, & Sagara, K. (2003). *Accelerated thermal cycle test of erythritol for the latent heat storage application.* Paper presented at the Proceedings of the EM4 Indore workshop IEA ECES IA annex.

Shukla, Anant, Buddhi, D, & Sawhney, RL. (2008). Thermal cycling test of few selected inorganic and organic phase change materials. *Renewable Energy, 33*(12), 2606-2614.

Shukla, Anant, Buddhi, D., & Sawhney, R. L. (2009). Solar water heaters with phase change material thermal energy storage medium: A review. *Renewable and Sustainable Energy Reviews, 13*(8), 2119-2125.

Soares, N., Costa, J. J., Gaspar, A. R., & Santos, P. (2013). Review of passive PCM latent heat thermal energy storage systems towards buildings' energy efficiency. *Energy and Buildings, 59*(0), 82-103.

Solé, Aran, Neumann, Hannah, Niedermaier, Sophia, Martorell, Ingrid, Schossig, Peter, & Cabeza, Luisa F. (2014). Stability of sugar alcohols as PCM for thermal energy storage. *Solar Energy Materials and Solar Cells, 126*(0), 125-134.

Solomon, Gnanadurai Ravikumar, & Velraj, Ramalingam. (2013). Analysis of the heat transfer mechanisms during energy storage in a Phase Change Material filled vertical finned cylindrical unit for free cooling application. *Energy Conversion and Management, 75*(0), 466-473.

Song, Shaokun, Dong, Lijie, Qu, Zhengyao, Ren, Jing, & Xiong, Chuanxi. (2014). Microencapsulated capric–stearic acid with silica shell as a novel phase change material for thermal energy storage. *Applied Thermal Engineering, 70*(1), 546-551.

Stovall, T. K., & Tomlinson, J. J. (1995). What are the Potential Benefits of Including Latent Storage in Common Wallboard? *Journal of Solar Energy Engineering, 117*(4), 318-325.

Stritih, U., & Butala, V. (2010). Experimental investigation of energy saving in buildings with PCM cold storage. *International Journal of Refrigeration, 33*(8), 1676-1683.

Tahan Latibari, Sara, Mehrali, Mohammad, Mehrali, Mehdi, Indra Mahlia, Teuku Meurah, & Cornelis Metselaar, Hendrik Simon. (2013). Synthesis, characterization and thermal properties of nanoencapsulated phase change materials via sol–gel method. *Energy, 61*(0), 664-672.

Talja, Riku A, & Roos, Yrjö H. (2001). Phase and state transition effects on dielectric, mechanical, and thermal properties of polyols. *Thermochimica acta, 380*(2), 109-121.

Talmatsky, Ella, & Kribus, Abraham. (2008). PCM storage for solar DHW: An unfulfilled promise? *Solar Energy, 82*(10), 861-869.

Tan, F. L. (2008). Constrained and unconstrained melting inside a sphere. *International Communications in Heat and Mass Transfer, 35*(4), 466-475.

Tang, Bingtao, Qiu, Meige, & Zhang, Shufen. (2012). Thermal conductivity enhancement of PEG/SiO< sub> 2</sub> composite PCM by in situ Cu doping. *Solar Energy Materials and Solar Cells, 105*, 242-248.

Tatsidjodoung, Parfait, Le Pierrès, Nolwenn, & Luo, Lingai. (2013). A review of potential materials for thermal energy storage in building applications. *Renewable and Sustainable Energy Reviews, 18*(0), 327-349.

Telkes, Maria. (1952). Nucleation of Supersaturated Inorganic Salt Solutions. *Industrial & Engineering Chemistry, 44*(6), 1308-1310.

Ting, KC, Giannakakos, PN, & Gilbert, SG. (1987). Durability of latent heat storage tube-sheets. *Solar Energy, 39*(2), 79-85.

Turnpenny, J. R., Etheridge, D. W., & Reay, D. A. (2000). Novel ventilation cooling system for reducing air conditioning in buildings.: Part I: testing and theoretical modelling. *Applied Thermal Engineering, 20*(11), 1019-1037.

Tyagi, V. V., Pandey, A. K., Giridhar, G., Bandyopadhyay, B., Park, S. R., & Tyagi, S. K. (2012). Comparative study based on exergy analysis of solar air heater collector using thermal energy storage. *International Journal of Energy Research, 36*(6), 724-736.

Tyagi, V. V., Pandey, A. K., Kaushik, S. C., & Tyagi, S. K. (2012). Thermal performance evaluation of a solar air heater with and without thermal energy storage. *Journal of Thermal Analysis and Calorimetry, 107*(3), 1345-1352.

Tyagi, Vineet Veer, & Buddhi, D. (2007). PCM thermal storage in buildings: A state of art. *Renewable and Sustainable Energy Reviews, 11*(6), 1146-1166.

van Miltenburg, J. C. (2000). Fitting the heat capacity of liquid n-alkanes: new measurements of n-heptadecane and n-octadecane. *Thermochimica Acta, 343*(1–2), 57-62.

Verma, Prashant, Varun, & Singal, S. K. (2008). Review of mathematical modeling on latent heat thermal energy storage systems using phase-change material. *Renewable and Sustainable Energy Reviews, 12*(4), 999-1031.

VijayaVenkataRaman, S., Iniyan, S., & Goic, Ranko. (2012). A review of solar drying technologies. *Renewable and Sustainable Energy Reviews, 16*(5), 2652-2670.

Wakao, N., & Kaguei, S. (1982). Heat and Mass Transfer in Packed Beds. *Gordon and Breach Science Publishers, New York*, 175-205.

Wang, Jifen, Xie, Huaqing, Guo, Zhixiong, Guan, Lihui, & Li, Yang. (2014). Improved thermal properties of paraffin wax by the addition of TiO2 nanoparticles. *Applied Thermal Engineering, 73*(2), 1541-1547.

Wang, Jifen, Xie, Huaqing, Li, Yang, & Xin, Zhong. (2010). PW based phase change nanocomposites containing γ-Al2O3. *Journal of thermal analysis and calorimetry, 102*(2), 709-713.

Wang, Jifen, Xie, Huaqing, & Xin, Zhong. (2009). Thermal properties of paraffin based composites containing multi-walled carbon nanotubes. *Thermochimica Acta, 488*(1–2), 39-42.

Wang, Weilong, Yang, Xiaoxi, Fang, Yutang, & Ding, Jing. (2009). Preparation and performance of form-stable polyethylene glycol/silicon dioxide composites as solid–liquid phase change materials. *Applied Energy, 86*(2), 170-174.

Wang, Weilong, Yang, Xiaoxi, Fang, Yutang, Ding, Jing, & Yang, Jianping. (2007). Preparation of polyethylene glycol/silicon dioxide phase change materials. *JOURNAL OF CHEMICAL INDUSTRY AND ENGINEERING-CHINA-, 58*(10), 2664.

Waqas, Adeel, & Ud Din, Zia. (2013). Phase change material (PCM) storage for free cooling of buildings—A review. *Renewable and Sustainable Energy Reviews, 18*(0), 607-625.

Wasp, F.J. (1977). Solid-liquid slurry pipeline transportation. *Trans. Tech. Berlin*.

Wu, Shuying, Zhu, Dongsheng, Zhang, Xiurong, & Huang, Jin. (2010). Preparation and melting/freezing characteristics of Cu/paraffin nanofluid as phase-change material (PCM). *Energy & Fuels, 24*(3), 1894-1898.

Xu, Biwan, & Li, Zongjin. (2013). Paraffin/diatomite composite phase change material incorporated cement-based composite for thermal energy storage. *Applied energy, 105*, 229-237.

Yavari, Fazel, Fard, Hafez Raeisi, Pashayi, Kamyar, Rafiee, Mohammad A., Zamiri, Amir, Yu, Zhongzhen, . . . Koratkar, Nikhil. (2011). Enhanced Thermal Conductivity in a Nanostructured Phase Change Composite due to Low Concentration Graphene Additives. *The Journal of Physical Chemistry C, 115*(17), 8753-8758.

Yinping, Zhang, & Yi, Jiang. (1999). A simple method, the-history method, of determining the heat of fusion, specific heat and thermal conductivity of phase-change materials. *Measurement Science and Technology, 10*(3), 201.

Yu, Wenhua, France, David M., Routbort, Jules L., & Choi, Stephen U. S. (2008). Review and Comparison of Nanofluid Thermal Conductivity and Heat Transfer Enhancements. *Heat Transfer Engineering, 29*(5), 432-460.

Yuan, Yanping, Zhang, Nan, Tao, Wenquan, Cao, Xiaoling, & He, Yaling. (2014). Fatty acids as phase change materials: A review. *Renewable and Sustainable Energy Reviews, 29*(0), 482-498.

Zábranský, Milan, Růžička, Vlastimil, & Domalski, Eugene S. (2001). Heat Capacity of Liquids: Critical Review and Recommended Values. Supplement I. *Journal of Physical and Chemical Reference Data, 30*(5), 1199-1689.

Zalba, Belén, Marín, José Ma, Cabeza, Luisa F., & Mehling, Harald. (2003). Review on thermal energy storage with phase change: materials, heat transfer analysis and applications. *Applied Thermal Engineering, 23*(3), 251-283.

Zeng, Ju-Lan, Gan, Juan, Zhu, Fu-Rong, Yu, Sai-Bo, Xiao, Zhong-Liang, Yan, Wen-Pei, . . . Cao, Zhong. (2014). Tetradecanol/expanded graphite composite form-stable phase change material for thermal energy storage. *Solar Energy Materials and Solar Cells, 127*, 122-128.

Zhang, Nan, Yuan, Yanping, Wang, Xi, Cao, Xiaoling, Yang, Xiaojiao, & Hu, Shuchun. (2013). Preparation and characterization of lauric–myristic–palmitic acid ternary eutectic mixtures/expanded graphite composite phase change material for thermal energy storage. *Chemical Engineering Journal, 231*(0), 214-219.

Zhang, Ping, Song, Lei, Lu, Hongdian, Wang, Jian, & Hu, Yuan. (2010). The influence of expanded graphite on thermal properties for paraffin/high density polyethylene/chlorinated paraffin/antimony trioxide as a flame retardant phase change material. *Energy Conversion and Management, 51*(12), 2733-2737.

Zhang, X. X., Fan, Y. F., Tao, X. M., & Yick, K. L. (2004). Fabrication and properties of microcapsules and nanocapsules containing n-octadecane. *Materials Chemistry and Physics, 88*(2–3), 300-307.

Zhang, Zhengguo, Shi, Guoquan, Wang, Shuping, Fang, Xiaoming, & Liu, Xiaohong. (2013). Thermal energy storage cement mortar containing n-octadecane/expanded graphite composite phase change material. *Renewable Energy*, *50*(0), 670-675.

Zhang, Zhengguo, Zhang, Ni, Peng, Jing, Fang, Xiaoming, Gao, Xuenong, & Fang, Yutang. (2012). Preparation and thermal energy storage properties of paraffin/expanded graphite composite phase change material. *Applied Energy*, *91*(1), 426-431.

Appendices

List of papers accepted for publication in journals

1. R.K. Sharma, P. Ganesan, V.V. Tyagi, H.S.C. Metselaar, S. Sandaran. (2016), "Thermal properties and heat storage analysis of palmitic acid-TiO_2 composite as nano-enhanced organic phase change material (NEOPCM)", Applied Thermal Engineering (Accepted for publication). (ISI-Cited).

2. R.K. Sharma, P. Ganesan, V.V. Tyagi. (2016). "Long term thermal and chemical reliability study of different organic phase change materials for thermal energy storage applications", Journal of Thermal Analysis and Calorimetry (Accepted for publication). (ISI-Cited).

3. R. K. Sharma, P. Ganesan, V. V. Tyagi, T.M.I. Mahlia. (2016). "Accelerated thermal cycle and chemical stability testing of Polyethylene glycol (PEG) 6000 for solar thermal energy storage", Solar Energy materials and Solar Cells, 147, 235-239. (ISI-Cited).

4. R. K. Sharma, P. Ganesan, V. V. Tyagi, H. S. C. Metselaar, S. C. Sandaran. (2015). "Developments in organic solid–liquid phase change materials and their applications in thermal energy storage", Energy Conversion and Management, 95, 193-228. (ISI-Cited).

5. R. K. Sharma, P. Ganesan, J. N. Sahu, H. S. C. Metselaar, T.M.I. Mahlia. (2014). "Numerical study for enhancement of solidification of phase change materials using trapezoidal cavity", Powder technology, 268, 38-47. (ISI-Cited).

Conference proceedings

1. R. K. Sharma, P. Ganesan, "*Numerical study of freezing of cu-water nanofluid in a trapezoidal cavity*", 3rd International Conference on Clean Energy and Technology (CEAT) 2014, held at Kuching, Malaysia between November 24-26, 2014. (Scopus-Cited)